THE UNIVERSITY OF CALGARY

Modelling the Hydrodynamics

of

Circulating Fluidized Bed Risers

by

Robert Wong

A THESIS

SUBMITTED TO THE FACULTY OF GRADUATE STUDIES

IN PARTIAL FULFILLMENT OF THE REQUIREMENTS FOR THE DEGREE OF

MASTER OF SCIENCE

DEPARTMENT OF CHEMICAL AND PETROLEUM ENGINEERING

CALGARY, ALBERTA

OCTOBER, 1991

ISBN 0-315-75247-5

Canada

THE UNIVERSITY OF CALGARY

FACULTY OF GRADUATE STUDIES
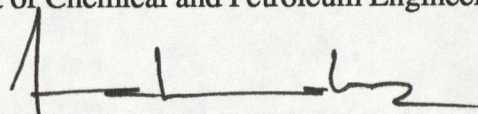
The undersigned certify that they have read, and recommend to the Faculty of Graduate Studies for Acceptance, a thesis entitled, "Modelling the Hydrodynamics of Circulating Fluidized Bed Risers" submitted by Robert Wong in partial fulfillment of the requirements for the degree of Master of Science.

Dr. F. Berruti (Supervisor)
Department of Chemical and Petroleum Engineering

Dr. L.A. Behie
Department of Chemical and Petroleum Engineering

Dr. A. Chakma
Department of Chemical and Petroleum Engineering

Dr. I. Wierzba
Department of Mechanical Engineering

November 28, 1991

ii

ABSTRACT

Although the commercial applications employing circulating fluidized bed (CFB) technology are developing rapidly, there is still a lack of fundamental research and understanding of fast fluidization. The objective of this study is to develop a more coherent picture of fast fluidization by examining the hydrodynamics of CFB risers. The study involves an experimental and theoretical investigation on the mechanisms responsible for creating the internal flow structure within the riser and on how entrance and exit effects, particle size and density and operating conditions affect riser hydrodynamics.

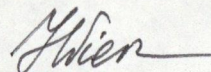A predictive model based on core/annular flow has been developed to estimate the axial voidage profile and internal flow structure of risers under fast fluidization conditions. The model assumes the riser to consist of three sections: 1) an acceleration zone where the solids accelerate upon entry into the riser, 2) a developed flow zone where the flow of gas and solids is assumed to be hydrodynamically fully developed and 3) an abrupt exit zone for CFB units equipped with an abrupt exit at the top of the riser. Using empirically developed equations for predicting the apparent voidage at the bottom of the riser, the length of the acceleration zone and the apparent voidage at the top of the riser (for CFBs with abrupt riser exits), the three sections of the riser are solved to yield the average voidage, core voidage, core radius, gas core velocity, solids core velocity, solids core-to-annulus interchange coefficient and solids annulus-to-core interchange coefficient

as a function of axial location.

Through comparison with experimental axial voidage profiles obtained in this study and reported in literature, the model was shown to be able to qualitatively and quantitatively predict the effect of operating variables such as superficial gas velocity, solids mass flux, solids diameter and density and riser geometry on the axial voidage profile. Because of uncertainties associated with experimental internal flow structure measurements, a meaningful comparison between the simulated and experimental results could not be made.

To illustrate an application of the hydrodynamic model to reactor design, the model was used to study the formation and evolution of environmentally damaging air pollutants such as SO_2 and NO_x emissions generated during circulating fluidized bed coal combustion. The study is a first attempt to model emissions from CFB coal combustors and may serve as a basis for more comprehensive simulations.

ACKNOWLEDGEMENTS

It gives me much pleasure to express my appreciation and gratitude to the many friends and colleagues who have assisted in this work. First of all, I wish to express my sincere thanks to Dr. Franco Berruti, whom without his guidance, support and friendship this study would not have been completed.

I would like to thank Todd Pugsley and Bruce Milne for many valued discussions throughout this study. Their advice and support was very much appreciated. In addition, I would also like to thank the undergraduate and graduate students in Chemical Engineering at The University of Calgary. Their enthusiasm, encouragement and zest for life helped to make my studies a very enjoyable experience.

Finally, I am indebted to my family for their inspiration, understanding and patient encouragement throughout this study.

TABLE OF CONTENTS

CHAPTER 1. - INTRODUCTION

CHAPTER 2. - EXPERIMENTAL EQUIPMENT

CHAPTER 3. - EXPERIMENTAL RESULTS

CHAPTER 4. - HYDRODYNAMIC MODELLING

CHAPTER 5. - MODEL VALIDATION AND SIMULATION RESULTS

CHAPTER 6. - MODELLING OF SO_2 AND NO_x EMISSIONS FROM CFB COAL COMBUSTORS

CHAPTER 7. - CONCLUSIONS AND RECOMMENDATIONS

CHAPTER 8. - REFERENCES

CHAPTER 9. - APPENDIX A

LIST OF TABLES

LIST OF FIGURES

NOMENCLATURE

A	constant in Equation 4.30 for K_{ca}, (-)
Ar	Archimedes number, (-)
B	constant in Equation 4.30 for K_{ca}, (-)
d_c	char particle diameter, m
C	concentration of SO_2 in sulfur capture model, mol/m^3
C_c	concentration of SO_2 at reaction interface within a grain in sulfur capture model, mol/m^3
C_{CO}	concentration of CO, $kmol/m^3$
C_{NH3}	concentration of NH_3, $kmol/m^3$
C_{NO}	concentration of NO, $kmol/m^3$
C_{O2}	concentration of O_2, $kmol/m^3$
C_{pl}	concentration of SO_2 in product layer, mol/m^3
D	molecular diffusivity, cm^2/s
D_{eff}	effective diffusivity, m^2/s
D_s	solid product layer diffusivity, m^2/s
D_h	riser hydraulic diameter, m
D_p	average solids particle diameter, m
D_t	riser diameter, m
E	upwards solids mass flux, $kg/(m^2 \cdot s)$
E_x	solids entrainment at any axial position x, $kg/(m^2 \cdot s)$
f_g	Fanning friction factor, (-)
f_i	interfacial friction factor, (-)
f_{io}	smooth pipe interfacial friction factor, (-)
f_s	solids friction factor, (-)
F_i	molar flowrate of species i, kmol/s
Fr	Froude number, (-)
g	acceleration due to gravity, m/s^2
G	solids mass flux, $kg/(m^2 \cdot s)$

k	proportionality constant in acceleration zone, m^{-1}
K_{ac}	solids annulus-to-core interchange coefficient, m/s
k_c	overall rate constant in Equation 6.8, cm/s
K_{ca}	solids core-to-annulus interchange coefficient, m/s
k_{cd}	diffusion rate constant in Equation 6.8, $mol/(cm^2 \cdot s \cdot atm)$
k_{cr}	chemical reaction rate constant in Equation 6.8, $mol/(cm^2 \cdot s \cdot atm)$
k_{SO2}	reaction rate constant in sulfation reaction, m/s
k_v	pseudo first order volumetric reaction rate constant, s^{-1}
L_{acc}	length of acceleration zone, m
m	constant in Equations 4.31 and 4.32 for K_{ca}, m
mw_c	molecular weight of carbon, kg/kmol
mw_{CC}	molecular weight of calcium carbonate, kg/mol
mw_n	molecular weight of nitrogen, kg/kmol
p	ratio of CO to CO_2 in Equation 6.6, (-)
P	pressure, Pa
Q	upward solids mass flowrate, kg/s
r_c	core radius, m
r_{CO}	reaction rate in Equation 6.13, $gmol/(cm^3 \cdot s)$
r_{char}	char combustion rate, gmol/(s·particle)
r_g	grain radius location, m
r_{go}	initial grain radius, m
r_{pl}	radial position in product layer, m
r_{SO2}	rate of sulfation in Equation 6.15, $gmol/(cm^3 \cdot s)$
r_1	reaction #1 rate expression in Table 6.1A, gmol/(s·particle)
r_2	reaction #2 rate expression in Table 6.1A, $gmol/(cm^3 \cdot s)$
r_3	reaction #3 rate expression in Table 6.1A, kmol/(kg·s)
r_4	reaction #4 rate expression in Table 6.1B, kmol/(kg·s)
r_5	reaction #5 rate expression in Table 6.1B, kmol/(kg·s)
r_6	reaction #6 rate expression in Table 6.1B, kmol/(kg·s)
r_7	reaction #7 rate expression in Table 6.1C, kmol/(kg·s)

r_8	reaction #8 rate expression in Table 6.1C, kmol/(kg•s)
R	riser radius, m
$R^{/}$	universal gas constant, J/(kmol•K)
R_g	universal gas constant, atm cm^3/(mol•K)
R_s	radius of solid particle, m
R_w	annular region film thickness, m
Re	Reynolds number, (-)
Re_p	particle Reynolds number, (-)
R_p	pellet radius, m
R_{po}	initial pellet radius, m
R_s	net particle radial flux, kg/(m^2•s)
S	Stokes number, (-)
$t_{0.5}$	half life, s
T	operating temperature, K
T_c	char particle temperature, K
U_{com}	combined phase gas-solid core velocity, m/s
U_{gc}	gas core veloctiy, m/s
U_o	superficial gas velocity, m/s
U_s	average solids velocity, m/s
U_{sc}	solids core velocity, m/s
U_t	single particle solids terminal velocity, m/s
V	volume of reactor
V_{co}	molar volume of calcium oxide, mol/m^3
V_{cs}	molar volume of calcium sulfate, mol/m^3
wf_c	weight fraction carbon in coal, (-)
wf_n	weight fraction nitrogen in coal, (-)
wf_s	weight fraction sulfur in coal, (-)
W	downwards solids mass flux, kg/(m^2•s)
x	axial location, m
X_L	local calcium oxide conversion per pellet, (-)

X_n weight fraction of nitrogen emitted during devolatilization, (-)

X_O overall calcium oxide conversion per pellet, (-)

X_s weight fraction of sulfur emitted during devolatiolization, (-)

y_{CO} mole fraction of carbon monoxide, (-)

y_{H2O} mole fraction of water, (-)

y_{O2} mole fraction of oxygen, (-)

y mole fraction of calcium carbonate in limestone, (-)

Z riser height, m

Greek Letters

α limiting core suspension density, kg/m^3

Γ constant in acceleration zone, (-)

δ mechanism factor in Equation 6.3, (-)

ε_b apparent voidage at riser bottom, (-)

ε_c core axial voidage, (-)

ε_{app} apparent axial voidage, (-)

ε_{avg} average axial voidage, (-)

ε_l limiting core voidage, (-)

ε_{ls} porosity of raw limestone, (-)

ε_{lsc} porosity of calcined limestone, (-)

ε_{mf} voidage at minimum fluidization, (-)

ε_o actual voidage at riser bottom, (-)

ε_t apparent voidage at riser top, (-)

ε_∞ voidage at end of acceleration zone, (-)

η effectiveness factor, (-)

μ_g gas viscosity, Pa-s

ζ constant in Equation 4.33 for f_i, (-)

ρ_b bulk density at minimum fluidization velocity, kg/m^3

ρ_{bulk} bulk density of catalytic material, kg/m^3

ρ_{cc} calcium carbonate particle density, kg/m^3

ρ_{com} combined phase gas-solid core density, kg/m^3

ρ_g gas density, kg/m^3

ρ_{ls} limestone particle density, kg/m^3

ρ_s solid particle density, kg/m^3

ρ_{susp} gas-solid suspension density, kg/m^3

τ interfacial shear stress, N/m^2

φ slip factor, (-)

ϕ proportionality constant in Equation 4.37 for interfacial shear, s^{-1}

ψ Thiele modulus, (-)

CHAPTER 1
INTRODUCTION

1.1 FLUIDIZATION

Fluidization occurs by passing a fluid at a sufficiently high velocity through a bed of solids such that an expanded, suspended mass is created. The liquid-like behaviour of the fluidized solids enables it to be easily moved from one vessel to another and/or drained through pipes and valves.

Many different types of fluidization exist. Particulate fluidization is characterized by uniform bed expansion with fluid velocity. As the velocity of the fluid is increased, the particles move farther apart uniformly until they are carried out of their holding vessel. Usually particulate fluidization occurs when solid particles are fluidized with liquids although depending on the fluidization conditions and the physical properties of the solids, particulate fluidization can also occur with gases. For example, fine catalyst solids fluidized by high pressure gas have exhibited behaviour characteristic of particulate fluidization. For the purposes of this study, only fluidization involving gases is considered.

Fluidization with gases resulting in the formation of bubbles is called aggregative or bubbling fluidization. In bubbling fluidization, most of the gas goes through the bed of solids as bubbles. The behaviour of the gas bubbles is hard to predict and depends on a multitude of factors. The nature and size distribution of the particles, the type of distributor plate, the superficial gas velocity, and the depth of the fluidized bed are examples (McCabe et al., 1985). Once the bubbles form, they have a tendency to

coalesce and grow as they rise through the fluidized bed of solids. It is possible for the bubbles to grow until they fill the entire cross section of the vessel containing the solids. Successive bubbles may then travel up the column separated by slugs of solids. This phenomena is called slugging and is highly undesirable because of pressure fluctuations in the bed, poor gas-solid contact and solids entrainment.

With increases in fluidizing gas velocity, the two phase character of the bubbling bed eventually gives way to a condition of increased uniformity. The resulting fluidized state has been defined by Lanneau (1960) and by Kehoe and Davidson (1971) as turbulent fluidization. There are two different views of turbulent fluidization. Kehoe and Davidson (1971) describes turbulent fluidization in terms of transitory voids moving obliquely upwards. Unlike the bubbles and slugs in lower velocity fluidization regimes, the voids are much smaller and occur much more frequently. Another description of turbulent fluidization is provided by Brereton (1987). According to Brereton (1987), turbulent fluidization is characterized by an absence of bubbles and by the existence of clusters or packets of solids in the bed. In both bubbling and turbulent beds, except for minor carryover of solids, the bed generally experiences no net flow and remains at the bottom of the holding vessel (Yerushalmi, 1986). Unlike a bubbling bed, in turbulent fluidization, the top surface of the bed of solids is considerably more diffuse because of the greater fluidizing gas velocity.

As the gas fluidization velocity is increased further, the rate of solids carryover rapidly increases. Without some sort of solids replenishment, the inventory of solids in the system would rapidly become depleted. By recycling the solids with external

cyclones and a standpipe, a fluidized system with a relatively high solids concentration can be maintained. According to Grace (1990), the fast fluidization regime occurs at a gas fluidizing velocity where there is no longer a clear interface between a dense bed of solids and a dilute freeboard region. Besides high solid concentrations, fast fluidization is also characterized by an extensive amount of solids backmixing.

Increases in gas velocity above the requirement for fast fluidization leads to what is known as pneumatic transport. In pneumatic transport, high velocity gas carries a lean gas-solid suspension upward in relatively straight paths with very little backmixing of the solid particles. Figure 1.1 show a schematic representation of the various hydrodynamic types of fluidization and Figure 1.2 represents a regime map of the various fluidization states.

1.2 FAST FLUIDIZATION AND THE CIRCULATING FLUIDIZED BED SYSTEM

One way of achieving fast fluidization conditions is to use a fast or circulating fluidized bed (CFB). A schematic of a typical circulating fluidized bed system is shown in Figure 1.3. Fast fluidization conditions are achieved by operating at a sufficiently high superficial gas velocity (6-8 m/s) and by using a cyclone and standpipe arrangement to recirculate the solids. The riser is the most important part of a CFB system since gas-solid chemical reactions occur in this region. Experimental studies of CFB risers have indicated that radial gradients exist with significantly higher concentrations of solids near the outer wall than in the interior of the riser (Yerushalmi et al., 1978; Weinstein et al., 1986; Geldart and Rhodes, 1986; Bolton and Davidson, 1988; Kwauk et al., 1986; Bader

INCREASING U, ε

FIXED BED
OR DELAYED
BUBBLING

BUBBLING
REGIME

SLUG FLOW

TURBULENT
REGIME

FAST
FLUIDIZATION
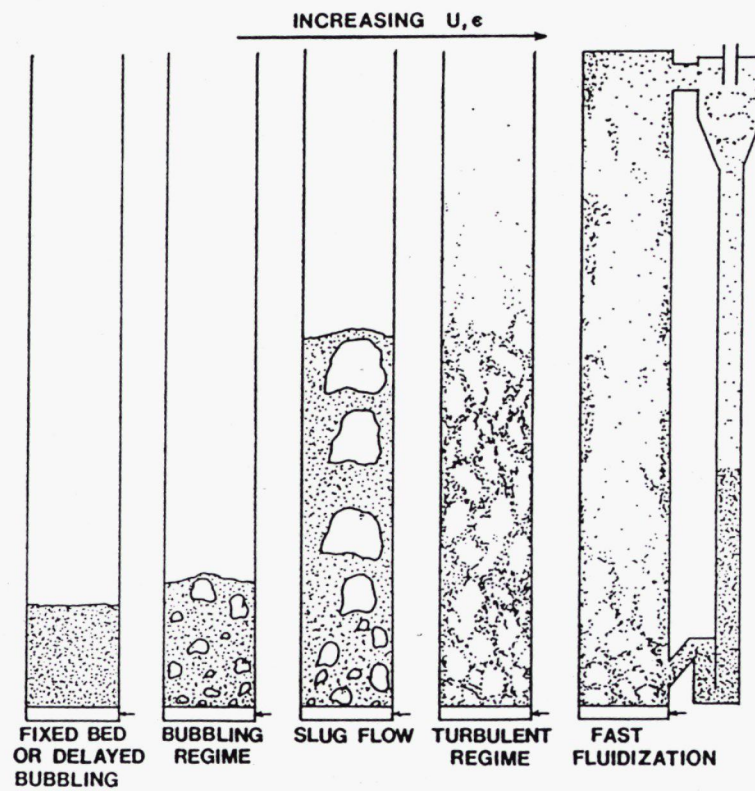
FIGURE 1.1 - SCHEMATIC OF HYDRODYNAMIC REGIMES OF
FLUIDIZATION, (GRACE, 1990)
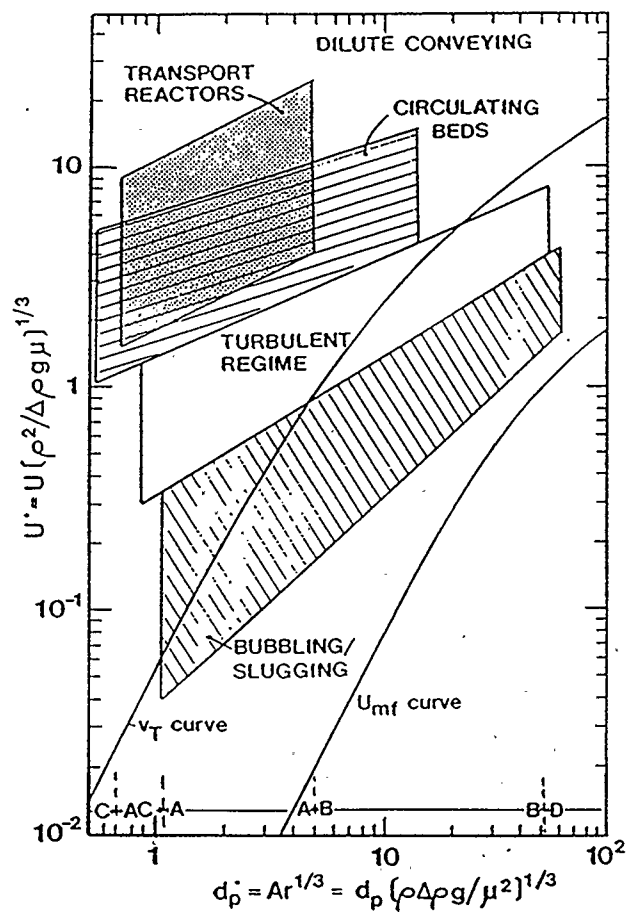
FIGURE 1.2 - FLUIDIZATION REGIME MAP, (GRACE, 1990)
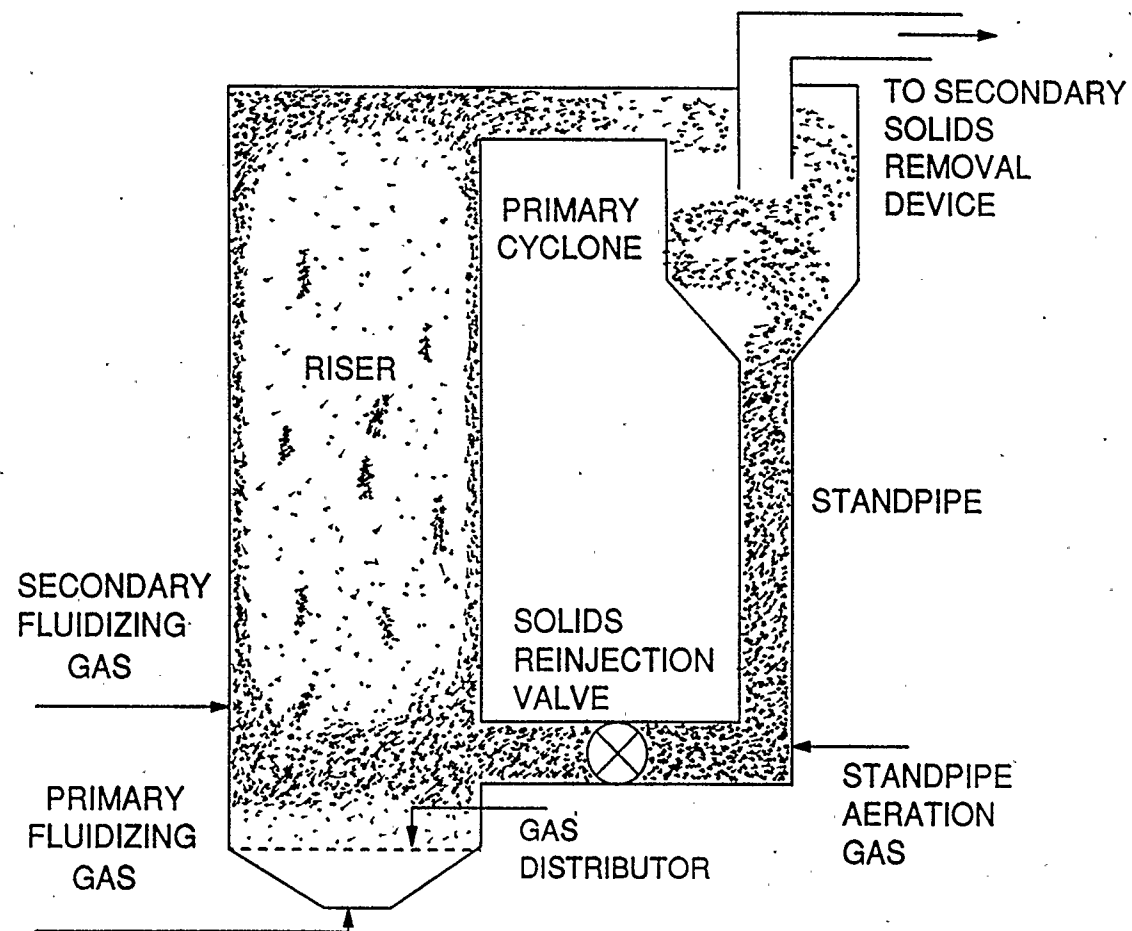
FIGURE 1.3 - SCHEMATIC OF CIRCULATING FLUIDIZED BED SYSTEM

et al., 1988; Horio et al., 1988; Rhodes, 1990; Kato et al., 1990; Dingrong et al., 1990).

Furthermore, pioneering studies by Kwauk et al. (1986) have shown that the riser also contains axial non-uniformities. According to Kwauk et al. (1986), the axial solids concentration profile is "S" shaped with a dense solid phase at the bottom of the column and a dilute solid phase at the top. The transition between the two solid phases is indicated by an inflection point in the axial solids holdup profile. Workers such as Kwauk et al. (1986) and Horio et al. (1988) have considered the riser to be made up of upward and downward moving clusters or packets of solids dispersed in a dilute continuum of discrete particles while others like Geldart and Rhodes (1986), Bader et al. (1988), Kato et al. (1990) and Dingrong et al. (1990) have considered the riser to be made up of a dilute upward moving gas-solid suspension surrounded by a film of downward falling solids. Others such as Bolton and Davidson (1988) have proposed that the lower region of the riser is similar to a slugging fluidized bed while the upper part consists of a lean gas-solid suspension similar to that found in pneumatic transport lines. Depending upon the exit configuration at the top of the riser, there may also be significant internal solids recirculation. As indicated by Brereton (1987) and Patience (1990), abrupt exits result in internal separation of entrained solids from the gas at the top of the riser and lead to considerable internal reflux of solids. The effect leads to an increase in solids hold-up at the top of the riser. Figure 1.4 shows the effect of riser exit configuration on the axial voidage profile.

Separation of solids leaving the riser is usually accomplished by external vertically oriented cyclones. Labyrinth separators can also be used in gas-solid separation (Dry and

RISER HEIGHT

B   A

VOIDAGE

B: ABRUPT EXIT
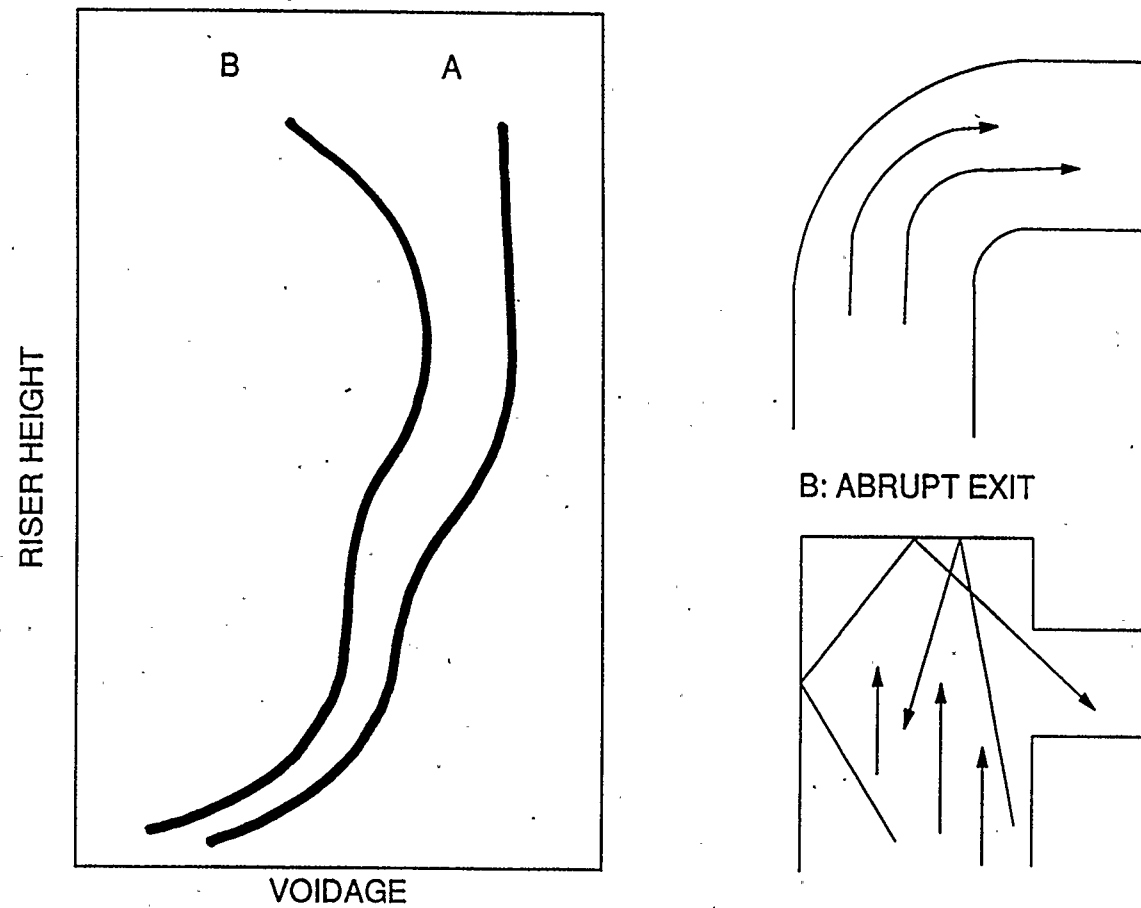
FIGURE 1.4 - EFFECT OF RISER EXIT GEOMETRY ON AXIAL SOLIDS HOLDUP

8

La Nauze, 1990). Labyrinth separators operate by changing the direction of flow many times and in the process trap solids in stagnant collection slides.

The solids from the gas-solid separation device fall into a standpipe where they are conveyed downward with the help of gravity. Usually, aeration is provided to keep the solids in the standpipe fluidized. The more solids in the standpipe, the greater the potential driving force for solids circulation and the higher the solids concentration in the riser (Dry and La Nauze, 1990).

The solids circulation loop is completed when the solids in the standpipe are reinjected back into the base of the riser. A critical aspect of the solids reinjection system involves designing the system so that gas cannot escape up the standpipe. Gas in the standpipe may entrain solids up the cyclone and possibly into downstream equipment. Loop seals, V valves and L valves are often used as part of the solids reinjection system.

1.3 ADVANTAGES OF A CIRCULATING FLUIDIZED BED

Circulating Fluidized Beds, operating in the fast fluidization regime have many advantages over lower velocity fluidization systems. Because of large external and internal recirculation, CFBs have the advantage of temperature uniformity or isothermal operation and like all fluidized beds have extremely good solids handling capabilities. The absence of bubbles in CFBs eliminates the gas bypassing problems that plagues bubbling fluidized beds. Heat and mass transfer rates are higher in CFBs since smaller solid particles, which have more interfacial area can be used (Ambler, 1988). Other advantages include adjustable retention time of solids by means of riser exit configuration

and choice of solids circulation rate, superior lateral mixing and high gas throughput per unit cross-sectional area. In the case of combustion reactions, due to better gas-solid mixing characteristics, CFBs can reduce the amount of NO_x emissions as well as the amount of unburned CO and hydrocarbons. In fast catalytic reactions involving rapidly deactivating catalysts, the recycle leg can be used as a continuous catalyst regenerator. The downside of CFBs include high gas compression costs due to the high pressure drop along the riser as the solid particles move upward, increased erosion of reactor components by the high velocity solids, solid particle attrition, a higher capital cost than lower velocity fluidization systems and most importantly, a lack of fundamental research and understanding into the phenomena of fast fluidization.

1.4 APPLICATIONS OF CIRCULATING FLUIDIZED BEDS

CFBs can be used in many industrial applications. Hartge et al. (1986) mentions that chemical reacting systems requiring high specific transfer rates, high solids throughput and thermal uniformity within the reactor are excellent candidates for application with CFB technology. Lurgi Chemie along with Vereinigte Aluminum Werke were the first to use CFBs. They developed a successful process for calcining aluminum hydroxide to supply cell-grade alumina (Yerushalmi, 1986). Reh (1986) have indicated that CFBs have been investigated for combustion of low grade fuels, pyrolysis of biomass, coal gasification, dry scrubbing of gases and Fischer-Tropsch synthesis. Catalytic reactions such as the production of maleic anhydride from n-butane have also been suggested. Presently, CFBs are largely used in the combustion of coal. Recent

developments in CFB technology include using CFB adsorbers for the recovery of uranium from seawater (Nakamura et al., 1990) and the use of CFBs for low temperature oxidation applications (Morooka et al., 1990).

1.5 OBJECTIVES OF STUDY

Although the commercial applications employing circulating fluidized bed technology are developing rapidly, there is still a lack of fundamental research and understanding of fast fluidization. The main objective of this study is to develop a more coherent picture of fast fluidization by examining the hydrodynamics of CFB risers. The study reported in this thesis involves an experimental and theoretical investigation on the mechanisms responsible for creating the internal flow structure within the riser and on how entrance and exit effects, particle size and density and operating conditions such as superficial gas velocity and solids circulation rate affect riser hydrodynamics. The results are used to develop a predictive hydrodynamic model which allows evaluation of the axial voidage profile and internal flow structure of CFB risers. Finally, the proposed model is used to study the formation and evolution of environmentally damaging air pollutants such as sulfur dioxide (SO_2) and nitric oxide (NO) generated during circulating fluidized bed coal combustion.

CHAPTER 2
EXPERIMENTAL EQUIPMENT

2.1 EXPERIMENTAL APPARATUS

A schematic of the experimental circulating fluidized bed used in this study is shown in Figure 2.1. The experimental unit was constructed at the University of Waterloo and previously used by Ambler (1988). The experimental system consists of a riser equipped with an abrupt exit configuration, two external vertically oriented cyclones in series for gas-solid separation and a flap valve diverter setup for measuring solids flowrate. The riser column is 3 m in height and 0.05 m in diameter. It is constructed from plexiglass to permit visual observation. The primary gas distributor is a sintered metal disk having approximately 100 μm diameters pores. Thirteen pressure taps are located along the length of the riser to measure the axial pressure drop. To prevent solid particles from plugging the pressure taps, each opening was lined with filter paper. High pressure air can also be used to flush out any solid particles trapped in the pressure taps. The location of the pressure taps along the riser is illustrated in Figure 2.2. Pressure measurements are made with a bank of manometers containing Meriam oil having a specific gravity of 1.0. The manometers are hooked up in such a way that the pressure measured at any tap is relative to the pressure at the base of the column. Solids from the recirculation leg enter the bottom of the riser through a 0.04 m transfer line at an angle of 45 degrees to the horizontal. An abrupt exit with a 0.12 m dead zone is employed at the top at the riser.
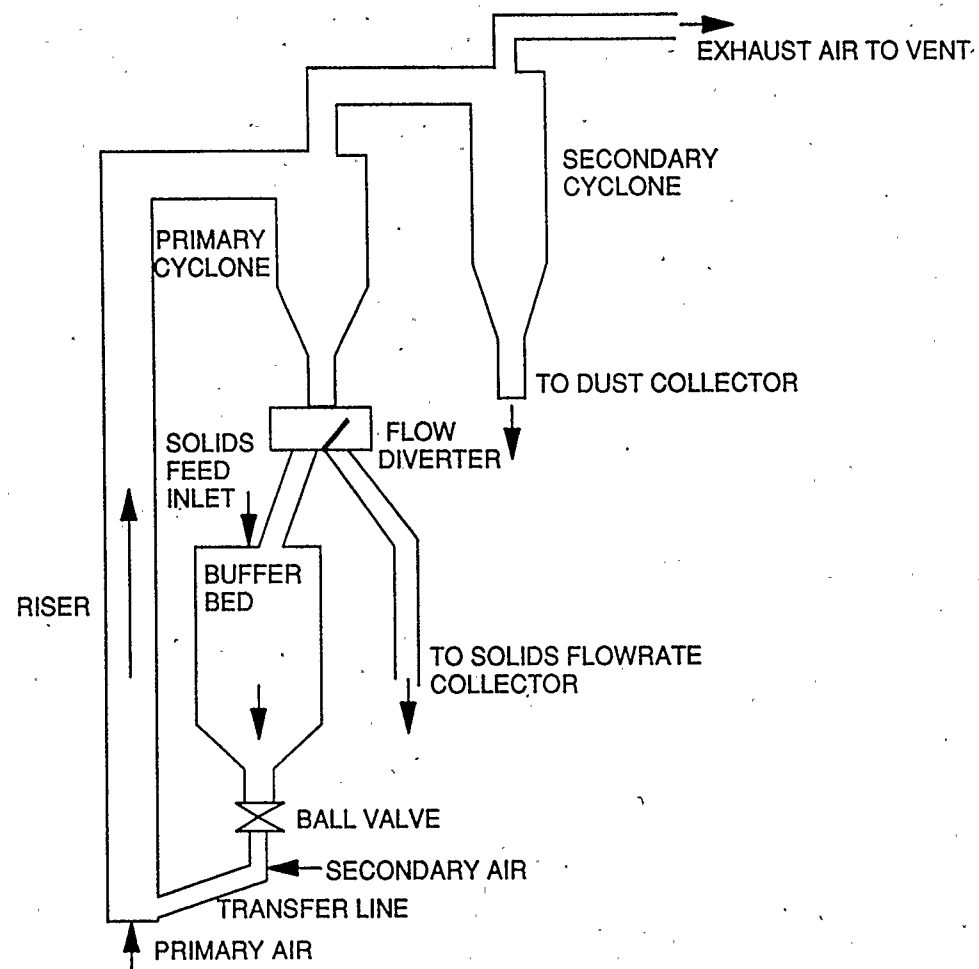
FIGURE 2.1 - SCHEMATIC OF EXPERIMENTAL CFB UNIT

ABRUPT EXIT
CONFIGURATION
AT TOP OF
RISER

A

0.10 m
0.15 m
0.25 m
0.25 m
0.25 m
0.25 m
0.25 m
0.25 m

3.0 m

0.25 m
0.25 m
0.25 m
0.25 m
0.25 m
0.25 m
0.15 m
0.10 m

PRESSURE
TAP
LOCATIONS

RISER TOP

(ABRUPT
EXIT
CONFIGURATION)

0.12 m

0.05 m

0.04 m

0.04 m

A

TO PRIMARY

CYCLONE

PRESSURE
TAP

RISER BOTTOM

0.10 m

0.05 m

0.04 m

TRANSFER LINE

45°

SINTERED METAL
PLATE
DISTRIBUTOR

PRIMARY AIR INLET

FIGURE 2.2 - RISER CONFIGURATION

14

2.2 RECIRCULATION LEG

Gas-solid separation is achieved by using two vertically oriented cyclones in series. The primary cyclone, having a low solids separation efficiency was originally designed by Ambler (1988) to separate primary high density solids while at the same time allowing for low density particles to continue with the gas. The captured solids from the primary cyclone then fall into a buffer bed. The secondary high efficiency cyclone collects any remaining solids carried with the gas in a 0.0508 m polyethylene pipe connected to a storage chamber. The gas passing through the secondary cyclone is vented to the atmosphere. Figure 2.3 shows the configuration and dimensions of the two cyclones.

A buffer bed is placed below the primary cyclone in the recirculation leg not only to store solids but also to prevent upsets during the solids flowrate measurement. The buffer bed is 1.4 m high and has a diameter of 0.20 m. The bottom of the buffer bed has a conical section with a 0.04 m diameter outlet. A 0.0125 m thick 0.125 m diameter aeration ring with 100 micron diameter holes is located within the bottom of the buffer bed. The purpose of the aeration ring is to aerate the solids in the buffer bed so that they remain in a fluidized state. Packed solids in the buffer bed is highly undesirable since bridging can occur at the neck of the buffer bed exit and prevent solids flow. Gas flow to the aeration ring is controlled by a needle valve connected to the secondary air supply.

A flap valve at the entrance to the buffer bed is used to divert solids to a collection vessel so that the solids flowrate can be evaluated. When the solids flowrate is being determined, the diameter of the buffer bed is large enough so that there is

FROM RISER

0.05 m

0.05 m

PRIMARY
CYCLONE (A)

Li

Lo

Do

Dc

Lcy

Ho

0.075 m

0.05 m

TO VENT

SECONDARY
CYCLONE (B)

0.05 m

0.05 m

Db

CYCLONE
DIMENSIONS (m)

	(A)	(B)
Dc	0.15	0.108
Do	0.075	0.054
Db	0.05	0.04
Lo	0.094	0.07
Li	0.075	0.054
Lcy	0.319	0.162
Ho	0.562	0.432
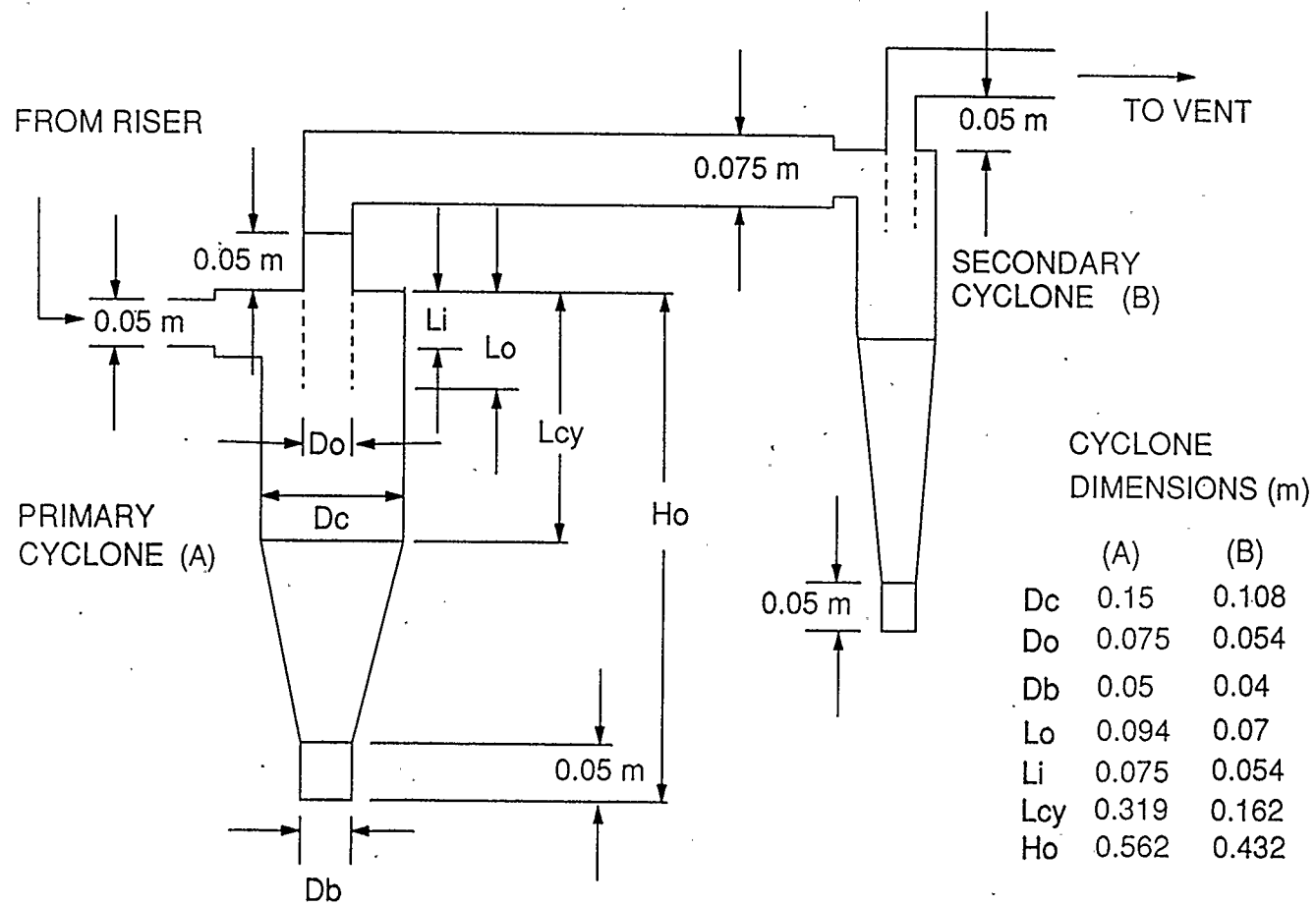
FIGURE 2.3 - CYCLONE CONFIGURATION

16

minimal reduction in the solids head during the diversion time and hence minimal upset to the system.

An opening is available at the top of the buffer bed to replenish any solids lost from the system and hence, keep the solids inventory constant. Solid flowrate is controlled by means of a 0.0381 m ball valve located immediately below the buffer bed. A secondary air injection port is installed in the transfer line between the solids recirculation leg and the riser to assist in the movement of solids through this zone.

Figure 2.4 show the specific dimensions of the buffer bed while Figures 2.5, 2.6 and 2.7 show the dimensions and configuration of the flap valve controlling the solids measurement system, the aeration ring and the transfer line between the solid recirculation leg and riser, respectively.

2.3 FLUIDIZING AIR CONTROL

The inlet air is divided into two streams: a primary air stream which goes to the base of the riser and a secondary air stream which goes to the solids recirculation leg. Because of static electricity buildup in the riser, the fluidizing air is first humidified by bubbling it through a water-filled vessel. The primary air is the principal fluidizing gas carrying solids up through the riser while the secondary air is used to facilitate the movement of solids in the recirculation leg. Primary air is metered by means of a Brooks type 1110-08B-A rotameter while the secondary air is controlled by a Brooks type 1110-08H2A1A rotameter. The secondary air stream is subsequently split by means of a needle valve so that a portion of it goes to the aeration ring in the buffer bed while the

BUFFER BED
TOP

BUFFER BED
BOTTOM

1.6 m

0.20 m

0.20 m

0.03 m

0.045 m

0.025 m

0.05 m

0.055 m

FRESH
SOLIDS
INLET

CIRCULATING
SOLIDS
INLET

0.05 m

0.04 m

0.16 m

0.04 m

CIRCULATING
SOLIDS
OUTLET
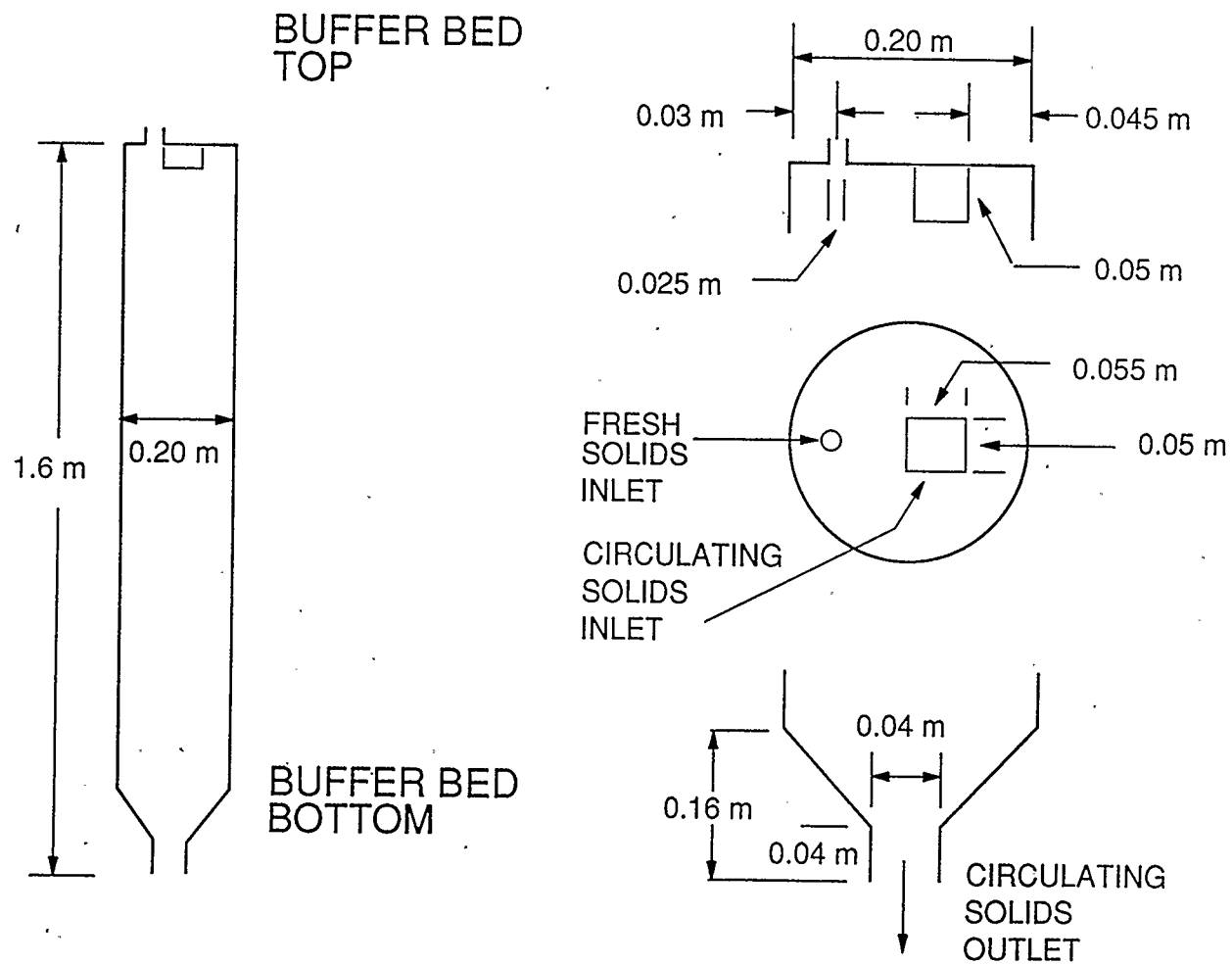
FIGURE 2.4 - BUFFER BED CONFIGURATION

FROM PRIMARY CYCLONE

0.03 m

0.03 m

0.05 m x 0.07 m

0.07 m

0.05 m

FLAP VALVE

0.04 m

0.27 m

0.16 m

0.05 m x 0.05 m

TO BUFFER BED

0.055 m | 0.05 m

0.06 m | 0.055 m

TO SOLIDS COLLECTOR
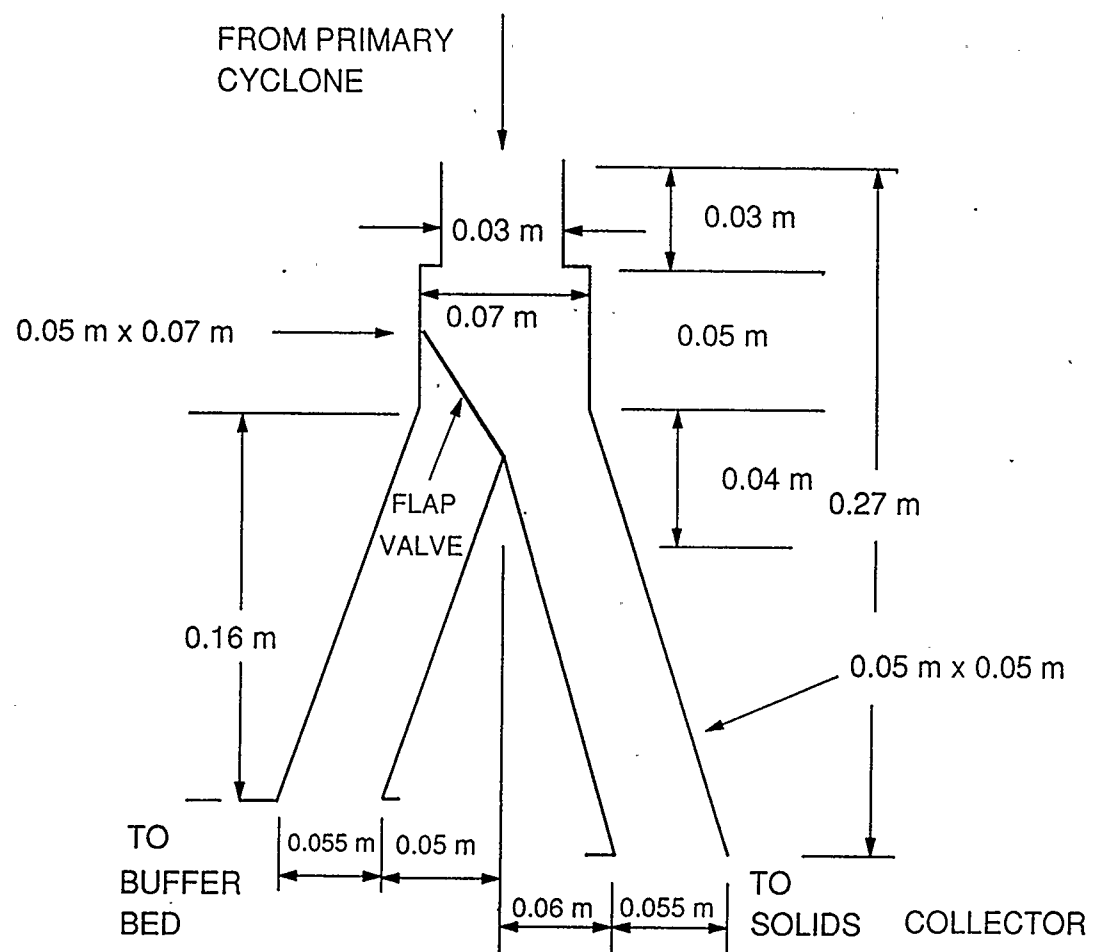
FIGURE 2.5 - FLAP VALVE CONFIGURATION

BUFFER BED

AERATION
RING

0.02 m

0.0125 m   0.125 m

0.20 m

0.0635 m TUBING

BUFFER BED
WALL

100 MICRON HOLES
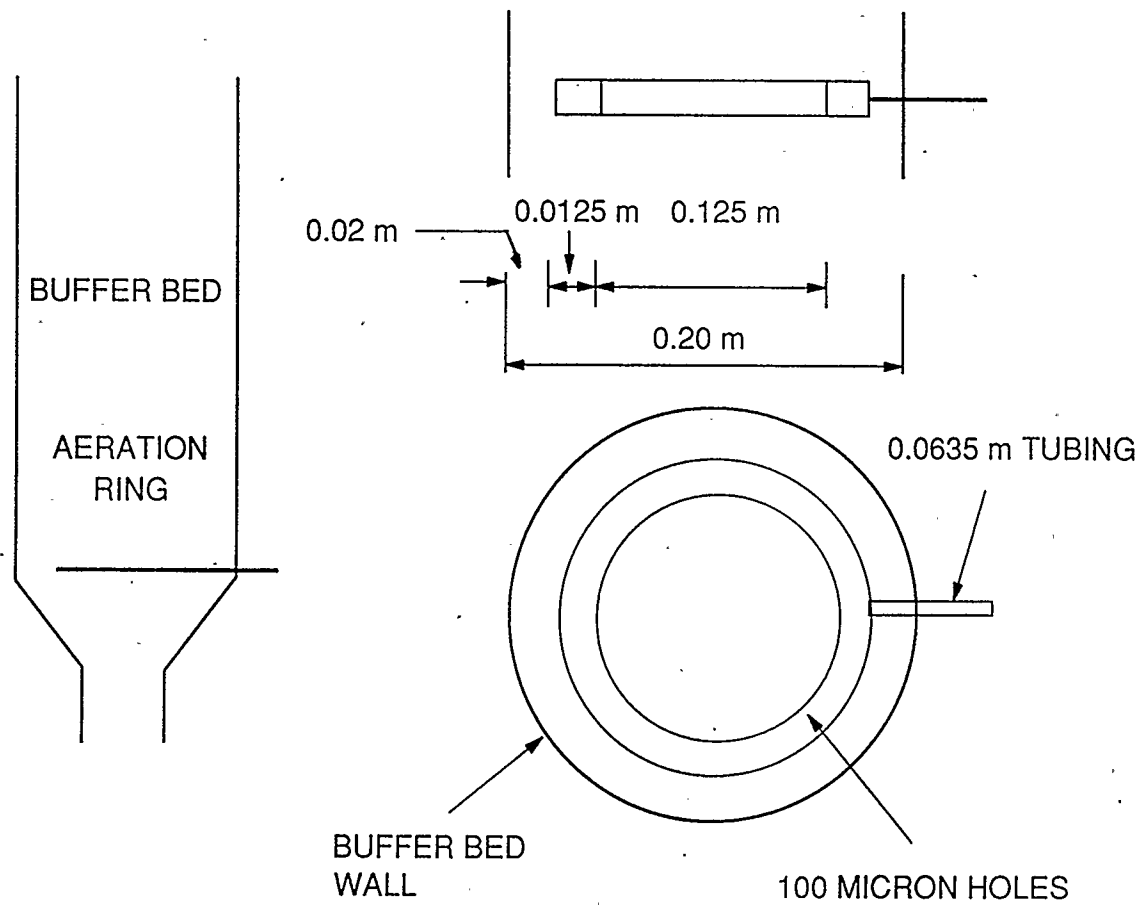
FIGURE 2.6 - AERATION RING CONFIGURATION

20

BUFFER BED

0.0381 m BALL VALVE

INLET FOR
SECONDARY AIR

0.0168 m

0.0232 m

0.04 m

0.0699 m

45 DEGREES

0.04 m

0.19 m

TO RISER

0.10 m
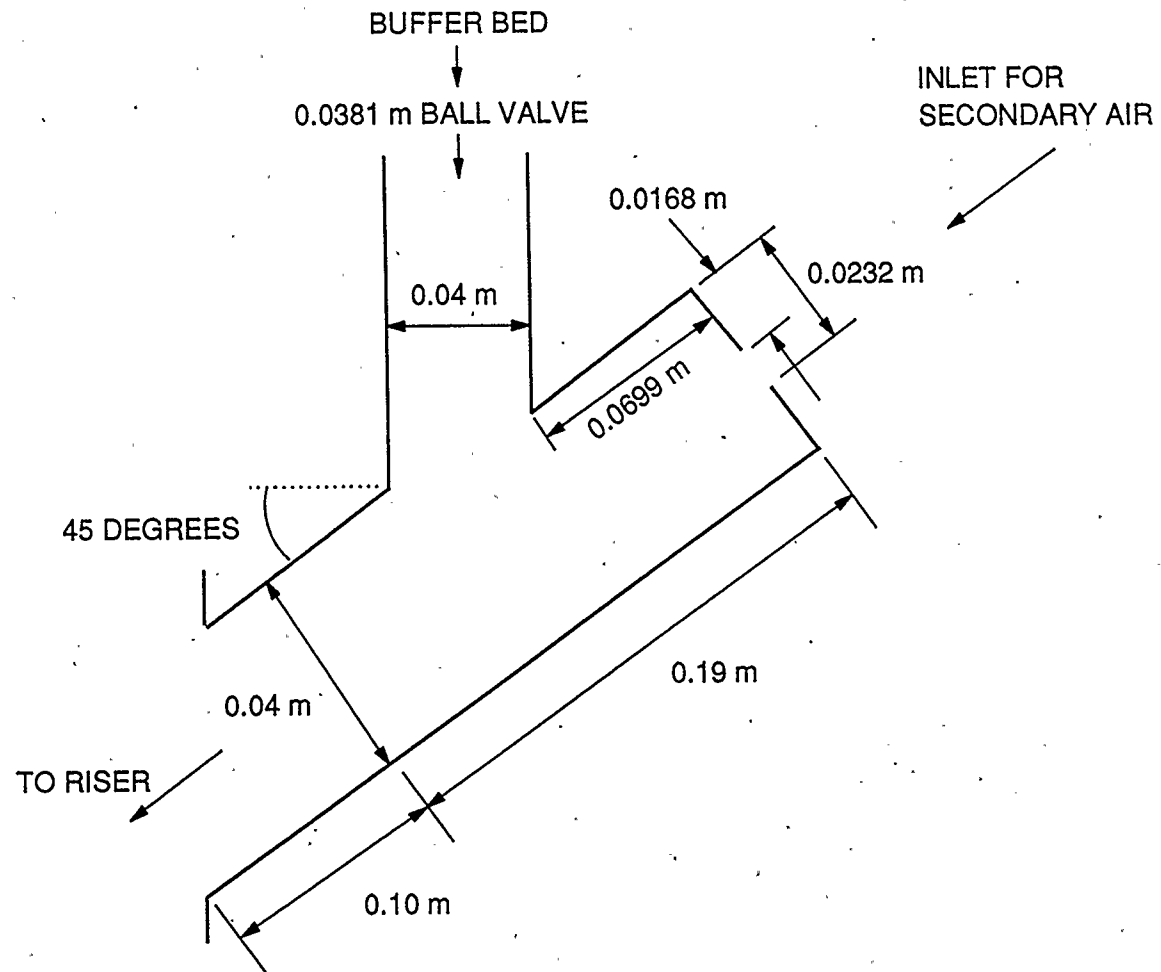
FIGURE 2.7 - TRANSFER LINE CONFIGURATION

remaining air goes into the solids transfer line connecting the riser and solids recirculation leg.

2.4 SOLIDS IN CFB SYSTEM

Ensuring fast fluidization conditions in the CFB was the main design criterion in determining the type of solids used in the experimental unit. As indicated in Figure 1.2, according to the Geldart (1973) classification of solids, group A and B particles meet the main design criterion. According to Grewal (1991), there is a relative abundance of CFB experimental studies involving group A particles but a lack of studies conducted with group B solids. Therefore, one batch of group B (D_p=174 µm, ρ_s=2500 kg/m^3) and one of group A (D_p=93 µm, ρ_s=2500 kg/m^3) solid particles were chosen. The relevant physical properties of the experimental solids are tabulated in Table 2.1. In the following chapters, the group A particles will be referred to as "sand A" while the group B particles will be referred to as "sand B".

2.5 EXPERIMENTAL PROCEDURE

Before any given experiment was performed, a series of steps was taken to ensure that the experimental CFB unit was operating correctly. To prevent any plugging in the pressure tap openings, which would affect the pressure tap measurements, air was used to "flush" out the openings and the filter paper lining each of the pressure taps was checked and replaced if damaged. The system was first filled with a desired inventory and type of solids. Then, the primary and secondary air rotameters were opened. The

PROPERTY	SAND 'A'	SAND 'B'
Sauter Mean Diameter, D_p, μm	93	174
Particle Density, ρ_s, kg/m^3	2500	2500
Minimum Fluidization Velocity, U_{mf}, m/s	0.0097	0.033
Minimum Fluidization Voidage, ε_{mf}, (-)	0.41	0.41
Terminal Velocity, U_t, m/s	0.55	1.55
Geldart (1973) classification	A	B

TABLE 2.1 - PHYSICAL PROPERTIES OF SOLIDS USED IN
EXPERIMENTS

primary air rotameter settings were adjusted so that the desired primary air flowrate was obtained. Solids flow was initiated by opening the ball valve located at the bottom of the buffer bed. Once the solids appeared to flow in a more or less continuous manner downward into the buffer bed, the flap valve arrangement was used to determine the solids flowrate. A series of measurements were taken to determine the average solids circulation rate in the system. The ball valve was then adjusted accordingly so that the desired solids flowrate was achieved. The secondary air rotameter settings were adjusted during the course of the experiment to ensure a sufficient state of fluidization in the buffer bed and hence, a sufficient movement of solids in the line connecting the recirculation leg to the bottom of the riser. The pressure drop along the riser was determined for each experiment by recording the pressure difference indicated by the bank of Meriam oil-filled manometers. To validate the reproducibility and accuracy of the results, multiple experiments were conducted to test the reproducibility of results and all measured quantities were determined more than once. Visual observations were made during each experiment to help qualitatively understand the phenomena occurring in different parts of the CFB system.

CHAPTER 3
EXPERIMENTAL RESULTS

3.1 VISUAL OBSERVATIONS

Under fast fluidization conditions, visual observations of solid and gas movement in different parts of the experimental CFB unit were made with both sand A and B. However, irregardless of the solid type, in a specific region of the experimental CFB unit, the movement of the solids and gas appeared to be the same. Consequently, the visual observations noted apply to both types of sand used in the experimental studies.

3.1.1 ENTRANCE REGION

In this study, the section of riser located immediately above the distributor plate and extending to the top of the solids re-entry point from the recirculation leg is defined as the entrance region.

Because of the turbulent motion of solids in the riser, observations in the entrance region could only be made at low solids fluxes (typically less than 15 kg/(m^2•s)). At a solids flux less than 5 kg/(m^2•s) and superficial gas velocity of approximately 5 m/s, which corresponded to fast fluidization conditions in the experimental unit, the solid particles seemed to accelerate immediately upon entry from the solids return leg. Closer examination of the region indicated very little downflow of solids along the walls of the riser. An interesting observation was the presence of small clumps of solids around the pores of the sintered plate distributor. The particles seemed to be trapped between the jets of air going through the pores in the distributor. Analysis of the particle size

distribution indicated that the observed effect may be due to a plugged distributor since it was possible for the sand to get stuck in the pores of the sintered metal plate. At a constant mass flux of 5 kg/(m^2•s), increases in superficial gas velocity clearly showed the immediate acceleration of particles upon entry into the riser from the recirculation leg. In addition, the small clumps of particles continued to appear and disappear at random intervals.

At intermediate solid mass fluxes (approximately 10 to 15 kg/(m^2•s)) and a superficial gas velocity around 5 m/s a small buildup of solids developed on the solids re-entry side of the riser. The existence of the clump of solids was attributed to the possibility of the force from the downward flow of solids from the recirculation leg being greater than the force of the upward gas flow in the vicinity of the solids return location. Particles from the solid transfer line seemed to collide into the clump and cause particles to be ejected from the mass of solids. At times, the flow of solids from the transfer line seemed to override the clump of stagnant solids and fall downwards before being accelerated by the upflowing gas. As a result, a recirculation pattern was visible. The presence of the apparently stagnant clump of solids created a maldistribution in the upflow of the gas-solid suspension. Instead of going upwards the solids seemed to move laterally first before being propelled upwards by the fluidizing gas. A small downflow of solids was present along the wall. Because of the predominant upward flow of gas-solid suspension in the entrance region, it was difficult to determine whether the amount of solids falling down the wall varied with increases in solids mass flux. Increases in superficial gas velocity did not break down the clump of solids although it was

significantly smaller. An immense amount of turbulence in the entrance region made visual observation much more difficult at higher superficial gas velocities.

At high solids fluxes (greater than 15 kg/(m^2•s)) observations were extremely difficult because of the turbulent motion of the solids. At times, it seemed that small voids of gas appeared but were quickly encapsulated by an influx of solids. At high solids fluxes, the entrance region consisted primarily of an upward flowing gas-solid suspension. When the superficial gas velocity was increased, there was so much mixing within the entrance region that observations of the flow pattern could not be made.

There is very little information on the entrance region of CFB units in literature. Very few, if any, studies have been conducted around the distributor to see how the region affects the hydrodynamics of the riser. Most studies have concentrated on the lower region of the riser well away from the distributor and solids re-entry point. Studies in the lower region of the riser have shown that radial solid concentration gradients exist. Weinstein et al. (1984) have modelled the gradient as consisting of a lean solids region in the centre of the riser surrounded by a dense and thick annular ring of solids. Yerushalmi et al. (1979) have characterized the gradient using clusters or packets of solids distributed across the cross-section of the riser. The experimental observations seemed to indicate that a combination of the Weinstein et al. (1984) and Yerushalmi et al. (1979) theories can be applied to describe the entrance region. Yang (1988) indicated that when solids are fed into the riser at an angle, countercurrent to the flowing gas, a turbulent refluxing pattern is often created at the entrance region. Visual observations during this experimental work at intermediate solid mass fluxes supported Yang's (1988) observation.

As solid particles falling down the wall approached the distributor, gas would force the particles up the centre of the riser. Many times, the accelerating particles would collide with fresh solids from the recirculation leg and appear to "swirl" back to the wall region. Patience (1990) using a 90 degree tee also noted similar observations. He further noted that increases in solids flowrate caused the particles to penetrate further towards the centre of the riser before being accelerated. In addition, Patience (1990) noted that at certain times the entrance region was completely emptied of solids.

3.1.2 EXIT REGION

For the purposes of this study, the exit region is defined as the section of riser immediately below the outlet at the top of the riser and encompassing the abrupt exit configuration.

As solids and gas reached the exit region, it was evident that the abrupt exit served to separate the gas-solid suspension by deflecting or diverting a portion of the solids back down into the riser. It appeared that the upflowing gas "swept" solids in the centre of the riser out towards the wall region. The solids then proceeded to fall down along the walls of the riser.

At low solid fluxes (around 5 kg/(m^2•s)) and a superficial gas velocity of 5 m/s, impingement of particles at the top of the riser section was not evident. It appeared that the particles that deflected downwards from the abrupt exit were "scooped" back up with the upflowing gas. Increases in superficial gas velocity at a constant solids flux revealed progressively smaller amounts of solids refluxing down the sides of the riser.

Similar to the entrance region, the turbulent motion of the solids made it very difficult to ascertain the flow pattern at intermediate and high solids mass fluxes.

Because the abrupt exit was not made from transparent plexiglass, it was not possible to determine whether there was actually a buildup of particles at the top of the abrupt exit. The existence of a stagnant zone of particles would not only dampen the effect of the abrupt exit configuration by reducing the amount of solids reflected back down into the riser but if thick enough, could act like a packed bed and create problems such as temperature nonuniformity and sintering of catalyst (if the solids were used as a catalyst).

As shown by Brereton (1987) an abrupt exit can create a significant increase in suspension density not only in the vicinity of the exit but extend throughout the column and hence, can affect the hydrodynamics of the entire riser. In systems where the extent of reaction depends upon the solids concentration, conversion can be increased because of the increased solids holdup. Another consequence of an abrupt exit is the increase in the residence time of the solids in the riser. With an abrupt exit, solid particles are separated from the gas by inertia when they hit the top of the exit and fall back down along the walls. Instead of going through the riser in one pass, the solids may circulate within the riser many times before going into the recirculation leg, thus increasing the amount of solids backmixing. Solids residence time distribution tests on CFB units with abrupt exits showed that a bimodal solids residence time distribution curve exists (Ambler et al., 1990). According to Ambler et al. (1990), a bimodal residence time distribution curve indicates two flow phenomena occurring in the riser. The first peak corresponds

to the fraction of tracer which goes rapidly through the riser while the second peak, representing the bulk of the tracer, is delayed by a certain extent due to extensive backmixing within the riser. Yong et al. (1988) have determined axial voidage distributions in fast fluidized beds with different exit structures. From the experimental studies, they developed an empirical correlation to predict the fraction of solids that is reflected back down into the riser because of an abrupt exit.

3.1.3 RISER

The flow pattern of the gas-solid mixture within the central portion of the riser was difficult to characterize. Except for the entrance region of the riser a definite downflow of solids along the wall was present at all values of solid mass fluxes and superficial gas velocities examined in the study. The downflow of solids was not constant but appeared to fall down in sheets. At times an immense amount of solids fell down while at other times there did not seem to be any appreciable downward flow. Except for the lowest quarter section of the riser, the downflow of solids was periodically disrupted by small packets of gas moving into the wall region and removing solids by pushing them towards the centre. The solids that were lost to the gas packet was quickly replenished by the solids falling down in the wall region. At the bottom quarter of the riser, the fluidizing gas moved predominantly upwards in almost one continuous phase at high gas velocities whereas a downward moving film at the wall was noted forming with reductions in gas velocity.

At high gas velocities, the upward movement of the fluidizing gas combined with

the accelerating solids from the recirculation leg was such that the large majority of the solids that would have moved down along the wall were captured by the upflowing suspension before the downward falling solids had a chance to reach the bottom of the riser. With reductions in superficial gas velocity, the portion of solids reaching the bottom of the riser before being captured in the upflowing suspension increased considerably. A dense gas-solid suspension was apparent at the bottom of the riser. Although quantitative analysis was not conducted, the experiments seem to show that the apparent dense phase at the bottom of the riser was not an actual deposition of solids as in a conventional bubbling fluidized bed but merely a consequence of the interaction between the upflowing accelerating suspension and downflowing solids. Thus the greater the degree of interaction between the upward and downward flowing phases the greater the apparent densification at the bottom of the riser.

In the middle section of the riser the solids seem to form a continuous interconnected phase with the gas. It appeared that although some streaks of solids were seen to move up with the fluidizing air in the centre of the riser, there was predominantly more gas than solids in the region. The true nature of the flow pattern was masked by the downflowing film of solids along the wall.

The upper section of the riser, just below the abrupt exit configuration also exhibited a densification of solids. The increase in solids concentration was clearly visible and was attributed to the effect of the abrupt exit, as described earlier.

The majority of research on CFBs have concentrated on the riser section of the system. Many workers have used devices such as tracers, fibre optics, photography,

capacitance probes to try and reveal the true nature of the flow pattern within the riser (Bader et al., 1988; Kojima et al., 1989; Arena et al., 1990; Brereton, 1987 and Hartge et al., 1986). From the experimental studies, two general schools of thought about the internal flow structure inside CFB risers have evolved. As previously mentioned, some workers believe that particles are agglomerated into clusters or packets of solids in a continuum of dilute particles while others believe in a core/annular flow structure. The core is essentially a dilute upward flowing gas-solid suspension while the annular region consists of a film of falling solids. There are also combinations of the two schools of thought. Studies by Patience (1990) and Brereton (1987) indicate the existence of clusters not only in the centre of the riser but also in the wall region. Their studies seem to indicate that the true flow pattern is a combination of the two theories. Based on the two schools of thought, many models have been proposed to describe the hydrodynamic structure with CFB risers. An overview of the models is given in Chapter 4.

3.1.4 BUFFER BED

In general, the solids falling in the buffer bed appeared to flow downwards in relatively straight lines. Voids, clusters or packets of solids and a densification of solids around the wall region was not present. Changes is superficial gas velocity did not affect the flow of solids in the buffer bed. The only difference was the uniform increase in the amount of solids flowing downward at the higher velocities.

As previously mentioned, the solid flowrate in the system was determined by means of a flap valve. Whenever the flap valve was diverted to measure the flowrate,

the change in solids bed height was noted. The observations revealed that there was very little change in the bed height and hence, proved that the diameter of the buffer bed was large enough to prevent an upset in gas and solid flow in the system.

There is a severe lack of information on the standpipe region of CFBs. Generally flow in standpipes is characterized as sliding packed bed in which the particles flow downward cocurrently with the gas (Patience, 1990). Most studies in the literature consider the standpipe in isolation of the other components of the system. A common procedure is to study a standpipe with an orifice at the bottom. Patience (1990) noted that the solids velocity at the buffer bed wall is lower than the solids velocity averaged over the entire cross-sectional area. Without proper calibration, significant errors can occur in the evaluation of the solids flux if based on the solids velocity at the wall. The error is magnified even more when one considers that the solids mass flux is the basis of most correlations pertaining to the hydrodynamics of a CFB system.

3.2 AXIAL PRESSURE DISTRIBUTION

By measuring the pressure drop using Meriam oil-filled manometers the pressure profile along the riser was determined. It is assumed that any radial pressure variation is negligible and hence, pressure is constant across the diameter of the riser. Attempts were made to determine axial pressure profiles as a function of both superficial gas velocity and solids mass flux. The experimental studies revealed that although it was very easy to maintain the superficial gas velocity constant while varying solids flowrate, the reverse was not true. The ball valve controlling the solids flowrate was very difficult

to adjust. Fine particles of sand and sometimes relatively large particles of sand caught in the crevices of the ball valve and made opening and closing the valve extremely difficult. Efforts were made to try and maintain a constant solids flux while varying gas velocity but because of difficulty in making small adjustments in the ball valve, the attempts were unsuccessful. As a consequence, the majority of the experimental studies performed used the superficial gas velocity as the main independent variable. Table 3.1 tabulates the superficial gas velocity, volumetric air flowrate, solids mass flux and sand type for each experiment conducted. From the slope of the experimentally determined axial pressure profiles, the pressure gradient was calculated at any axial location and used in the calculation of the axial apparent suspension density and the axial apparent voidage profiles. The suspension density and voidage profiles are called "apparent" and not "average" because they also include acceleration and friction effects. Both the suspension density and the voidage profile provide a picture of how the solids and gases are distributed along the riser and hence can help in understanding the hydrodynamics of CFB risers.

The apparent suspension density, ρ_{susp}, is related to the axial pressure gradient by

$$\rho_{susp}=-\frac{1}{g}\frac{dP}{dx}$$ 3.1

Once the suspension density is known, the apparent voidage, ε_{app}, can be calculated.

The relation between apparent suspension density and apparent voidage is

TRIAL #	U_0 m/s	Q L/s	G kg/(m^2•s)	SAND TYPE
1A	1.1	0.28	3.2	A
1B	6.6	0.95	26.9	A
1C	5.0	1.31	109.0	A
2A	8.0	2.11	106.0	A
2B	7.7	2.00	74.0	A
3A	2.1	0.56	31.6	A
3B	2.2	0.57	33.2	A
3C	5.5	1.44	46.0	A
3D	8.0	2.06	67.0	A
4A	2.3	0.61	13.4	B
4B	2.4	0.64	10.4	B
5A	5.2	1.37	41.0	B
5B	5.3	1.39	46.3	B
6A	8.0	2.06	57.0	B
6B	8.0	2.09	104.0	B
7A	4.0	1.10	123.0	B
7B	4.3	1.13	69.0	B
8A	7.7	2.03	75.0	B
8B	7.7	2.03	126.0	B

TABLE 3.1 - SUMMARY OF EXPERIMENTS

$$\rho_{susp} = \rho_s (1 - \varepsilon_{app}) + \rho_g (\varepsilon_{app}) \qquad 3.2$$

To obtain an estimate of how much particle acceleration and deceleration (for CFB risers equipped with an abrupt exit) and frictional effects contribute to the total riser pressure drop the methodology proposed by Kato et al. (1986) was used. The total riser pressure drop used in this study is simply the difference in pressure between the uppermost and the lowermost taps.

According to Kato et al. (1986) the total axial pressure drop along a riser, ΔP_t, is comprised of four components: ΔP_a, pressure drop due to acceleration of particles, ΔP_s, pressure drop due to hold-up of particles, ΔP_{fg} and ΔP_{fs}, pressure drops due to frictional effects of gas and solid, respectively.

$$\Delta P_t = \Delta P_a + \Delta P_s + \Delta P_{fs} + \Delta P_{fg} \qquad 3.3$$

ΔP_a can be determined from the change in kinetic energy of the particles as they accelerate from the base of the riser. If it is assumed that the vertical velocity at which the solids enter the riser is approximately zero, then the pressure drop due to solids acceleration is given by .

$$\Delta P_a = \frac{\rho_s (1 - \varepsilon) U_s^2}{2} \qquad 3.4$$

where ε according to methodology proposed by Kato et al. (1986) is the average voidage in the riser.

The average solids velocity after the acceleration region, U_s, can be calculated by

$$U_s = \frac{G}{\rho_s(1-\varepsilon)} \qquad\qquad 3.5$$

where G is the net solids mass flux.

The component of the total riser pressure drop attributed to solids holdup in the riser is calculated from

$$\Delta P_s = \rho_s g(1-\varepsilon)\Delta x \qquad\qquad 3.6$$

The Fanning equation can be used to estimate the contribution of the gas frictional effects on the total riser pressure drop:

$$\Delta P_{fg} = 4 f_g \rho_g \varepsilon \frac{\Delta x}{2D_t}\left(\frac{U_o}{\varepsilon}\right)^2 \qquad\qquad 3.7$$

where f_g is the Fanning friction factor.

For the solid friction component of the total riser pressure drop, the expression is

$$\Delta P_{fs} = 2 f_s \rho_s (1-\varepsilon)\frac{\Delta x}{D_t} U_s^2 \qquad\qquad 3.8$$

where f_s is the solid friction factor.

The solids friction factor can be determined from correlations proposed by Yang (1977) or Capes and Nakamura (1973). Breault and Mathur (1989) have reviewed many of the correlations proposed for estimating the solid friction factor.

Table 3.2 tabulates the contribution of solids acceleration, solids holdup and gas and solid frictional effects on the total riser pressure drop for a representative sample of

TRIAL #	ΔP_t, (Pa)	ΔP_a (%)	ΔP_s (%)	ΔP_{fg} (%)	ΔP_{fs} (%)
1C	3924	1.3	88.7	9.5	0.5
2A	3300	1.8	85.0	11.5	1.7
2B	2943	1.1	88.8	8.4	1.7
3D	1766	2.6	80.4	14.1	2.9
7A	4414	1.3	88.9	9.5	0.3
7B	1962	2.7	80.5	14.3	2.5

TABLE 3.2 - COMPONENTS OF TOTAL RISER PRESSURE DROP

the experiments performed. The results indicate that the pressure drop component due to solids holdup contributes the most to the total riser pressure drop. The acceleration component contribution typically varies from 0 to 3 percent. The result indicates that the net contribution of solids acceleration to the total riser pressure drop is relatively small. The pressure drop due to accelerating solids at the bottom of the riser is cancelled out by the solid deceleration effects at the top of the riser. However, it should be pointed out that the local solids acceleration contribution can be very significant in the lower part of the riser. For example, Weinstein and Li (1989) estimated that as much as 40% of the pressure drop in the lower reactor region can be attributed to particle acceleration. In the experimental work, gas frictional effects contributes between 0 and 3 percent and solid frictional effects account for 3 to 12 percent of the total pressure drop. Based on the results in Table 3.2, it can be concluded that for the operating conditions used in the experimental CFB unit frictional effects are negligible and that particle acceleration and deceleration should be considered locally in the lower and upper regions of the riser, respectively.

Figure 3.1 to 3.5 show typical experimental axial apparent voidage profiles. Based on an error analysis calculation, the maximum error associated with the experimental results is approximately 1%. Figure 3.1 shows the effect of particle diameter on the apparent voidage. The largest differences appear at the base and the top of the riser. The results indicate that the smaller the particle diameter the more dense the gas-solid suspension at the bottom of the riser. As indicated in Table 2.1, the smaller diameter particle is a Geldart group A particle. Such solids can be moved much more readily than
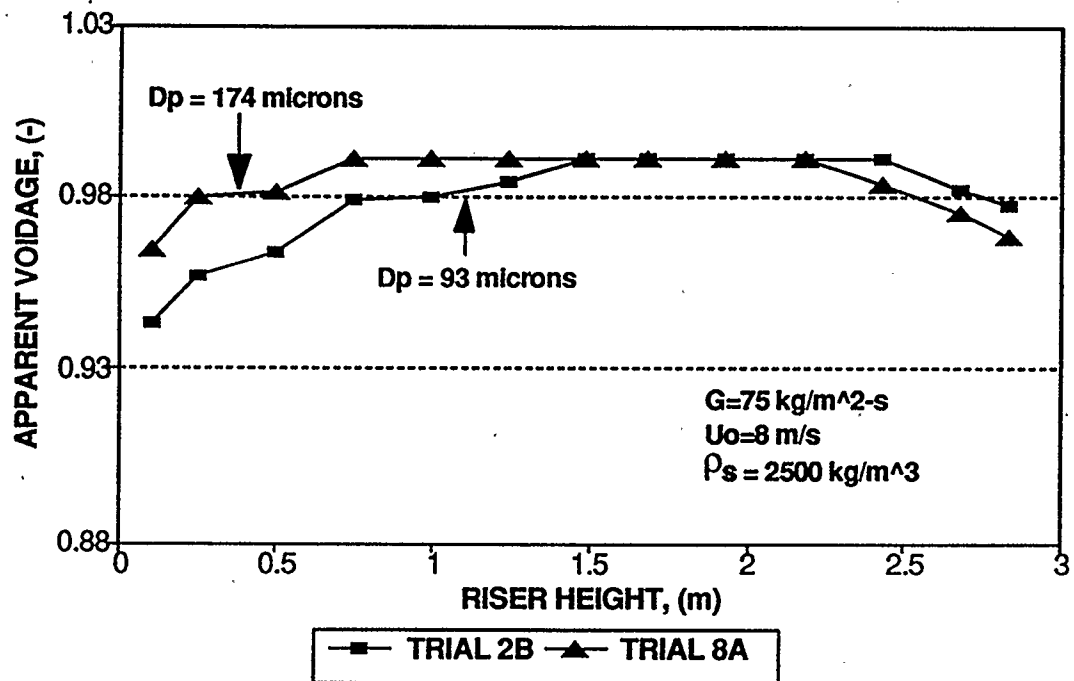
FIGURE 3.1 - EFFECT OF PARTICLE DIAMETER ON AXIAL APPARENT VOIDAGE

the larger diameter particles (group B of the Geldart classification). Perhaps at the bottom of the riser, the gas with a high fluidizing velocity has so much momentum that it preferentially moves the smaller solids out towards the sides of the riser to a greater extent than with the larger solids. Instead of the gas entraining the small solids upwards, it actually channels right through leaving a dense phase in the lower region of the riser. At the top of the riser, the larger the solids the greater the abrupt exit effect. The larger the solid, the greater the momentum and therefore the backmixing of the solids reflected by the top of the abrupt exit.

Figures 3.2 and 3.3 show the effect of solids mass flux on the apparent voidage. The figures generally indicate that the higher the solids mass flux the greater the solids holdup, or equivalently the lower the apparent voidage. For a given superficial gas velocity, increases in solids mass flux lowers the ability of the gas to entrain the solids. If the solids mass flux is continuously increased, a point will be reached where choking occurs. At this point the gas does not have enough momentum to push the solids up the riser and as a result, a dense phase similar to that of a slugging bed forms. It is interesting to note that in Figure 3.3, in the upper region of the riser, the experimental results seem to indicate that the lower the solids mass flux the greater the abrupt exit effect. Besides experimental error, the apparent contradiction with results reported in literature can be explained by discussing the difficulties in obtaining consistent fast fluidization conditions with sand A. When sand A was used, many times the line connecting the top of the riser to the cyclone would become partially plugged. Whenever there was some sort of clog in the line, the flow of solids through the system was

significantly reduced. Visual observations indicated that the solids actually built up in the upper portion of the riser. Consequently, any pressure measurements used to determine the axial apparent voidage would be distorted by the buildup of solids at the top of the riser.

Figures 3.4 and 3.5 shows the effect of inlet superficial gas velocity on the axial apparent voidage profile. The figures indicate that at the bottom portion of the riser, the higher the superficial gas velocity the leaner the gas-solid suspension in the riser. At a constant solids mass flux, increasing the superficial gas velocity increases the carrying capacity of the gas. In Figure 3.4, the difference between the apparent voidage profile in the middle and top of the riser is very small. In Figure 3.5, the difference between the apparent voidage profiles in the middle and upper portion of the riser can be attributed to the periodic constricted flow in the line connecting the top of the riser to the cyclone, as explained earlier. In Trial 1C (Figure 3.5), because of the combination of high solids mass flux and low velocity, the effect of the constricted flow on the apparent voidage is magnified. Figure 3.5 indicates that approximately half of the riser was affected by the reduced solids flow. A complete set of the experimentally determined data can be found in Appendix A.
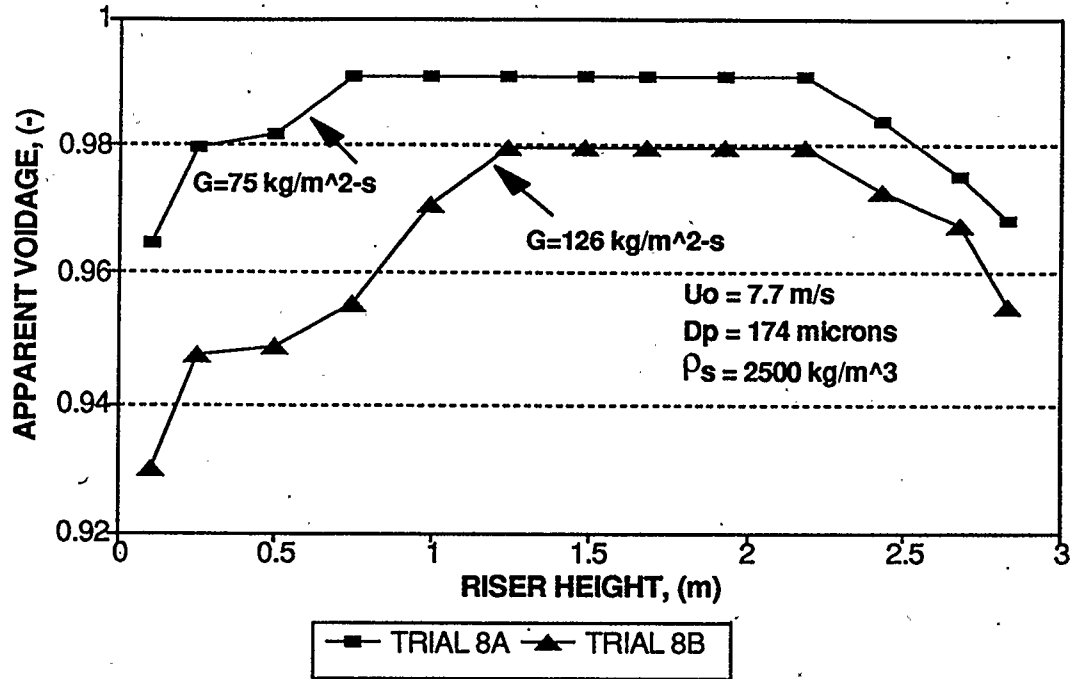
FIGURE 3.2 - EFFECT OF SOLIDS MASS FLUX ON AXIAL APPARENT VOIDAGE-
SAND B
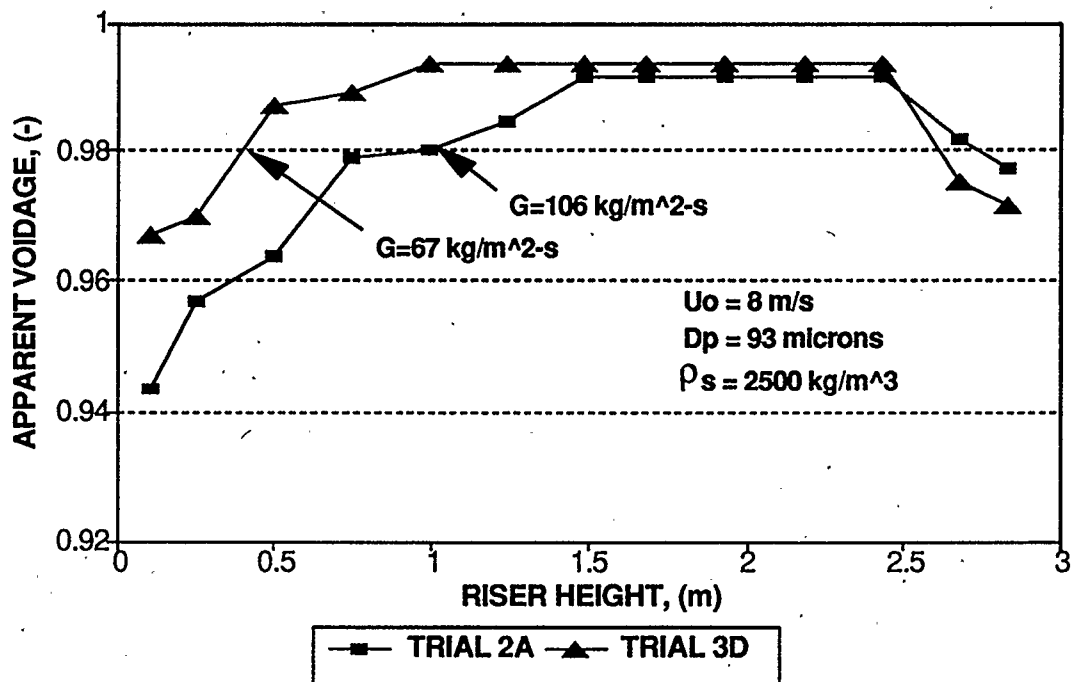
FIGURE 3.3 - EFFECT OF SOLIDS MASS FLUX ON AXIAL APPARENT VOIDAGE-
SAND A
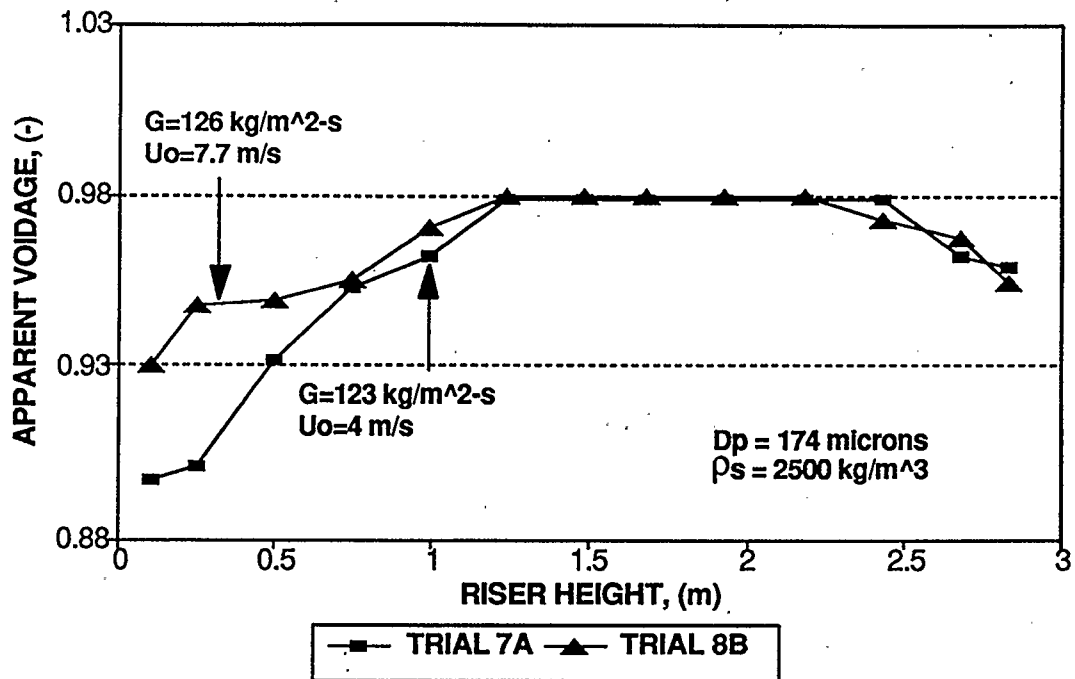
FIGURE 3.4 - EFFECT OF SUPERFICIAL GAS VELOCITY ON AXIAL APPARENT
VOIDAGE - SAND B
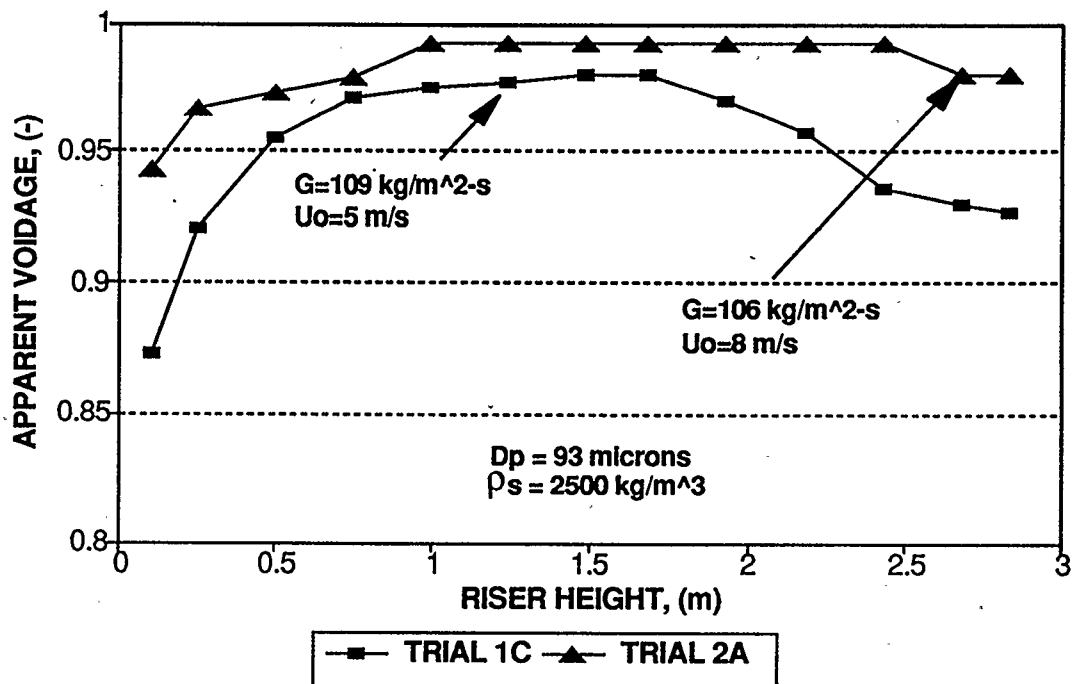
FIGURE 3.5 - EFFECT OF SUPERFICIAL GAS VELOCITY ON AXIAL APPARENT
VOIDAGE - SAND A

CHAPTER 4
HYDRODYNAMIC MODELLING

4.1 LITERATURE REVIEW

Having qualitatively described the flow of gas and solids through the different components making up a CFB system, the next step in the study focused on developing a generalized hydrodynamic model to describe the visual observations. Simply stated, a hydrodynamic model allows the distribution of gas and solids in the CFB to be determined. The distribution provides an idea of the degree of gas-solid interaction in the reactor and allows calculation of the conversion and/or concentration of a species at any point in the system. More importantly, a successful model can be used to predict the effect of parameters such as system geometry, physical properties of gas and solids and operating conditions on system performance.

In general, there is a lack of understanding of CFB systems. The complex hydrodynamics, combined with the many parameters that influence it, makes the development of a CFB hydrodynamic model an imposing task. One way to improve the knowledge of CFB systems and to simplify the hydrodynamic modelling is to break a CFB system into modules. Like a jigsaw puzzle, the complete picture is formed by putting the pieces together. The piece of the puzzle this study looks at is the CFB riser.

Many riser hydrodynamic models have been proposed in literature. Generally, the models follow one of two schools of thought: a dilute upward moving gas-solid suspension surrounded by a denser annulus of downflowing solids (core-annulus models) or packets of upward and downward moving solids occupying a dilute continuum of

discrete particles (cluster models). There are also empirical models based on experimental data, models that treat the riser like the freeboard of a bubbling fluidized bed and models based on phenomenological equations of mass and momentum.

Models based on core-annular flow include those proposed by Nakamura and Capes (1973), Morooka et al. (1980), Kmeic and Leschonski (1987), Berruti and Kalogerakis (1989) and Rhodes (1989). The Nakamura and Capes (1973) model assumes pneumatic transport of gas and solid in the riser and does not consider a transfer of particles from the core to the annulus. The Morooka et al. (1980) model is based on measurements of radial variations in particle velocity and voidage in bubbling fluidized beds. From equations of mass continuity and momentum, Kmeic and Leschonski (1987) varied the degrees of gas-solid interaction and determined that a model based on annular flow best represented their experimental data. Once again, their model was based on pneumatic transport. Given the axial pressure profile, the Berruti and Kalogerakis (1989) core-annular model predicts the internal hydrodynamic structure within the riser under fast fluidization conditions. Furthermore, the model can also predict the net particle radial flux at any given axial location. The Rhodes (1989) model applies to the dilute phase region not only in CFBs but also the riser of vertical pneumatic conveying lines and the freeboard of bubbling fluidized beds. The models assumes a net transfer of solids from the dilute core to the dense annular region at any axial location.

Models based on the cluster or packets phenomena include those by Arastoopour and Gidaspow (1979), Li and Kwauk (1980), Dingrong et al. (1988), Horio et al. (1988), Ishii et al. (1989), Horio et al. (1990) and Zhang et al. (1990). Assuming the existence

of large clusters of particles throughout the bed and characterizing the clusters by equivalent diameters, the model proposed by Arastoopour and Gidaspow (1979) successfully predicts pressure drops in columns under fast fluidization. The Li and Kwauk (1980) and Zhang et al. (1990) models are very similar. Both are based on the basic diffusivity equation and the randomness of particle motion in a fluidized bed. The models propose a "S" shaped longitudinal voidage profile with a dense solid phase at the bottom of the column and a dilute solid phase at the top. The transition between the two phases is indicated by an inflection point in the axial voidage profile. Empirical expressions are given for the point of inflection, and limiting voidages in both the dense and lean solid phases. The Dingrong et al. (1988) model combines the two schools of thought. The model assumes the clusters that exist within the riser occupy positions near the wall region. These workers give expressions for predicting the transfer rates of particles from the core to annulus and from the annulus to the core region. The models by Horio et al. (1988,1990) are extensions of the Capes and Nakamura (1973) model. The main difference lies with the inclusion of cluster phenomena in the models by Horio et al. (1988, 1990). The Ishii et al. (1989) model assumes that the riser consists of clusters that ascend in the core as well as fall along the wall.

Empirical axial voidage correlations which describe the distribution of solids and gases along the riser include those by Kato et al. (1989), Mori et al. (1990) and Choi et al. (1990). The range of applicability of the empirical equations are restricted to CFB units similar to the ones used to develop the correlation.

The models of Bolton and Davidson (1988), Geldart and Rhodes (1986) and Kunii

and Levenspiel (1990) treat CFB risers like the freeboard region of bubbling fluidized bed reactors. Bolton and Davidson (1988) measured a decrease in downward flux of particles in the annulus with riser height in their experimental studies. The effect was modelled in terms of a mass transfer coefficient. Using the entrainment correlations of Wen and Chen (1982), Geldart and Rhodes (1986) described the entrainment of solids at any height in the lean phase of a CFB riser. The dense phase of the CFB was modelled as if it were similar to the dense phase of a bubbling fluidized bed. Kunii and Levenspiel (1990) viewed a CFB riser as having a lower region of constant bulk density and an upper region whose bulk density decreases with height. Taking data from literature, they developed a correlation to describe the decay in density with height. The model was used to describe the effect of various operating parameters on riser performance.

Using a generalization of the Navier-Stokes equation for two fluids, Tsuo and Gidaspow (1990) were able to compute the flow regimes within a CFB. The analysis showed that at high solid concentrations a core-annular flow exists while in lean solid suspensions, clusters predominate the flow.

Table 4.1 lists the empirical axial voidage correlations reported in literature. In an attempt to determine the accuracy of the correlations, they have been used to evaluate the axial voidage profile from experimental data reported in literature. Figure 4.1 compares the axial voidage profile predicted from the correlations with a calculated voidage profile from the experimental data of Patience (1990). The figure indicates that the empirical axial correlations do not provide a good representation of the actual voidage profile. The Kato et al. (1989) correlation could not be used because the operating

TABLE 4.1 EMPIRICAL AXIAL VOIDAGE CORRELATIONS

•Li and Kwauk (1980):

$$\frac{\varepsilon - \varepsilon_a}{\varepsilon^* - \varepsilon} = \exp\left(-\frac{(z - z_i)}{z_0}\right)$$

where z_i=point of inflection in voidage profile

$\varepsilon_a, \varepsilon^* =$ limiting voidages and z_0 is a constant

•Kato et al. (1989):

$$\frac{\varepsilon}{1-\varepsilon} = 0.048 \frac{\exp(z - z_i)}{1 + \exp(z - z_i)} (U_0 - U_t)^{1.35} \left(\frac{G}{\rho_s U_t}\right)^{-1.28} Re_p^{0.23} D_t^{-0.42}$$

where $1.4 < U_0 < 6$ m/s $0.1 < U_t < 0.9$ m/s $30 < G < 130$ kg/(m^2•s)
          $0.45 < Re_p < 10$ $0.04 < D_t < 0.1$ m

•Rhodes and Geldart (1989):

$$U_t \varepsilon^2 - (U_0 + U_t + \frac{E_x}{\rho_s}) \varepsilon + U_0 = 0$$

where $E_x =$ solids entrainment at any axial location x

•Zhang et al. (1990):

for $z < z_i$,

$$\varepsilon = \varepsilon^* - (\frac{\varepsilon^* - \varepsilon_a}{2}) \exp(\frac{z - z_i}{A})$$

for $z > z_i$,

$$\varepsilon = \varepsilon_a + (\frac{\varepsilon^* - \varepsilon_a}{2}) \exp(\frac{z_i - z}{A})$$

where $\varepsilon_a, \varepsilon^*$ are the same as for Li and Kwauk (1980) model and A is a constant

•Kunii and Levenspiel (1990):

$$\varepsilon - \varepsilon^0 = (\varepsilon^{sat} - \varepsilon^0) \exp(-az)$$

where $a, \varepsilon^0, \varepsilon^{sat}$ are constants
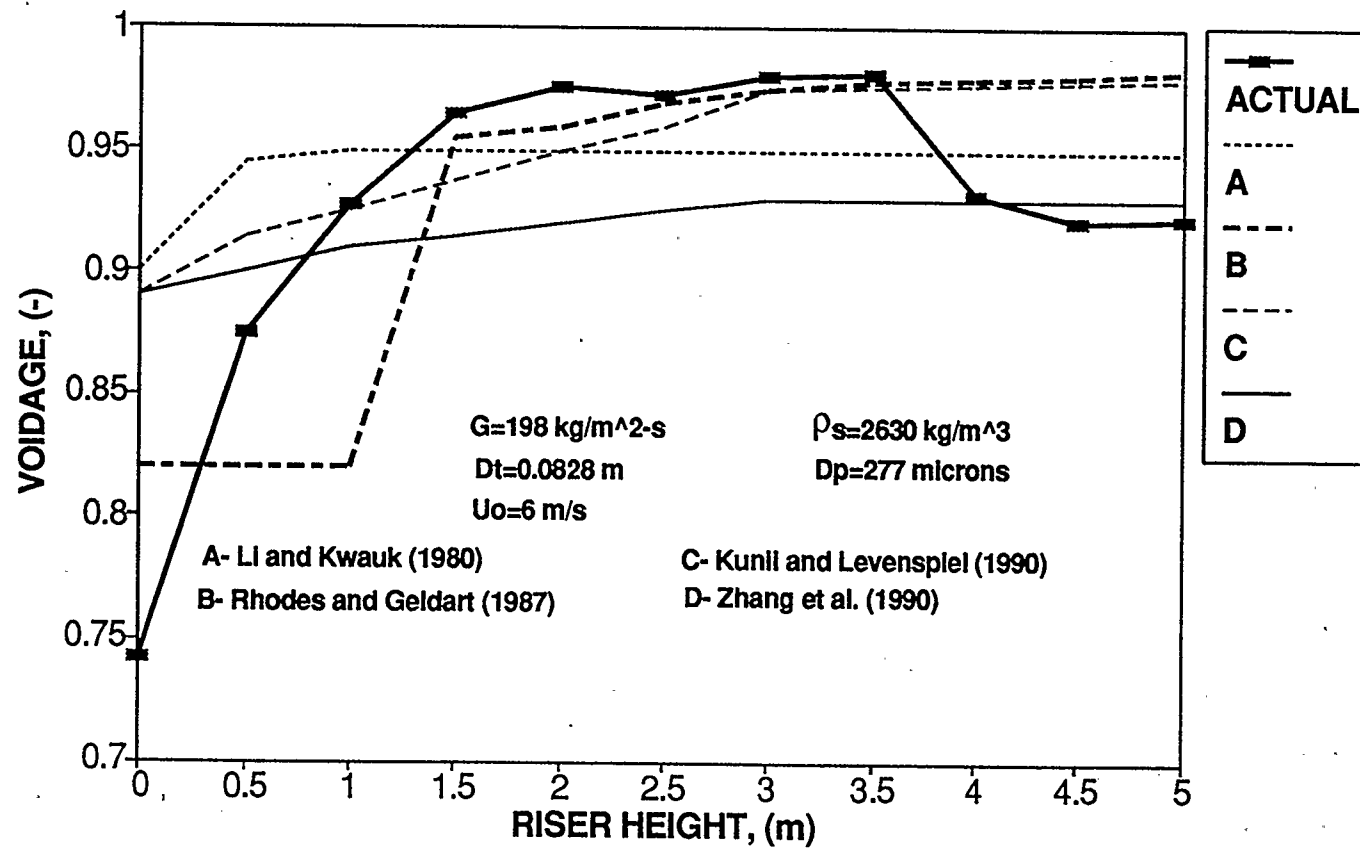
FIGURE 4.1 - COMPARISON OF EMPIRICAL AXIAL VOIDAGE CORRELATIONS
- ACTUAL DATA FROM PATIENCE (1990)

conditions employed by Patience (1990) were outside the range of applicability of the correlation. The Li and Kwauk (1980), Kunii and Levenspiel (1990) and Zhang et al. (1990) correlations severely underestimated the actual voidage in the lower portion of the riser. In the middle portion of the riser, the Li and Kwauk (1980) and Zhang et al. (1990) correlations overpredicted the solids holdup while the Kunii and Levenspiel (1990) correlation approximated the solids holdup reasonably well. None of the available correlations could predict the increase in solids holdup at the top of the riser due to the abrupt exit configuration.

4.2 BASIS FOR PROPOSED MODEL

Because the above solids holdup models could not predict the axial voidage profile with any degree of accuracy, there is a need to develop a generalized model able to describe experimental data from literature. The objective is a predictive model for the axial holdup profile to be used in conjunction with the Berruti and Kalogerakis (1989) model for the evaluation of the internal flow structure characteristics. Such a model would remove the requirement for experimental work and enable the model to be used over a wide range of operating conditions with substantial savings in money and time. Moreover, the model can be used in conjunction with reaction kinetics to simulate the performance of reaction processes such as the combustion of coal or catalytic processes such as oxidation of n-butane to maleic anhydride.

4.2.1 BERRUTI-KALOGERAKIS MODEL

The Berruti and Kalogerakis (1989) model assumes a core-annulus type of flow structure exists within the riser of CFBs. A mass balance across any section of the riser gives

$$E = G + W \qquad 4.1$$

where E is the upward solids mass flux limited to the core region and based on a unit cross sectional area of riser, W is the downward solids mass flux which is limited to the annular region and G is the net solids mass flux.

The upwards solids flux in the core region is given at any axial location by

$$E = U_{sc} (1 - \varepsilon_c) \rho_s \left(\frac{r_c}{R} \right)^2 \qquad 4.2$$

where U_{sc} is the actual solids velocity in the core, ε_c is the core voidage, r_c is the core radius and R is the riser radius. Solving Equation 4.2 with respect to ε_c yields

$$\varepsilon_c = 1 - \frac{E}{U_{sc} \rho_s \left(\frac{r_c}{R} \right)^2} \qquad 4.3$$

If the rising particles in the core do not interfere with each other significantly, then according to Bolton and Davidson (1988) and Yang (1988), the upward solids velocity in the dilute core can be expressed as

$$U_{sc} = U_{gc} - U_t \qquad 4.4$$

where U_{gc} is the interstitial gas velocity in the core and U_t is the single particle terminal velocity based on the Sauter mean diameter.

Assuming that the gas phase travels upward only in the core region, the interstitial gas velocity can be calculated from

$$U_{gc} = \frac{U_o}{\varepsilon_c} \left(\frac{R}{r_c} \right)^2 \qquad 4.5$$

where U_o is the inlet superficial gas velocity.

According to Yang (1988), the solid particles in the dense annular region move downward at a velocity close to the terminal velocity of a single particle and the voidage in the annular region is close to that of a bubbling fluidized bed at minimum fluidization conditions, ε_{mf}. With these assumptions, the downward flux, W, based on unit riser cross sectional area can be calculated from

$$W = \left(1 - \left(\frac{r_c}{R} \right)^2 \right) \rho_s (1 - \varepsilon_{mf}) U_t \qquad 4.6$$

Substitution of Equation 4.1 and Equations 4.4 to 4.6 into Equation 4.3 gives

$$\varepsilon_c = 1 - \frac{G + \left(1 - \left(\frac{r_c}{R} \right)^2 \right) \rho_s (1 - \varepsilon_{mf}) U_t}{\rho_s \left(\frac{r_c}{R} \right)^2 \left(\frac{U_o}{\varepsilon_c} \left(\frac{R}{r_c} \right)^2 - U_t \right)} \qquad 4.7$$

A solids balance within a differential volume along the riser gives

$$\left(\frac{r_c}{R}\right)^2 = \frac{\varepsilon_{avg} - \varepsilon_{mf}}{\varepsilon_c - \varepsilon_{mf}} \qquad 4.8$$

The average riser voidage, ε_{avg} at any given axial location is generally obtained from the pressure drop profile along the riser of a CFB unit. Equations 4.7 and 4.8 are independent and thus can be solved simultaneously to yield the values of r_c and ε_c at any axial location along the riser. Once the core radius and voidage are known, W, E, U_{gc} and U_{sc} can be calculated as a function of riser length.

The net particle radial flux between core and annulus, R_s, at any axial location can be determined from a mass balance around a differential volume along the riser.

$$R_s = -\frac{1}{2\pi r_c}\frac{dQ}{dx} \qquad 4.9$$

where Q is the upward solids mass flowrate and is given as

$$Q = E\pi r_c^2 \qquad 4.10$$

4.3 MODEL FORMULATION

The major assumptions of the proposed model are

1) the riser can be divided into three sections: an acceleration zone, a developed flow zone and a deceleration zone. The deceleration zone is considered only when the riser is equipped with an abrupt exit configuration. In the case of a smooth elbow-type of exit, the developed flow region is considered to extend to the exit.

2) the solids in the dense annular region move downwards at a velocity equal to the terminal velocity of a single particle with a diameter equivalent to the Sauter mean diameter and the voidage at any axial location in the annular region corresponds to that of a bubbling fluidized bed at minimum fluidization (Berruti and Kalogerakis, 1989),

3) the dilute core can be treated as a dilute phase pneumatic transport line with the majority of gas going through in plug flow,

4) the interface between the core and annular regions is considered to be parallel to the riser wall although it is recognized that waves or ripples may be present on the interface surface and

5) clusters may be present in both the annular and core regions but they exist for only short periods of time. In the core, any clusters that form are rapidly dissolved by the upflowing gas. Clusters in the annular region are formed by gas entering the annular region and isolating clumps of solid from the wall region. The isolated clumps are quickly swallowed up by the downflowing solids. Therefore, on a time-averaged scale, any non-uniformity caused by clusters and voids is neglected.

4.3.1 ACCELERATION ZONE

According to Weinstein and Li (1989), in the acceleration zone, the actual density profile required for reactor design can only be determined if the effect of accelerating particles is separated from the apparent density measured from the axial pressure gradient.

Thus, to properly model a CFB riser, it is important to describe the acceleration zone correctly. From experimental observations, in the lower regions of the riser, there is a predominant upflow of gas and solids. Although some solids fall down the sides of the riser, the upward momentum of the gas and accelerating solids causes the majority of the falling solids to go upwards. Assuming a predominantly upward flowing gas-solid suspension exists in the acceleration zone of the riser, a gas and solids momentum balance gives

$$\frac{d}{dx}\left(\rho_s(1-\varepsilon)U_s^2 + \rho_g\varepsilon U_g^2\right) = -\frac{dp}{dx} - (\rho_s(1-\varepsilon) + \rho_g\varepsilon)g \qquad 4.11$$

Neglecting the gas component because $\rho_s >> \rho_g$, and expressing Equation 4.11 in terms of solids mass flux and the pressure gradient in terms of apparent voidage gives

$$1 - \varepsilon_{app} = \frac{G}{\rho_s g}\left(\frac{dU_s}{dx} + \frac{g}{U_s}\right) \qquad 4.12$$

Weinstein and Li (1989) assumed that dU_s/dx is proportional to the velocity difference between solids in the acceleration region and those at the end of the acceleration zone.

$$\frac{dU_s}{dx} = k(U_{s\infty} - U_s) \qquad 4.13$$

Integrating Equation 4.13 from an initial solids velocity of U_{so} at the bottom of the riser to a velocity U_s at a position x in the acceleration zone yields

$$\frac{U_{s\infty}-U_s}{U_{s\infty}-U_{so}} = \exp(-kx) \qquad 4.14$$

Assuming that the initial solids velocity, U_{so} is zero and substitution of Equations 4.13 and 4.14 into 4.12 and noting that

$$\frac{G}{\rho_s U_{s\infty}} = 1 - \varepsilon_\infty \qquad 4.15$$

reduces Equation 4.12 to

$$\frac{1-\varepsilon_{app}}{1-\varepsilon_\infty} = \frac{U_{s\infty}^2 k}{g}\exp(-kx) + \frac{1}{1-\exp(-kx)} \qquad 4.16$$

It should be noted that in some cases the initial solids velocity, U_{so} may not be zero. Weinstein and Li (1989) have solved the above equations for the situation where the initial solids velocity is not zero. In this case Equation 4.12 becomes

$$\frac{1-\varepsilon_{app}}{1-\varepsilon_\infty} = \frac{U_{s\infty}^2 k\Gamma}{g}\exp(-kx) + \frac{1}{1-\Gamma\exp(-kx)} \qquad 4.17$$

where Γ is a constant and is expressed as

$$\Gamma = 1 - \frac{1-\varepsilon_\infty}{1-\varepsilon_0} \qquad 4.18$$

In Equation 4.18, ε_∞ is the voidage at the end of the acceleration zone and ε_0 is the actual voidage at the bottom of the riser. In order to determine the constant Γ, ε_b, the apparent voidage at the bottom of the riser must be known. Once the bottom voidage,

the voidage at the end of the acceleration zone and k are known, they can be substituted into Equation 4.17 to determine Γ. To estimate the voidage at the bottom of the riser the empirical correlations of Kato et al. (1988) and Senior and Brereton (1990) were initially used. The correlations are shown as "Case 1" and "Case 2" in Table 4.2. Difficulties arose with the Kato et al. (1988) correlation because of the limited operating conditions under which it could be applied. Many experimental studies involved operating conditions outside the range of applicability of the correlation. Although the Senior and Brereton (1990) correlation provided a reasonable estimate of the bottom zone voidage, the correlation was not realistic because it suggested that the riser diameter had no effect on the bottom voidage. The studies by Kato et al. (1988) indicated that the diameter has an important effect on the voidage profile. Consequently, modified forms of the Kato et al. (1988) and Senior and Brereton (1990) correlations have been proposed and tested. The modified forms are shown as "Case 3" through "Case 5" in Table 4.2. "Case 3" is a modified form of the Kato et al. (1988) correlation. It is obtained by assuming that the voidage at the bottom is independent of the point of inflection in the axial voidage profile. Many experimental studies do not show a point of inflection, which separates the dense solid phase from the lean solid phase (Arena et al.,1986; Brereton, 1987; Patience, 1990). "Case 4" incorporates the effect of riser diameter into the correlation proposed by Senior and Brereton (1990). "Case 5" is another modified form of the Kato et al. (1988) expression. The term involving the point of inflection is neglected and instead of the left hand side being equal to $\varepsilon_b /(1-\varepsilon_b)$ it is assumed to be simply equal to ε_b. During the riser bottom voidage analysis, the latter was found to give a much better prediction of the

TABLE 4.2 - EMPIRICAL BOTTOM VOIDAGE CORRELATIONS

•CASE 1:

$$\frac{\varepsilon_b}{1-\varepsilon_b}=0.048\frac{\exp(z-z_i)}{1+\exp(z-z_i)}(U_o-U_t)^{1.35}(\frac{G}{\rho_s U_t})^{-1.28}(Re_p)^{0.23}(D_t)^{-0.42}$$

•CASE 2:

$$1-\varepsilon_b=A\left(U_o(\frac{\rho_g^2}{\mu_g(\rho_s-\rho_g)})^{1/3}\right)^B(\frac{G}{\rho_s(U_o-U_t)})^C$$

where A,B,C are constants

•CASE 3:

$$\frac{\varepsilon_b}{1-\varepsilon_b}=A(U_o-U_t)^B(\frac{G}{\rho_s U_t})^C Re_p^D D_t^E$$

where A,B,C,D,E are constants

•CASE 4:

$$1-\varepsilon_b=A\left(U_o(\frac{\rho_g^2}{\mu_g(\rho_s-\rho_g)})^{1/3}\right)^B(\frac{G}{\rho_s(U_o-U_t)})^C D_t^D$$

where A,B,C,D are constants

•CASE 5:

$$\varepsilon_b=A(\frac{G}{\rho_s U_o})^B D_t^C Re_p^D$$

where A,B,C,D are constants

bottom voidage. During the analysis, it was determined that a single expression could not accurately predict the riser bottom voidage. It was evident that Geldart (1973) group A particles behaved differently from Geldart group B particles. In CFB risers involving group B and borderline group A and B particles, an expression illustrated as "Case 5", has been developed to estimate the riser bottom voidage:

$$\varepsilon_b = 0.249 \left(\frac{G}{\rho_s U_o} \right)^{-0.10794} D_t^{-0.23396} Re_p^{0.018583}, \quad R^2 = 0.8690 \qquad 4.19$$

with $20 < G < 198$ kg/(m^2•s), $4 < U_o < 8$ m/s, $90 < D_p < 277$ µm and $Re_p = U_t \rho_g D_p / \mu_g$

The coefficient of multiple determination, R^2, is a statistic which is used to illustrate the adequacy of the fitted regression model (Equation 4.19). The quantity indicates the portion of the regressed data that is explained by the fitted model. A R^2 value of 1 suggests a perfect fit. If Geldart (1973) group A solids are used, then the corresponding expression for estimating the riser bottom voidage is

$$\varepsilon_b = 0.714 \left(\frac{G}{\rho_s U_o} \right)^{-0.02528} D_t^{-0.0794} Re_p^{-0.12016}, \quad R^2 = 0.8551 \qquad 4.19a$$

with $60 < G < 251$ kg/(m^2•s), $4 < U_o < 9.1$ m/s, $50 < D_p < 90$ µm

The source of the data (from this work as well as from data reported in literature) utilized in the development of the above correlations as well as pertinent riser geometry dimensions and gas and solid physical properties are shown in Table 4.3. The calculated

DATA SOURCE	G kg/m^2-s	ρ_s kg/m^3	Uo m/s	Dt m	Dp μm
Patience (1990) ▫	198	2630	6	0.0828	277
	151	2630	6	0.0828	277
	102	2630	6	0.0828	277
	70	2630	6	0.0828	277
	45	2630	6	0.0828	277
	20	2630	6	0.0828	277
this work ✚	109	2500	5	0.05	93
	106	2500	8	0.05	93
	74	2500	8	0.05	93
	67	2500	8	0.05	93
	41	2500	5	0.05	174
	46	2500	5	0.05	174
	104	2500	8	0.05	174
	123	2500	4	0.05	174
	69	2500	4	0.05	174
	75	2500	8	0.05	174
	126	2500	8	0.05	174
Arena et al. (1986) ✳	489	2600	5	0.041	88
	500	2600	7	0.041	88
	390	2600	5	0.041	88
	382	2600	7	0.041	88
Hartge et al. (1986) ▲	65	2500	5	0.4	56
	118	2500	5	0.4	56
Bader et al.(1988) ■	147	1714	9	0.305	76
Arena et al. (1990) ✖	114	2543	5	0.4	90
	215	2543	5	0.4	90
	251	2543	5	0.4	90
Rhodes and Geldart (1986) ⧓	115	1800	4	0.152	64
	102	1800	4	0.152	64
	86	1800	4	0.152	64

TABLE 4.3 - REFERENCES AND EXPERIMENTAL CONDITIONS FOR DATA IN FIGURES 4.2A AND 4.2B

coefficient of multiple variation indicates that over 85% of the riser bottom voidage regression data can be fitted by either Equation 4.19 or 4.19a. Figure 4.2A shows graphically the accuracy of Equation 4.19 while Figure 4.2B shows the accuracy of Equation 4.19a.

The first term on the right hand side of Equation 4.17 represents the contribution of the accelerating particles to the pressure drop in the acceleration zone while the second term represents the contribution of the weight of the solids. The real or average voidage profile in the acceleration zone can be determined by omitting the effect of the accelerating particles and assuming frictional effects to be negligible.

The proportionality constant k can be determined from Equation 4.14 if the length of the acceleration zone is known. The end of the acceleration zone is defined as the point where the axial voidage profile does not change with height. It can also be defined as the point on a pressure drop versus height curve (measured from the solids inlet) where the pressure gradient becomes constant. Assuming that U_s is $0.99U_{s\infty}$ when x is approximately equal to L_{acc}, an expression for k can be derived from Equation 4.14:

$$k = -\ln(\frac{0.01}{L_{acc}})$$ 4.20

In order to solve Equation 4.20 the acceleration zone length must be known. If experimental data is available then the length can easily be determined. However, in a predictive hydrodynamic model, one must be able to evaluate the acceleration zone length without the benefit of experimental data. An analysis was performed to determine whether such a model or correlation exists in literature.
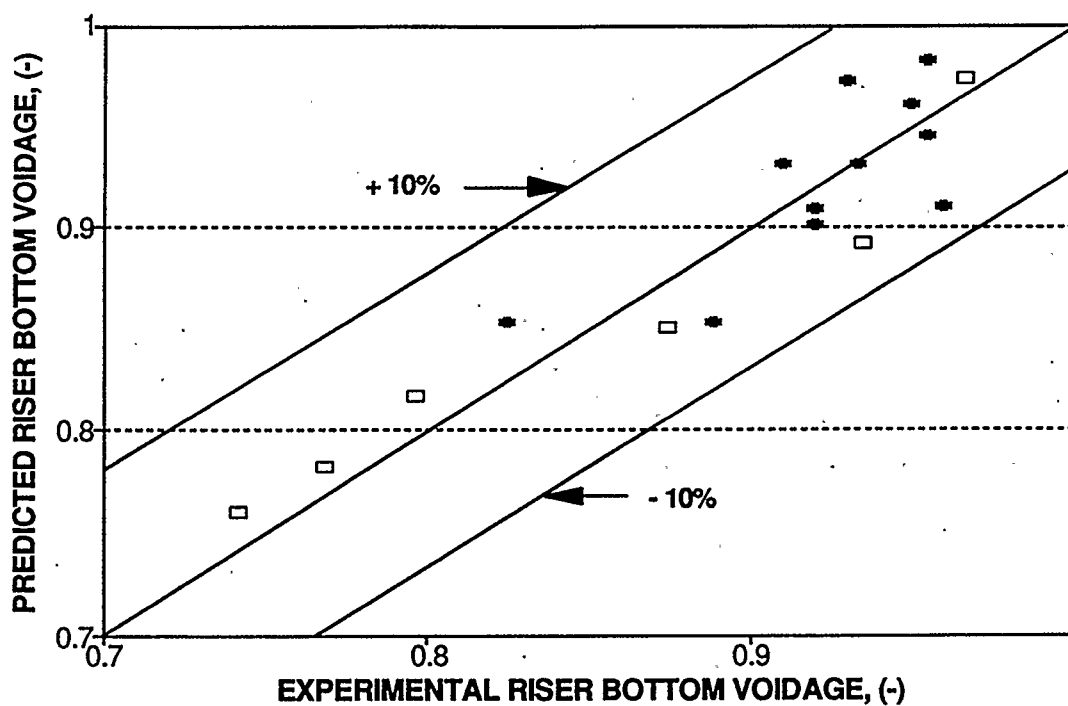
FIGURE 4.2A - COMPARISON OF PREDICTED AND EXPERIMENTAL RISER
BOTTOM VOIDAGE - GELDART GROUP B SOLIDS-EQN. 4.19
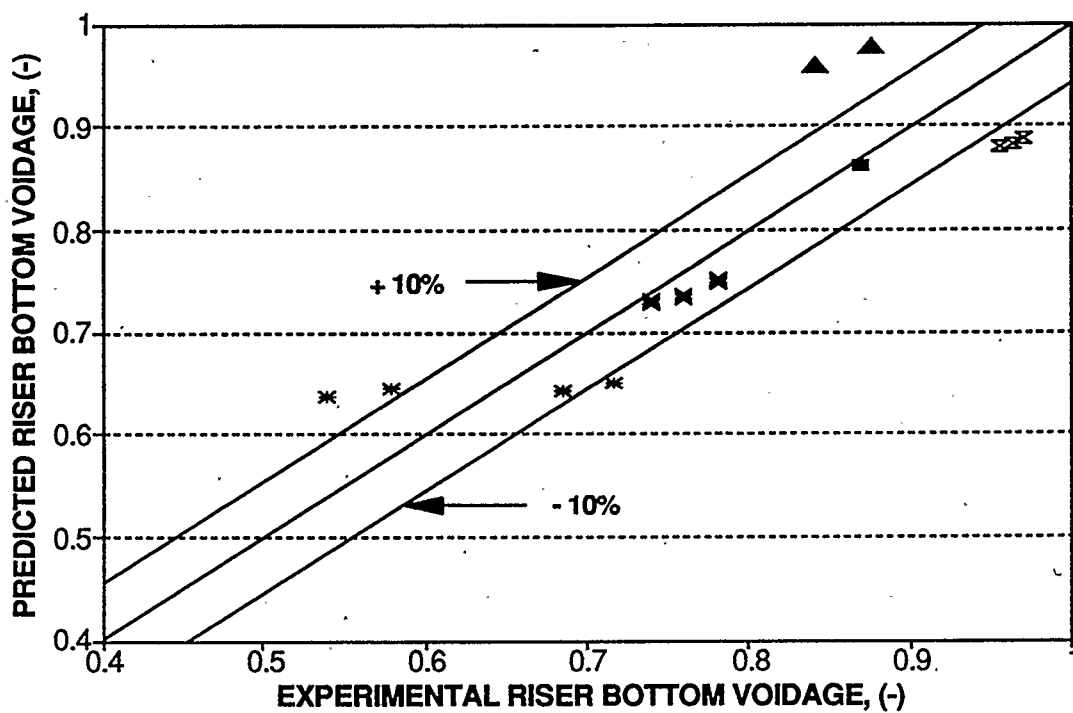
FIGURE 4.2B - COMPARISON OF PREDICTED AND EXPERIMENTAL RISER
BOTTOM VOIDAGE - GELDART GROUP A SOLIDS- EQN. 4.19a

Kalpakov and Donat (1970) studying the use of vertical pipelines for conveying solid particles developed a relationship for the pressure drop in the acceleration zone. They divided the acceleration pressure drop into two terms: one corresponding to the consumption of energy to overcome the inertia of particles fed from the feed device and the other term for the acceleration of particles. In order to use the equation, experimental studies must be performed to determine several fitting parameters. Rose and Duckworth (1969) suggested that the acceleration length is related to the Stokes number, Froude number and the loading rates of solids and fluid. Based on theoretical analysis, the workers developed an empirical acceleration length correlation. The correlation is said to be able to take into account acceleration effects in the transport of solids in gases or fluids. A drawback of the correlation is that gas and frictional effects are not taken into account in the correlation. Work by Yang and Keairns (1976) and Enick et al. (1987) showed that the frictional effects, especially the solids friction factor must be determined correctly to produce accurate results. Jotaki and Tomita (1976) developed a one-dimensional solids flow model for analyzing the acceleration region of pneumatic transport of granular solids in vertical pipes. Based on a solids force balance, they showed that the acceleration pressure drop was dependent on solids to air feed ratio, air velocity, solids free falling velocity and solids friction coefficient. Except for solids to air feed ratio, the acceleration length is also dependent on the same factors.

Yang and Keairns (1976) and Enick et al. (1987) analyzed the length of the acceleration zone based on evaluating an integral composed of a force balance between drag forces, gravity forces and solids friction. The resulting model was found to be very

sensitive to the value used for solids friction factor. Depending on the solids friction factor used, there was a wide range in the accuracy of the predicted results. Because of the difficulty in generating accurate results, Enick et al. (1987), using observed trends reported in literature, developed an empirical formula for predicting the acceleration length in horizontal and vertical pneumatic transport lines.

Attempts were made to try and determine the validity of the different models and correlations available. Some correlations like the Kolpakov and Donat (1970) expression required fitting parameters for different types of solids. Using suggested fitting parameters, the calculated acceleration lengths were significantly different from the experimental results. In many cases, the calculated acceleration lengths were many times smaller than the actual length. As expected, the deviations indicate that the parameters are not suitable for conditions prevalent in fast fluidization. Most models were not suitable for the types of solids and conditions typically found in fast fluidization. The Yang and Keairns (1976) model could not predict the correct acceleration zone length for fine solid particles typically found in CFB units. Furthermore, the voidage profile in the acceleration zone must be known before the acceleration length can be determined. In the proposed model formulation the acceleration length is needed in order to determine the voidage.

It became evident that the existing correlations in literature could not describe the acceleration zone length under conditions of fast fluidization. The development of a new correlation for estimating the acceleration zone length involved an attempt to combine all the observed trends reported in literature into one equation. The empirical equation of

Enick et al. (1987) was used as a starting point since their method of analysis was similar to the one proposed. For vertical pneumatic transport the expression of Enick et al. (1987) is

$$\frac{L_{acc}}{D_t} = 1.84 \times 10^{-5} (\frac{D_t}{D_p})^{-0.173} (\frac{\rho_s}{\rho_g})^{1.24} (1 + \frac{G}{U_o \rho_g})^{0.915} Re^{0.415} \qquad 4.21$$

where $Re = U_o \rho_g D_p / \mu_g$

Figure 4.3 shows the acceleration length predictions of the Enick et al. (1987) correlation for various risers under fast fluidization. Table 4.4 shows the source of the experimental data (from work performed in this study and work reported in literature) used in this investigation. The figure indicates a wide disagreement between predicted and actual results. In almost all instances, the Enick et al. (1987) correlation severely underestimates the acceleration zone length.

Previous analysis of the Kolpakov and Donat (1970) expression suggested that due to dissimilar types and degrees of gas-solids mixing in pneumatic transport and fast fluidization, different constants should apply. Using the experimental data from the studies referenced in Table 4.4, a regression analysis was performed to determine new constants in Equation 4.21. The modified Enick et al. (1987) correlation for fast fluidization conditions, based on the regression analysis, is :

$$(\frac{L_{acc}}{D_t}) = 7.92 \times 10^8 (\frac{D_t}{D_p})^{-0.7642} (\frac{\rho_s}{\rho_g})^{-1.213} (1 + \frac{G}{U_o \rho_g})^{0.2789} (Re)^{-0.9692} \qquad 4.22$$

DATA SOURCE	G kg/m^2-s	ρs kg/m^3	Uo m/s	Dt m	Dp μm
Patience (1990) □	198	2630	6	0.0828	277
	151	2630	6	0.0828	277
	102	2630	6	0.0828	277
	70	2630	6	0.0828	277
	45	2630	6	0.0828	277
	20	2630	6	0.0828	277
this work ✚	106	2500	8	0.05	93
	74	2500	8	0.05	93
	67	2500	8	0.05	93
	104	2500	8	0.05	174
	75	2500	8	0.05	174
	126	2500	8	0.05	174
Arena et al. (1986) ✖	489	2600	5	0.041	88
	500	2600	7	0.041	88
	390	2600	5	0.041	88
	382	2600	7	0.041	88
	180	2600	5	0.041	88
	199	2600	7	0.041	88
Bader et al.(1988) ■	147	1714	9.1	0.305	76
Arena et al.(1990) ✖	215	2543	5	0.4	90
Harge et al.(1986) ▲	65	2500	5	0.4	56

TABLE 4.4 - REFERENCES AND EXPERIMENTAL CONDITIONS
FOR DATA IN FIGURES 4.3 AND 4.4

Equation 4.22 is used to determine the acceleration length in the hydrodynamic model. The results of the analysis are presented in Figure 4.4. The coefficient of multiple variation is 0.9021 indicating that 90% of the regression data is described by Equation 4.22.

Figures 4.5 and 4.6 show how the experimental apparent voidage profile compares with the calculated apparent voidage profile based on the assumption of gas-solid upflow in the acceleration zone. The figures also shows how acceleration effects alter the axial voidage profile in the bottom of the riser. The figures indicate a reasonable agreement between calculated and experimental profiles. More importantly, the results show the correct trends in the voidage profiles. The highest concentration of solids is at the very bottom of the riser and decreases with height. Also, Equations 4.16 or 4.17 provides an easy procedure for evaluating the effect of acceleration on the axial voidage profile in the bottom of the riser.

4.3.2 DEVELOPED FLOW ZONE

The developed flow zone is the region of the riser where the voidage remains relatively constant with height. It is well away from the entrance zone affected by solids acceleration and the exit zone where there may be effects caused by the presence of an abrupt exit. The flow of gas and solids in the region can be characterized as steady state flow. That is, the velocity of the gas and solids are relatively constant with variations in riser height.

The slip factor criterion of Patience et al. (1991) is used to describe the developed
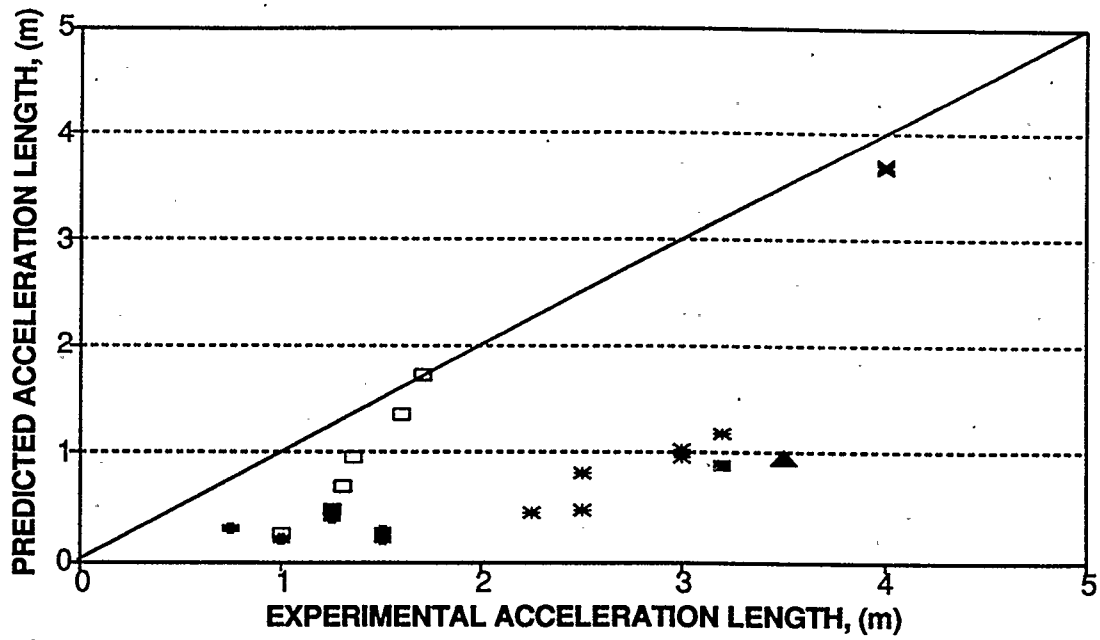
FIGURE 4.3 - COMPARISON OF PREDICTED AND EXPERIMENTAL
ACCELERATION LENGTH - ENICK ET AL. (1987) - EQN. 4.21
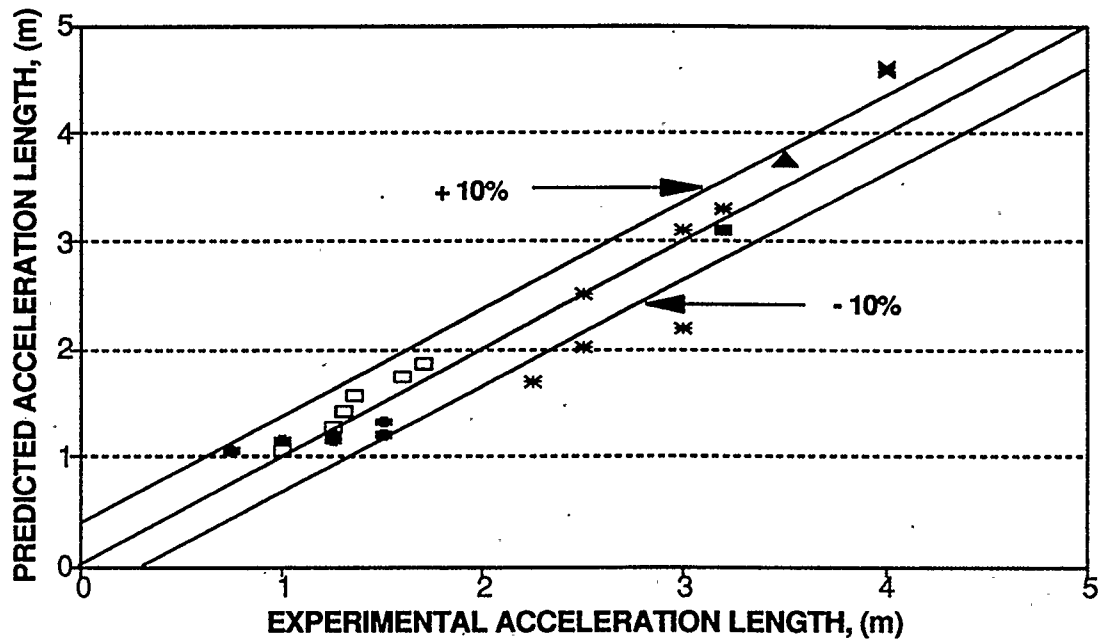
FIGURE 4.4 - COMPARISON OF PREDICTED AND EXPERIMENTAL
ACCELERATION LENGTH - EQN. 4.22
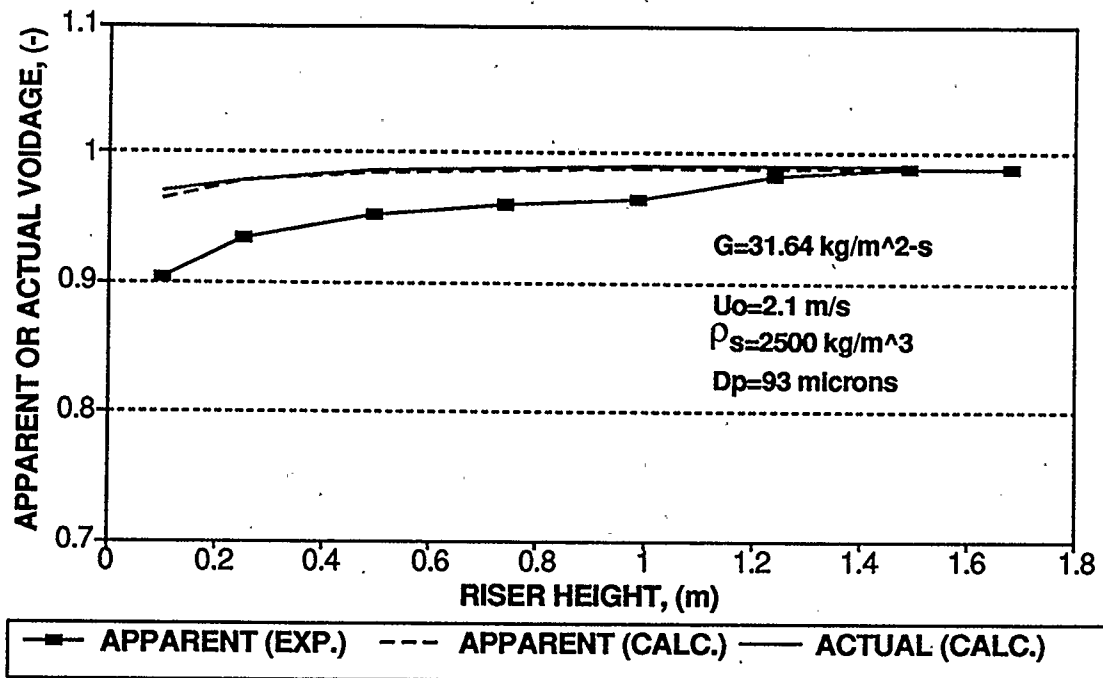
FIGURE 4.5 - EXPERIMENTAL AND CALCULATED APPARENT VOIDAGE-TRIAL 3A
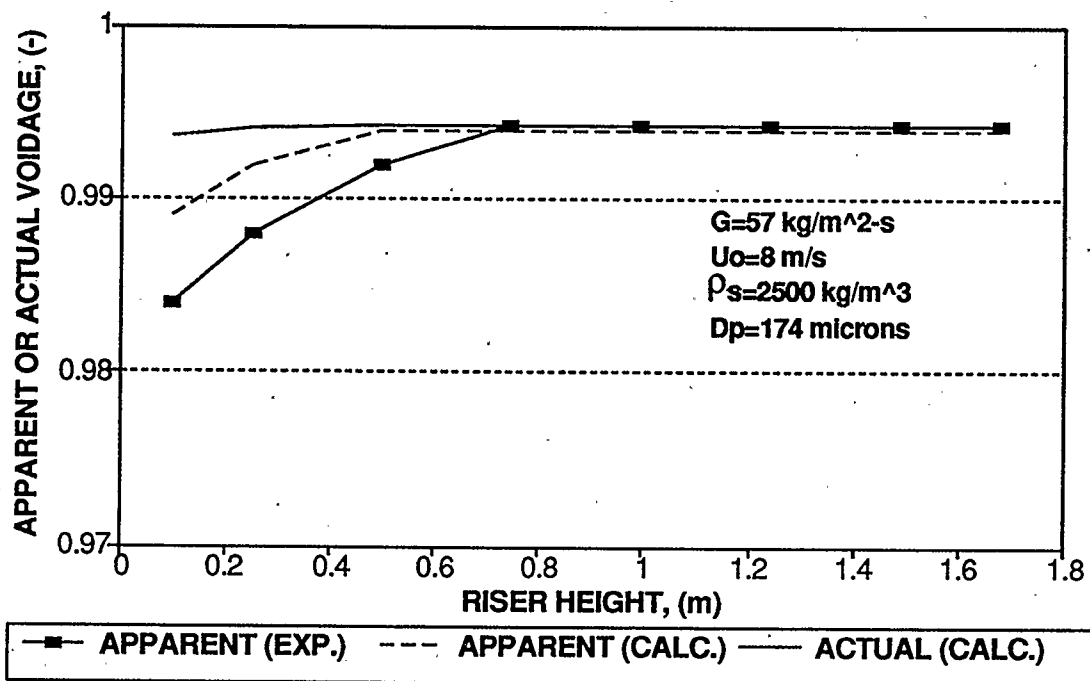
FIGURE 4.6 - EXPERIMENTAL AND CALCULATED APPARENT VOIDAGE-TRIAL 6A

flow zone in the hydrodynamic model. The slip factor criterion states that in the fully developed region of CFB risers the slip factor, which is defined as the ratio of interstitial gas to average solids velocity is approximately equal to two:

$$\varphi = \frac{U_o}{\varepsilon_{avg}} \frac{1}{U_s} = 2$$

4.23

φ is the slip factor while U_o and U_s are the superficial gas and average solids velocity, respectively.

The average solids velocity is calculated based on the net solids circulation rate, G, as:

$$U_s = \frac{G}{\rho_s(1 - \varepsilon_{avg})}$$

4.24

As mentioned before, ε_{avg}, the average voidage can be calculated from the longitudinal riser pressure drop profile. In the developed flow zone, solids acceleration does not contribute to the riser pressure drop and assuming frictional effects are negligible, the experimentally determined pressure gradient can be used in evaluating the average voidage:

$$\varepsilon_{avg} = 1 - \frac{1}{\rho_s g} \frac{dP}{dx}$$

4.25

The slip factor criterion only applies in the developed flow region of a CFB riser. Figures 4.7 and 4.8 compare the experimental apparent slip factor with the calculated actual slip factor in the solids acceleration region of the riser. The apparent slip factor incorporates the effect of accelerating solids while the actual slip is based solely on the hydrostatic head of the solids in the region. The figures indicate that the apparent slip
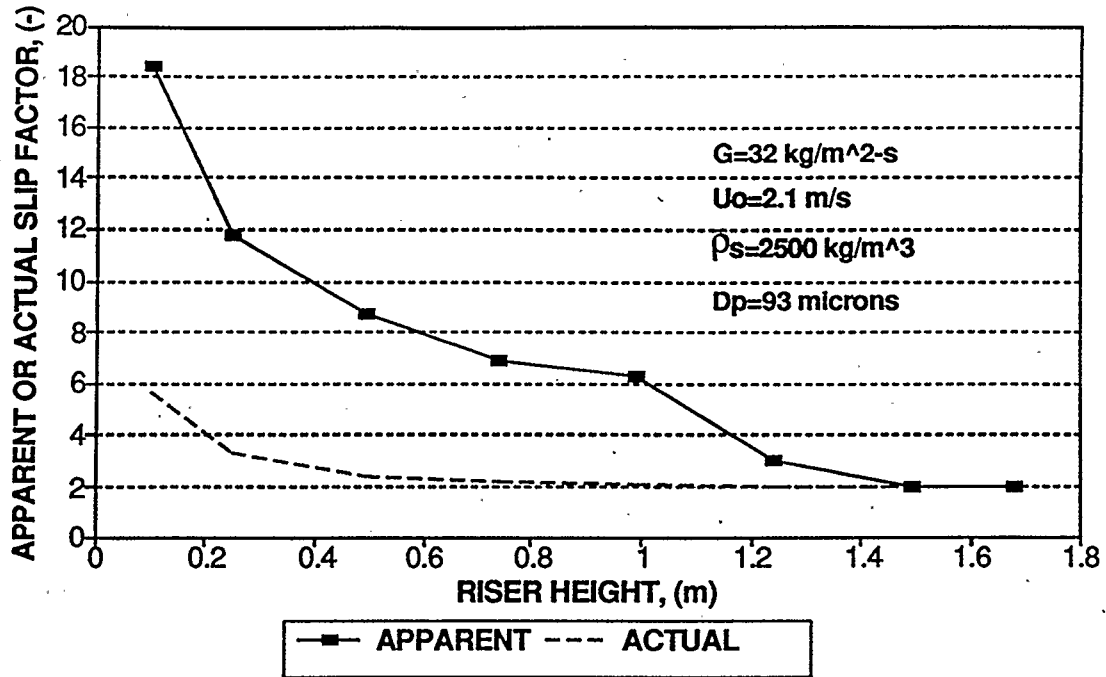
FIGURE 4.7 - APPARENT AND ACTUAL SLIP FACTOR - TRIAL 3A
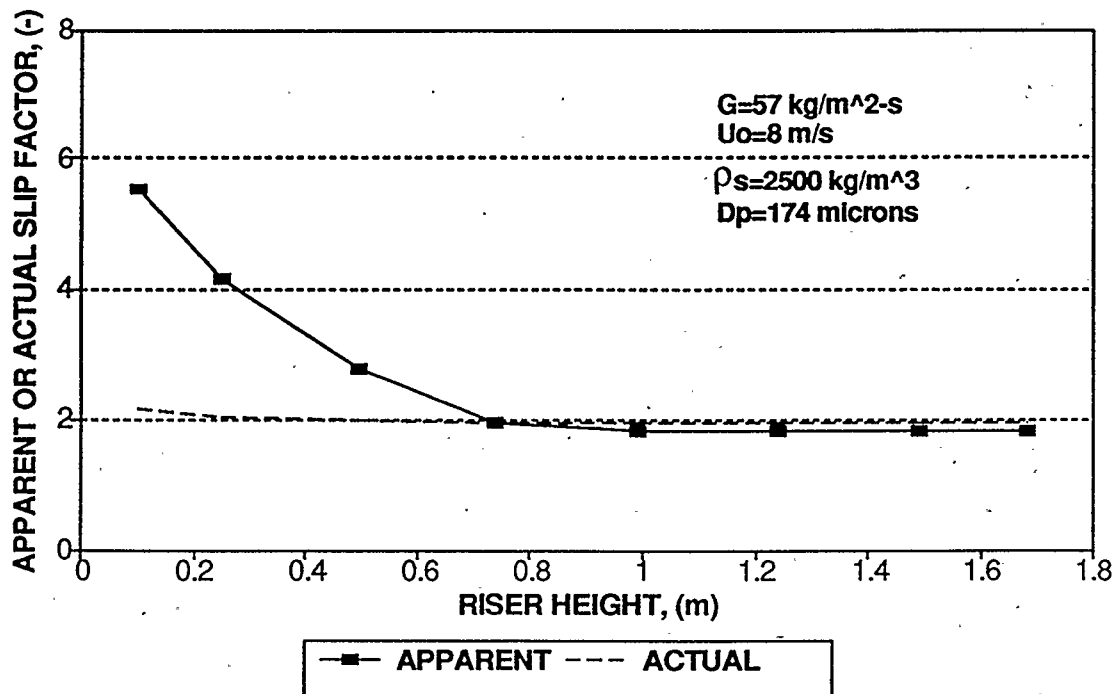
FIGURE 4.8 - APPARENT AND ACTUAL SLIP FACTOR - TRIAL 6A

factor is significantly greater than two in the acceleration region. The slip factor decreases when the solids acceleration contribution is removed and tends to a constant value equal to two. In the developed flow zone, where the solids have stopped accelerating, the apparent and actual slip factors coincide and are approximately equal to two.

The slip factor criterion applies over a wide range of operating conditions, particle characteristics and furthermore, in both large industrial and small experimental units. Matsen (1970) has reported that the slip factor in the risers of industrial scale fluidized catalytic crackers (with diameters up to 1.5 m) is approximately equal to two. Experimental studies by Van Swaaij (1970) in a 0.18 m diameter riser and Patience (1990) in a 0.0825 m diameter unit have validated the slip factor criterion in small experimental units. The experiments performed in this study have also shown that the slip factor is approximately equal to two in the developed flow zone of a small diameter CFB riser. As mentioned by Patience et al. (1991), in general, the values of the slip factor lies between 1.5 and 2.5. However, in some experimental studies, like those of Brereton (1987) the calculated slip factors are much higher than two. The anomaly may be attributed to the secondary air supplied to the column in Brereton's (1987) studies. The introduction of secondary air has a significant impact on the voidage profile. The developed flow zone is never reached due to the extension of the acceleration zone by the secondary air supplied to the column. The right angled abrupt exit in Brereton's experimental unit cannot be used to explain the high slip factors. Studies by Patience (1990) and work in this study with right angled exits resulted in slip factors

approximately equal to two. Other studies have also resulted in slip factors deviating from a value of approximately two in the developed flow zone (Arena 1986). The effect may be attributed to inaccurate solids flowrate measurements. As indicated by Patience et al. (1991) any error in solid flowrate measurement can affect the slip factor significantly. Burkell et al. (1988) has examined various methods for evaluating solids flowrate and has indicated the limitations of the commonly used methods.

Assuming a slip factor of two in the developed flow zone, Equations 4.23 and 4.24 can be combined and solved with respect to ε_{avg} to yield

$$\varepsilon_{avg} = \frac{U_o \rho_s}{2G + U_o \rho_s} \qquad 4.26$$

Equation 4.26 allows the average voidage in the developed flow zone to be determined.

Once the average voidage is known, the internal flow structure can be fully determined. The internal flow structure allows the net solids radial flux to be evaluated, according to the Berruti and Kalogerakis model (1989). The net solids radial flux, R_s, can be written in terms of the core-to-annulus solids interchange coefficient, K_{ca}, and the annulus-to-core solids interchange coefficient, K_{ac}:

$$R_s = K_{ca} \alpha - K_{ac} \rho_b \qquad 4.27$$

where α is the suspension density in the dilute core region and ρ_b is the bulk density of the solids in the annular region. The bulk density corresponds to that of a bubbling fluidized bed at minimum fluidization and can be determined experimentally. The suspension density in the dilute core is given by

$$\alpha = \rho_s (1 - \varepsilon_c) + \rho_g \varepsilon_c \qquad\qquad 4.28$$

The core-to-annulus solids interchange coefficient can be attributed to either the turbulent diffusion of solids from the core to the annulus or to the interactions occurring through solid-solid collisions. The exact mechanism is not known since only a few experimental studies have been conducted to deduce the core to annulus solids transfer mechanism. In the process of evaluating the degree of internal circulation in a fast fluidized bed, Bolton and Davidson (1988) noted that their experimental observations were consistent with the assumption of turbulent mass transfer of particles from the dilute core to the film of solids in the annulus region. Using the results of various workers, they came up with an empirical expression for the deposition of solids from the core to the annulus:

$$K_{ca} = 0.1 \sqrt{\pi} \, U_o \frac{(1 - 2.8 \, Re^{-1/8})}{1 + S/12} \qquad\qquad 4.29$$

where Re, is the Reynolds number and $S = \rho_s D_p^2 U_o / (18 \mu_g U_t)$ is the Stokes number.

Senior and Brereton (1990) assumed that solid-solid collisions accounted for the lateral movement of solids from the core to the annular region in their hydrodynamic model of a CFB coal combustor. There is no mention of the validity of their assumption although from experiments performed on the experimental CFB unit at The University of British Columbia, they deduced that the value of the core-to-annulus solids interchange coefficient ranges from 0.05 to 1.0 m/s. A value of 0.20 m/s provided the best results in their hydrodynamic model. Chandok and Pei (1972) in studying solid dynamics in gas-solid flow and Min (1967) researching the intensity of particle motion in gas-solid suspensions also noted a similar range of K_{ca} values.

Dingrong et al. (1988) with experimental work and data reported in literature proposed an empirical correlation for the movement of solids from the core to the annular region. The empirical correlation is given as

$$K_{ca} = \frac{\mu_g}{D_t \rho_g}(A - B)$$ 4.30

where A is defined by

$$A = 7.67 m^{-0.75} Re^{1.042} Fr^{-0.802} Ar^{-0.416}$$ 4.31

and B by

$$B = 9.18 m^{-1.111} Re^{0.935} Fr^{-0.953} Ar^{-0.57}$$ 4.32

In Equations 4.31 and 4.32, $Fr = U_t/(gD_t)^{0.5}$, is the Froude number, $Ar = D_t^3 \rho_g^2 g/\mu^2$, is the Archimedes number and m is equal to $\rho_g U_o/G$. Again, there is no mention of the postulated mechanism responsible for core to annulus solids transfer.

In the present hydrodynamic model, the Bolton and Davidson (1988) correlation was used to evaluate the solids core-to-annulus interchange coefficient. As will be explained in the next section, a constant value of 0.20 m/s as used by Senior and Brereton (1990) and the value determined from the correlation of Dingrong et al. (1988) could not be used to simulate the solid densification due to an abrupt exit configuration.

The solids annulus-to-core interchange coefficient is based on an analogy with two-phase countercurrent annular flow. Observations by Bader et al. (1988), Rhodes (1989), Senior and Brereton (1990) and Takeuchi and Hirama (1990) suggest that the instabilities in the annulus region are similar to that described in liquid flow literature.

According to Wallis (1969) the interfacial friction factor is related to the dimensionless liquid layer thickness, R_w/D_h by

$$f_i = f_{io}\left(1 + \zeta\frac{R_w}{D_h}\right)$$ 4.33

where f_{io} is the smooth pipe friction factor, R_w is the thickness of the liquid layer in the annular region, D_h is the riser hydraulic diameter which is equal to the riser diameter for a circular pipe and ζ is a constant fitted parameter accounting for the wavy nature of the annular film.

The interfacial friction factor is defined as

$$\tau_i = \frac{1}{2}\rho_{com}U_{com}^2 f_i$$ 4.34

where ρ_{com} is a combined phase core density and U_{com} is a combined phase core velocity.

The combined phase density is given by

$$\rho_{com} = \frac{U_{gc}\varepsilon_c\rho_g + U_{sc}(1-\varepsilon_c)\rho_s}{U_{gc}\varepsilon_c + U_{sc}(1-\varepsilon_c)}$$ 4.35

while the combined phase velocity is defined as

$$U_{com} = (U_{gc}\varepsilon_c + U_{sc}(1-\varepsilon_c))\frac{r_c^2}{R^2}$$ 4.36

Senior and Brereton (1990) assumed that the interfacial shear is proportional to the vertical momentum change of solids removed from the annular region. Following a

similar approach the interfacial shear is related to the solids annulus-to-core transfer coefficient by

$$\tau_i = \phi K_{ac} \rho_b (U_{sc} - U_{sa})$$ 4.37

where ϕ is the proportionality constant relating the interfacial shear to the annulus-to-core solids interchange coefficient and U_{sa} is the solids velocity in the annular region which according to the Berruti and Kalogerakis (1989) model is equal to the single particle terminal velocity. Combining Equations 4.33, 4.34, 4.35, 4.36 into 4.37 results in the following expressing for the solids core-to-annulus interchange coefficient.

$$K_{ac} = \frac{\phi \rho_{com} U_{com}^2 f_{io}}{2 \rho_b (U_{sc} - U_{sa})} \left(1 + \zeta \left(\frac{R - r_c}{D_t} \right) \right)$$ 4.38

The proportionality constant can be evaluated by considering the situation where the wall thickness approaches zero. At such a condition, a certain limiting apparent voidage exists in the riser. According to Senior and Brereton (1990), the limiting apparent voidage or equivalently, the limiting suspension density corresponds to the situation where a negligible thin film of solids exist on the riser wall and where the net transfer of solids is zero. Consequently, setting R_s, the net solids radial flux to zero and substituting Equation 4.38 into Equation 4.27 yields

$$K_{ca} (\rho_g \epsilon_l + \rho_s (1 - \epsilon_l)) = \phi \frac{\rho_{com} U_{com}^2 f_{io}}{2 \rho_b (U_{sc} - U_{sa})}$$ 4.39

where ϵ_l is the limiting core voidage and ρ_{com} and U_{com} are evaluated at the limiting

core voidage. Once the limiting core voidage is known, it can be used to solve for the core radius and voidage and core gas and solids velocity. Consequently, everything except for ϕ is known in Equation 4.39. The limiting voidage can be physically measured by lowering the net solids circulation rate until a negligible thin film of solids is evident on the riser wall (Senior and Brereton, 1990). Senior and Brereton (1990) used a limiting suspension of 2 kg/m^3, which is a typical upper limit found in dilute pneumatic literature in their hydrodynamic model. Attempts were made to determine the limiting suspension density in the experimental CFB unit at the University of Calgary by lowering the solids circulation rate until there was no downflow of solids along the wall. However, due to large fluctuations in the manometer unit, the measured pressure drop along the riser was not very accurate. The limiting suspension density typically varied between 1 and 50 kg/m^3. The limiting suspension value used by Senior and Brereton (1990) was therefore incorporated in the proposed model.

The only unknown parameter remaining in the expression for the solids annulus-to-core interchange coefficient is ζ. The value is expected to vary depending upon the conditions prevalent in the riser. Wallis (1969) and Dukler (1970) have noted that in two-phase countercurrent flow that the wavy nature of the gas-liquid interface is proportional to the gas velocity. The researchers have also noted that the amount of fluid flowing down the sides of a vertical pipe also has a significant effect on the amount of instability on the gas-liquid interface. At low liquid flowrates, there is a tendency for the gas to entrain large amounts of liquid from the wall region. As the liquid flow is increased, the interface flattens out and there is less entrainment of fluid. However, an increase in film

thickness is accompanied by an increases in liquid flowrate. The increased film thickness leads to increased interstitial gas velocity because of the reduced cross-sectional area. Applying similar reasoning to CFB risers, it is expected that high interstitial gas velocities which have a greater ability to entrain solids from the annular region result in a higher annulus-to-core solids interchange coefficient when compared to a situation involving a lower interstitial gas velocity. The amount of solids in the downward flowing film can be expected to affect the interchange of solids from the annulus to the core in the same manner as for two-phase countercurrent gas-liquid annular flow. The less solids along the riser wall, the greater the chance for the gas to penetrate into the annular region and sweep out the solids. As the amount of solids in the annulus region increases the annulus to core interchange coefficient decreases because of the increased difficulty for the gas to penetrate into the annular region. A trial and error approach is generally used to determine the magnitude of ζ because of the many factors that affect it.

4.3.3 ABRUPT EXIT ZONE

The abrupt exit zone in this study is defined as the region of riser that is affected by the presence of an abrupt exit configuration. As mentioned earlier, the effect of an abrupt exit is a densification of solids at the top and sometimes throughout the riser due to the internal recirculation of solids. Only a few experimental studies involving CFB units with abrupt exits have been reported in literature. Using right-angled abrupt exits, Brereton (1987) was the first to notice the increased solids concentration at the top portion of the riser due to the exit. The greater the net solids circulation rate at a

constant inlet superficial gas velocity, the greater the densification at the top of the riser. The higher the net solids circulation rate, the greater the interaction between the solids flowing upwards and the solids reflecting off the abrupt exit. Although there is still a densification of solids in the upper region of the riser with increases in gas velocity at a constant net solids circulation, the effect is not as significant. High gas velocities lead to a leaner gas-solid suspension in the riser. With leaner gas-solid suspensions there is. less chance of solids interaction. The experimental results suggest that an abrupt exit can have important effects on the conversion of a reaction process because of the increased solids residence time due to the reflection of solids off the exit configuration. Patience (1990) and the experimental work in this study (both using right angled abrupt exits) have confirmed the experimental results of Brereton (1987). Solids residence time tests by Patience (1990), Ambler et al. (1990) and by Milne and Berruti (1990) in CFBs with right-angled abrupt exits have resulted in a bimodal solids residence time curve. The first peak corresponds to the fraction of solids which leaves the riser in one pass while the second peak represents the fraction of solids which reflects off the abrupt exit and circulates within the riser for a period of time before exiting. Studying various types of exit configuration Yong et al. (1988) developed an empirical formula for predicting the fraction of solids reflected off a certain type of abrupt exit configuration.

In the present modelling development, the approach taken in evaluating the axial voidage profile and the internal flow structure in the abrupt exit zone is different from the strategy used in both the developed flow zone and the acceleration region. In both the acceleration zone and the developed flow zone of the riser, correlations have been used

to determine the axial voidage first and from that the internal flow structure was then evaluated. Preliminary modelling involved trying to determine an empirical formula to model the apparent voidage in the upper region of the riser. Difficulties arose because of 1) a limited amount of experimental data involving abrupt exits, 2) the inability to match the available data even though the same type of abrupt exit was employed and 3) complications in evaluating the portion of the riser affected by the abrupt exit.

Because of the difficulties encountered, the method used in the abrupt exit region involved solving for the internal flow structure first and then determining the apparent voidage. Equation 4.27 expressing the net solids radial flux as a function of the interchange coefficients is used as the basis for determining the internal flow structure in the abrupt exit region. Q, the upward solids flowrate can be expressed in terms of core radius by combining Equations 4.1 and 4.6 to yield

$$Q = \left(G + (1 - (\frac{r_c}{R})^2) \rho_s (1 - \varepsilon_{mf}) U_t \right) \pi r_c^2 \qquad 4.40$$

The net solids radial flux expression remains the same as before. Substitution of Equation 4.40 into 4.27 gives

$$-\frac{1}{2\pi r_c} \frac{d\left([G + (1 - (\frac{r_c}{R})^2) \rho_s (1 - \varepsilon_{mf}) U_t] \pi r_c^2 \right)}{dx} = K_{ca} \alpha - K_{ac} \rho_b \qquad 4.41$$

As a first approximation, the solids core-to-annulus interchange coefficient, K_{ca} is assumed to be the same as that in the developed flow zone. As mentioned before, there is very little information reported in literature which can be used to infer a specific interchange coefficient in the abrupt exit zone. It should be noted that the formulation

of the model is very flexible so that any expression for K_{ca} can be easily incorporated into the model. Consequently, as more experimental data becomes available, more reliable expressions for K_{ca} can be used in the model. The expression for K_{ac} is the same as for the developed flow and acceleration regions except that the value of ζ is not expected to be the same because the degree of solids interaction is vastly different. The unknowns in Equation 4.41 are $\dot{e}_c$, r_c and ζ. The core voidage can be eliminated by incorporating the relationship between ε_c and r_c from the Berruti and Kalogerakis (1989) model. As a result, knowing ζ, Equation 4.41 can be solved as a boundary value problem to yield the core radius profile in the abrupt exit zone. The boundary condition at the top of the riser is given by the apparent voidage at the top of the riser. Knowing the riser top apparent voidage, the core radius can be determined from the Berruti and Kalogerakis (1989) model. Similarly, knowing the apparent voidage in the developed flow zone, the boundary condition at the bottom of the abrupt exit zone can be determined.

Empirical forms similar to the bottom zone analysis were evaluated and the best equation was used to estimate the riser top voidage. Table 4.5 tabulates the data used to develop the riser top voidage expression. Based on a formulation similar to "Case 4" in Table 4.2, the final form of the equation used to predict the average voidage profile at the top of the riser is:

$$\frac{\varepsilon_t}{1-\varepsilon_t} = 130.934 \left(U_o \left(\frac{\rho_g^2}{\mu_g(\rho_s-\rho_g)} \right)^{1/3} \right)^{-0.8578} \left(\frac{G}{\rho_s(U_o-U_t)} \right)^{-0.2999} A \qquad 4.42$$

where A is defined by

DATA SOURCE	G kg/m^2-s	ρs kg/m^3	Uo m/s	Dt m	Dp m	Z μm
Patience (1990)▫	198	2630	6	0.0828	277	5
	151	2630	6	0.0828	277	5
	102	2630	6	0.0828	277	5.
	70	2630	6	0.0828	277	5
	45	2630	6	0.0828	277	5
	20	2630	6	0.0828	277	5
this work ✚	106	2500	8	0.05	93	3
	74	2500	8	0.05	93	3
	41	2500	5	0.05	174	3
	57	2500	8	0.05	174	3
	104	2500	8	0.05	174	3
Brereton (1987)▲	35	2650	6.1	0.152	148	9.3
	45	2650	6.1	0.152	148	9.3
	59	2650	6.1	0.152	148	9.3
	45	2650	7.1	0.152	148	9.3
	73	2650	7.1	0.152	148	9.3
	66	2650	8.1	0.152	148	9.3
	82	2650	8.1	0.152	148	9.3

TABLE 4.5 - REFERENCES AND EXPERIMENTAL CONDITIONS
FOR DATA IN FIGURE 4.9

$$A = D_t^{-0.53642} Re_p^{-0.10143} Z^{10.3377} \qquad 4.43$$

Figure 4.9 shows how the apparent voidage at the top of the riser predicted by Equation 4.42 compares with experimental data obtained in this work and reported in literature. Although there is a very good fit between the experimental and predicted results (R^2=0.9629), as Table 4.5 indicates there is a lack of data on the apparent voidage at the top of the riser. The experimental studies have all involved CFB riser with small diameters and solids with a narrow range of physical properties. Consequently, it should be mentioned that Equation 4.42 is valid only for conditions similar to the ones outlined in Table 4.5. The reasonable fit provided by the equation suggests that the form can be used to determine the apparent voidage at the top of a CFB riser equipped with a right-angled abrupt exit. However, much more experimental studies with larger diameters, different solids and gas physical properties as well as with different types of exit configurations are required to validate Equation 4.42.

4.4 SOLUTION METHOD

The solution of the model equations presented in the preceding three sections is a three step procedure. First, the internal flow structure and apparent voidage in the abrupt exit zone is determined. Using Equation 4.42, an estimate of the riser top voidage is obtained. The core radius and core voidage corresponding to the riser top voidage is then calculated by simultaneous solution of Equations 4.7 and 4.8. The calculated core radius becomes the boundary conditions at the top of the abrupt exit zone. Using the slip factor criterion of Patience et al. (1991), the average voidage in the developed flow zone
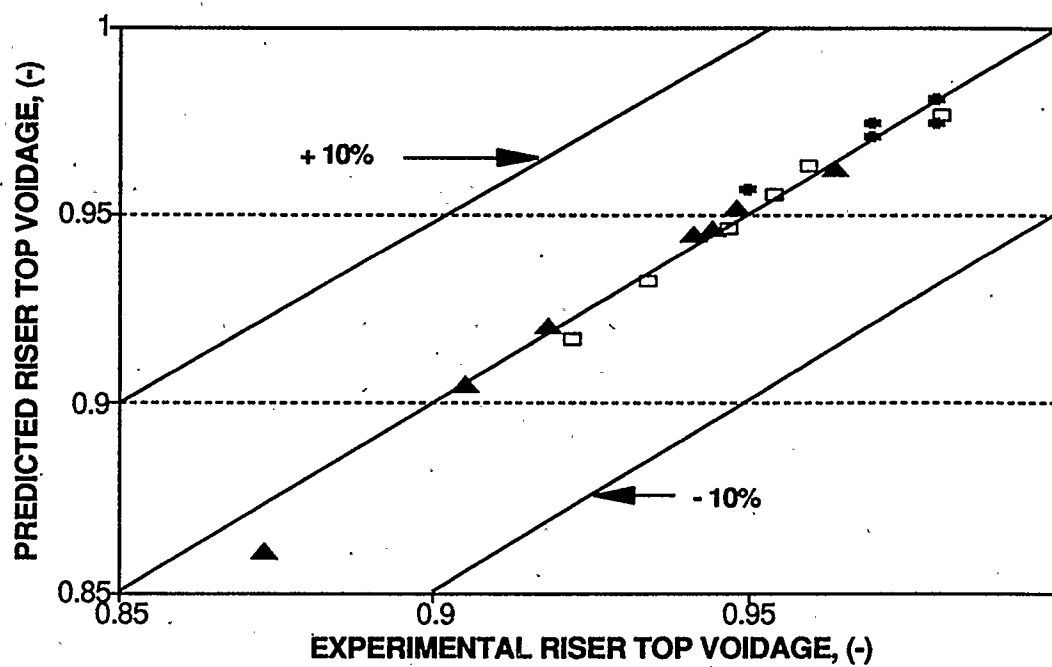
FIGURE 4.9 - COMPARISON OF PREDICTED AND EXPERIMENTAL
RISER TOP VOIDAGE - EQN. 4.42

(since there are no solid acceleration effects and frictional effects are assumed to be negligible) can be calculated. The corresponding core radius becomes the boundary condition at the bottom of the abrupt exit zone. Discretizing Equation 4.41 and starting from the top of riser a modified Euler's algorithm is used to determine the core radius profile in the abrupt exit zone. If the calculated core radius profile does not converge with the core radius in the developed flow zone, the value of ζ is varied until convergence occurs. Once convergence is obtained, internal flow quantities such as core radius and voidage, core gas and solids velocity and solids interchange coefficients can be calculated as a function of axial location. The portion of the riser affected by the abrupt exit configuration is determined from the location where the core radius from the developed flow zone coincides with the core radius from the bottom of the abrupt exit zone. Once the core radius and voidage are known, Equation 4.8 can be used to determine the apparent voidage in the abrupt exit zone. In situations where a CFB unit does not have an abrupt exit, the abrupt exit zone calculation is not required as the average voidage along the riser remains approximately constant throughout the entire fully developed flow region and up to the riser exit. The second step involves calculation of the axial voidage profile and internal flow structure in the developed flow zone. Equation 4.26, developed from the slip factor criterion of Patience et al. (1991) is used to determine the voidage in the developed flow zone. The core radius and voidage and core gas and solids velocity are subsequently calculated from the equations of the Berruti and Kalogerakis (1989) model. The value of ζ determined from the abrupt exit zone calculation is used to calculate the solids annulus-to-core interchange coefficient while the

solids core-to-annulus coefficient is obtained from the Bolton and Davidson (1988) correlation. The third step involves determining the axial apparent voidage profile and the internal flow structure in the acceleration zone. Estimating the length of the acceleration zone and the riser bottom voidage from empirically developed expressions, Equation 4.17 is used to determine the apparent or real voidage in the acceleration zone. Equation 4.7 and 4.8 are then solved simultaneously to determine the core radius, core voidage, core gas velocity and core solids velocity. Although the apparent voidage or equivalently, the net solids radial flux is known in the acceleration zone of the riser, the evaluation of the solids interchange coefficients is made more difficult because the solids core-to-annulus interchange coefficient is not constant. At the bottom of the riser, the greater concentration of solids combined with the momentum of the gas causes more lateral movement of the solids than in the developed flow zone. The calculation of the core-to-annulus interchange coefficient involves evaluation of K_{ac} first and then back calculation of K_{ca}. At the top of the acceleration zone or equivalently, the bottom of the developed flow zone, K_{ca} is known. Using Equation 4.27, an initial value of ζ is assumed and K_{ca} is calculated as a function of riser height. The computed value of K_{ca} at the end of the acceleration zone is compared with the value at the bottom of the developed flow zone and if they are not the same, the value of ζ is varied until convergence is achieved. Once convergence is achieved, Equation 4.38 is used to calculate K_{ac} and Equation 4.27 can be solved to yield K_{ca}.

CHAPTER 5
MODEL VALIDATION AND SIMULATION RESULTS

5.1 MODEL VALIDATION METHODOLOGY

To determine the validity of the proposed model, computer simulations were performed to compare the apparent axial voidage profile and/or internal flow structure characteristics predicted using the model with data obtained in experimental CFB units. Comparisons were also made between the simulated and experimental results to illustrate the ability of the model to predict the effect of operating parameters such as superficial gas velocity, solids mass flux, solids diameter and density and riser geometry. Furthermore, a sensitivity analysis was performed to illustrate the effect of the same operating parameters on riser performance.

5.2 APPARENT VOIDAGE PROFILE

The simulated and experimental apparent axial voidage profiles from the experimental CFB unit at the University of Calgary are shown in Figures 5.1 through 5.7. Both the simulated and experimental axial apparent voidage profiles show the same characteristic shape. At the bottom of the riser there is a gradual decrease in the solids holdup or equivalently, an increase in apparent voidage with increases in riser height. The effect is due to the acceleration of the solids as they enter the riser from the recirculation leg. Once the solids stop accelerating the apparent voidage becomes relatively constant with further increases in riser height. The flow of gas and solids is thought to be hydrodynamically developed once the voidage becomes constant with
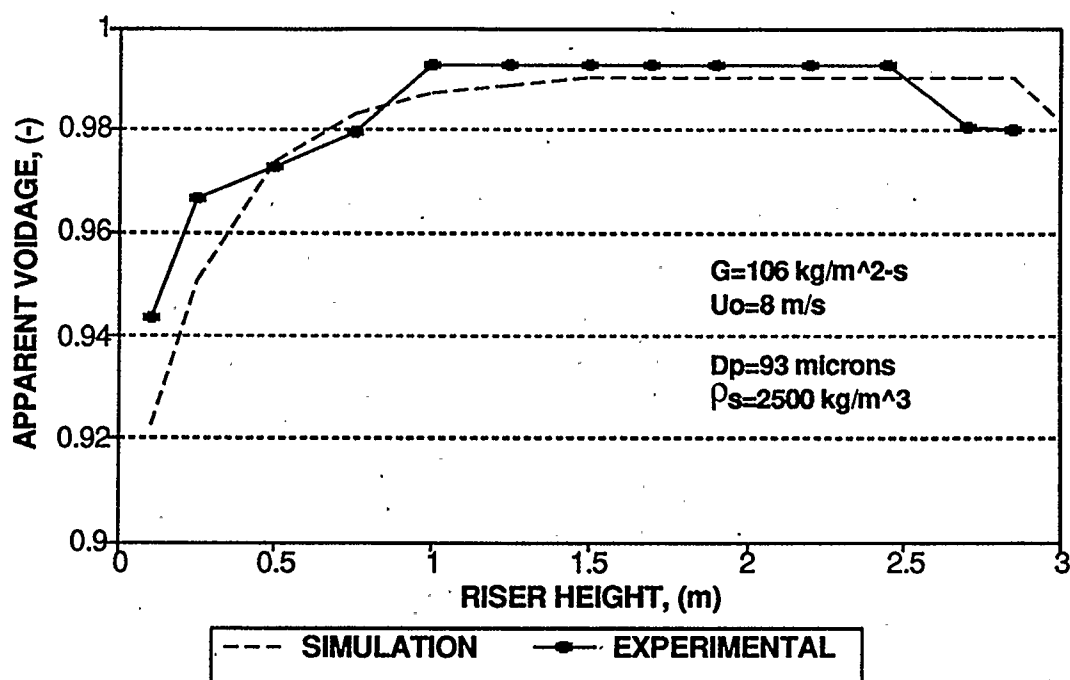
FIGURE 5.1 - COMPARISON OF APPARENT VOIDAGE PROFILE - TRIAL 2A
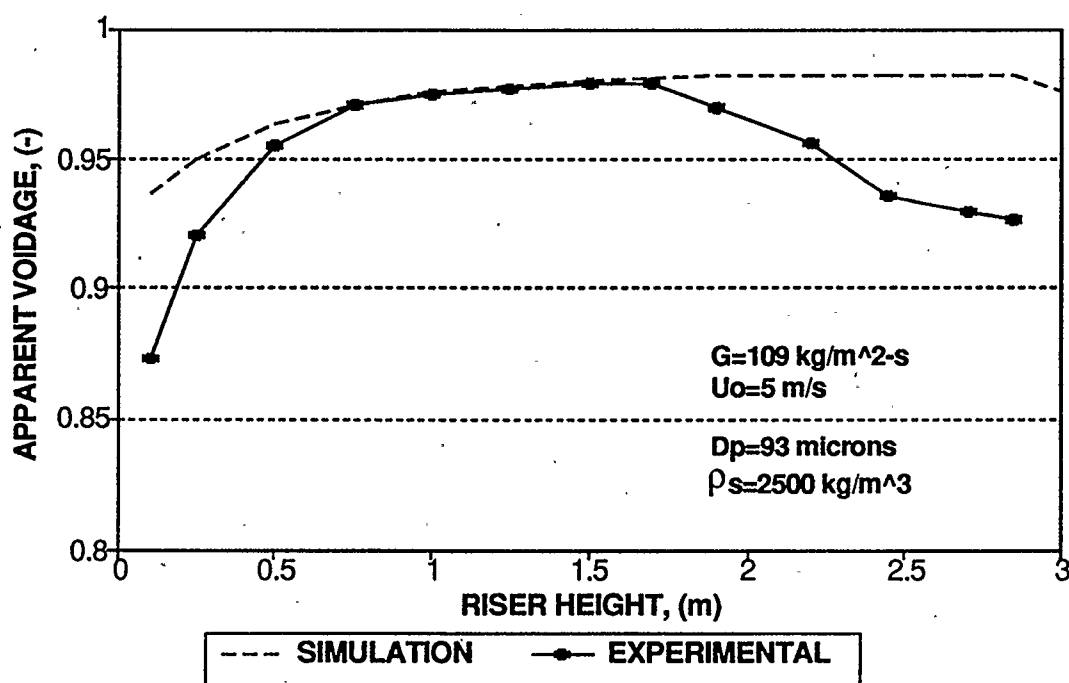
FIGURE 5.2 - COMPARSION OF APPARENT VOIDAGE PROFILE- TRIAL 1C
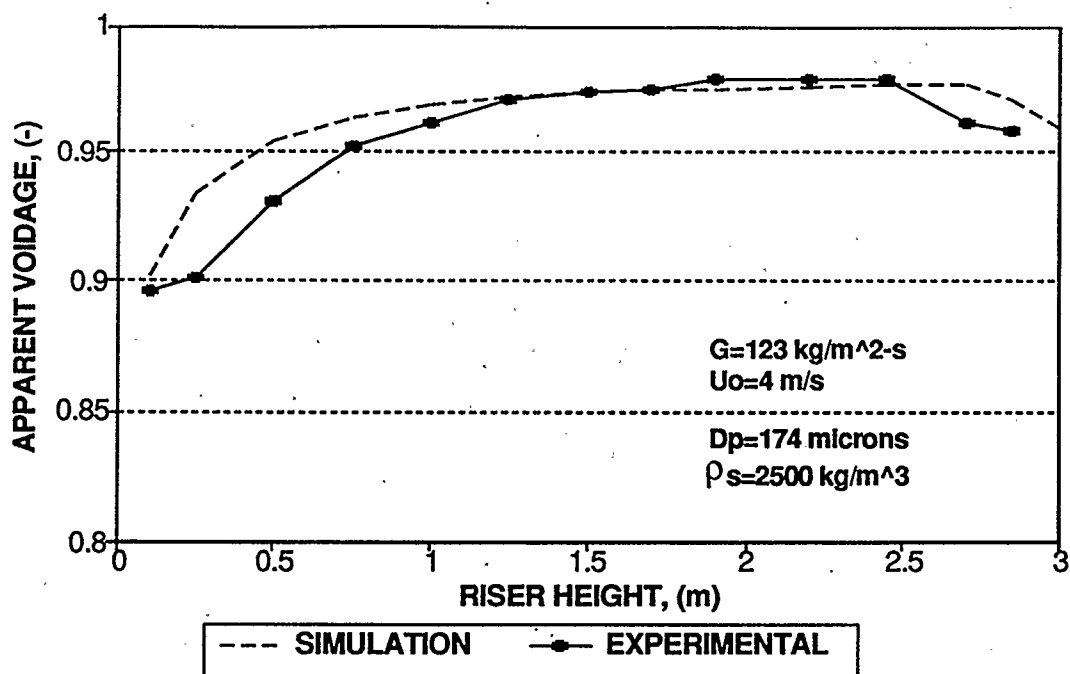
G=123 kg/m^2-s
Uo=4 m/s

Dp=174 microns
ρs=2500 kg/m^3

--- SIMULATION   --•-- EXPERIMENTAL

FIGURE 5.3 - COMPARSION OF APPARENT VOIDAGE PROFILE- TRIAL 7A

G=126 kg/m^2-s
Uo=7.7 m/s

Dp=174 microns
ρs=2500 kg/m^3

--- SIMULATION   --•-- EXPERIMENTAL
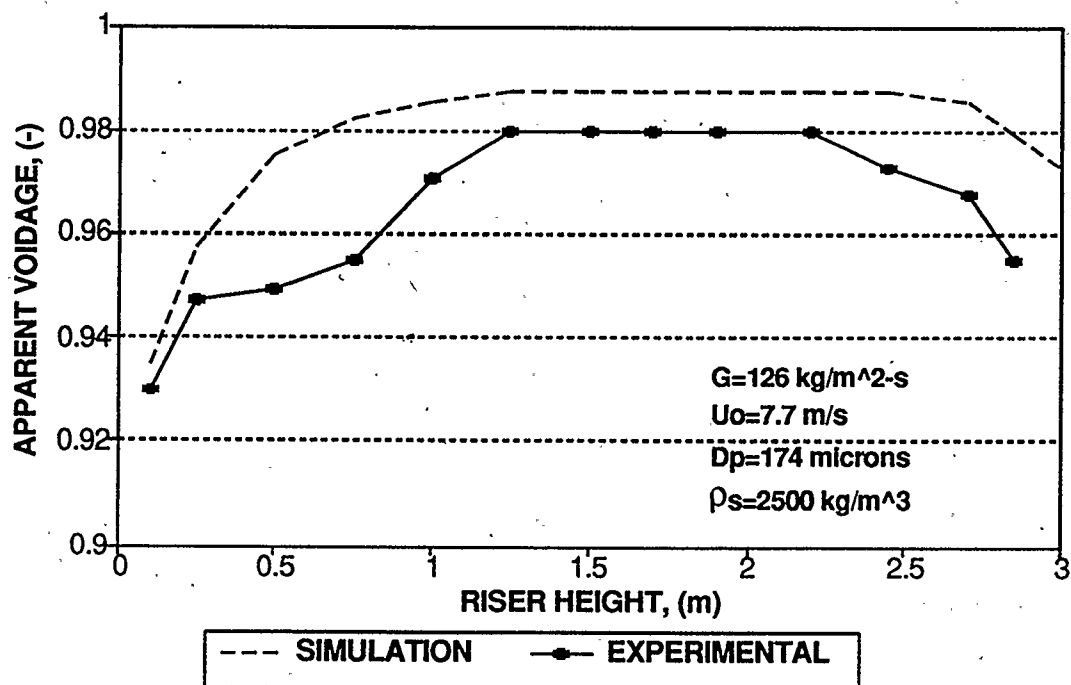
FIGURE 5.4 - COMPARSION OF APPARENT VOIDAGE PROFILE- TRIAL 8B
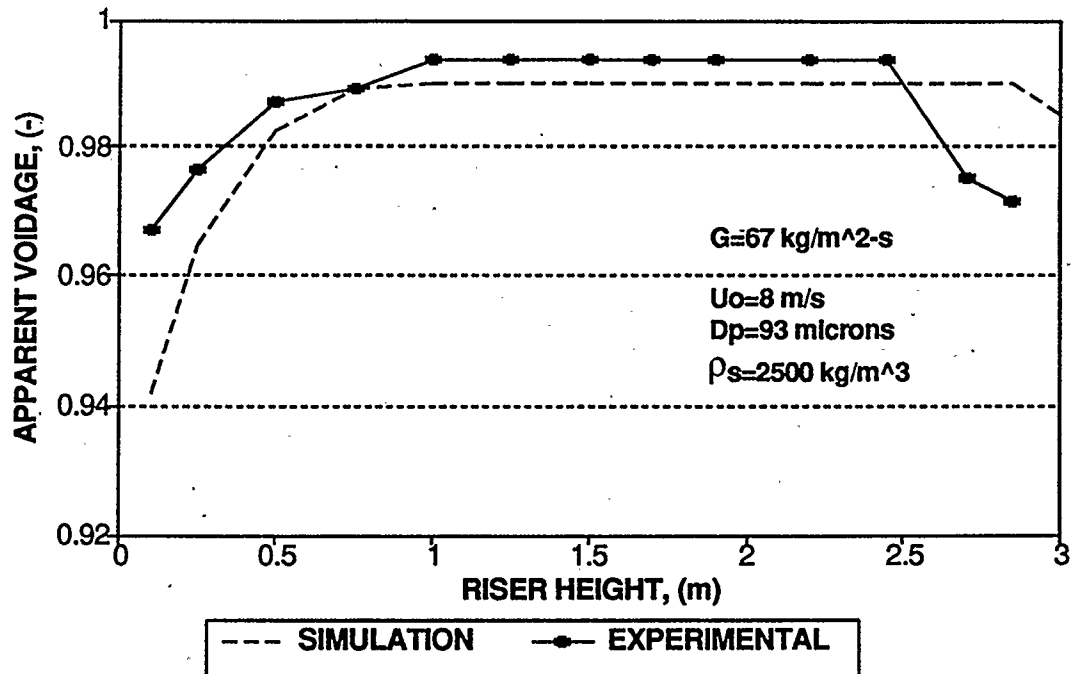
FIGURE 5.5 - COMPARSION OF APPARENT VOIDAGE PROFILE- TRIAL 3D
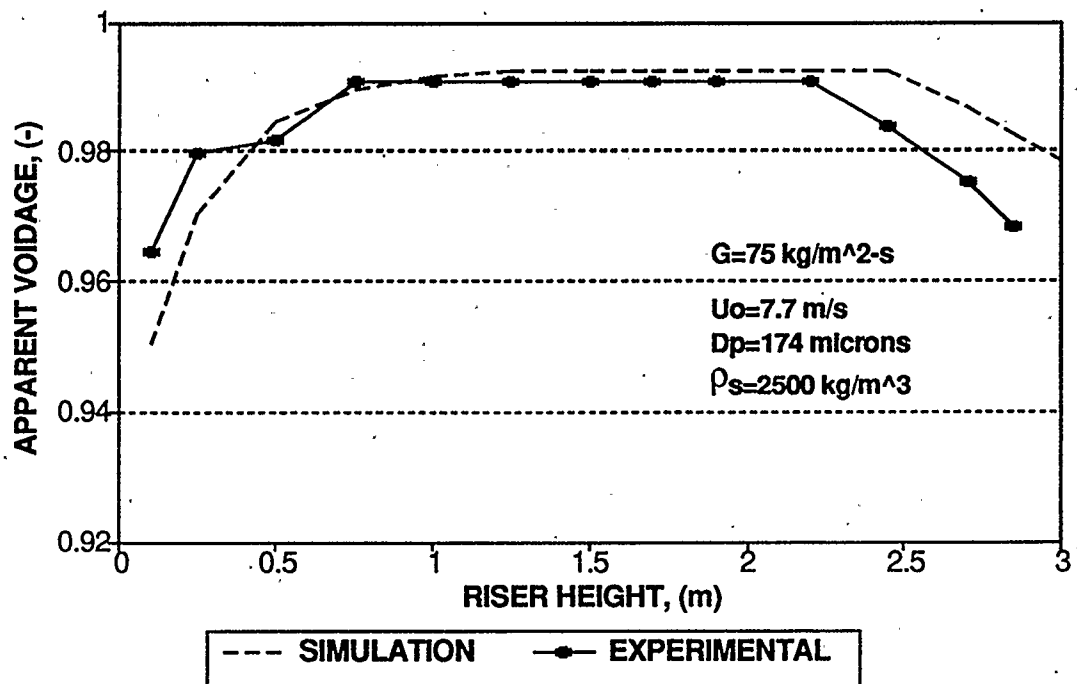
FIGURE 5.6 - COMPARISON OF APPARENT VOIDAGE PROFILE- TRIAL 8A
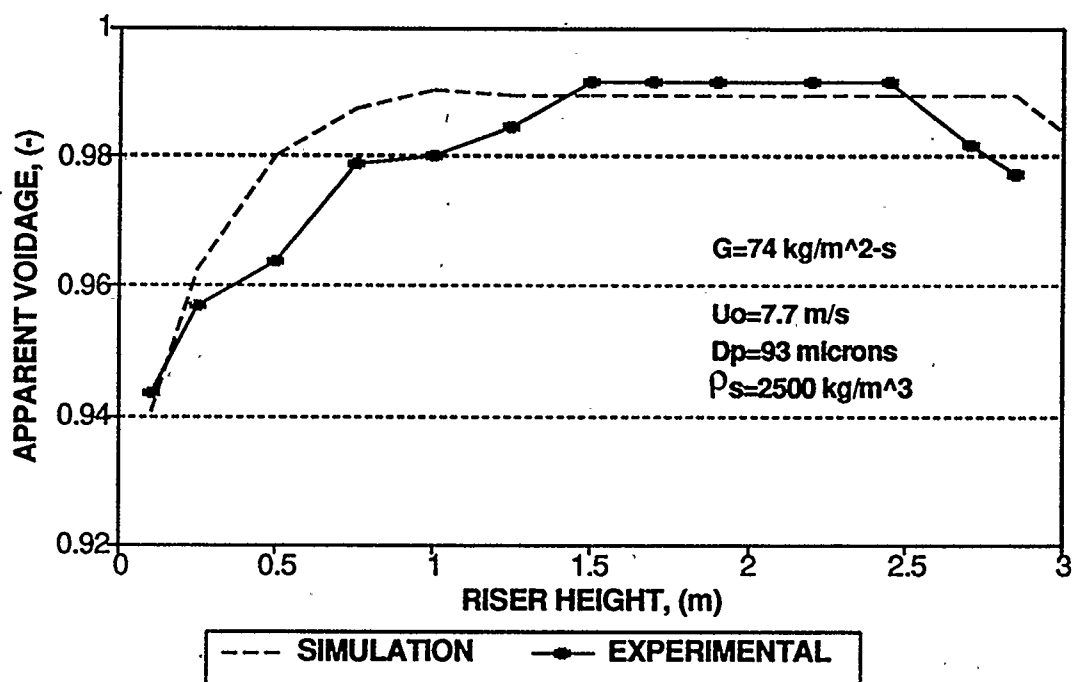
FIGURE 5.7 - COMPARSION OF APPARENT VOIDAGE PROFILE- TRIAL 2B

height. Because of the abrupt exit configuration used in this work there is a densification of solids in the upper portion of the riser.

Detailed examination of Figures 5.1 through 5.7 indicates a reasonably good fit between the simulated and experimental apparent voidages. Although it may appear that there are some localized differences in the simulated and experimental results, in all cases the percent difference is less than 10%. The largest percent difference in apparent voidage values occurs in Figure 5.2. At the bottom of the riser the percent difference between the simulated and experimental voidage is approximately 7% while at the top of the riser the error is roughly 6%. However, as will be discussed shortly, the differences can be attributed to the difficulties encountered in maintaining uniform flow through the line connecting the riser to the cyclone rather than the inability of the proposed model to simulate the axial apparent voidage profile. In Figure 5.5, which also appears to have large differences between the simulated and experimental results, the actual percent difference in apparent voidage is small. At the bottom of the riser the difference is roughly 2.5% while the percent difference at the top of the riser is approximately 1.5%. Similarly, in Figure 5.4, at an axial location of 0.75 m, although it appears much larger, the percent difference between the simulated and apparent voidage is actually only 2.5%. In the developed flow zone of the riser, the predicted and experimental voidages almost always coincide.

The choice of superficial fluidizing gas velocity can significantly affect the shape of the apparent voidage profile. For example, experimental studies by Jotaki and Tomita (1976) and Yang and Keairns (1976) have demonstrated that at a constant solids flux, the

greater the superficial fluidizing gas velocity the shorter the acceleration region in the riser. The higher the gas velocity and hence the larger the gas momentum, the easier it is to push the solids up through the riser. Because of this, the greater the gas velocity at a constant solids flux the lower the solids concentration at the bottom. In fact, it can be surmised that if the superficial gas velocity is lowered enough, the fluidization state in the riser will change from fast to turbulent fluidization and then to bubbling fluidization. Bader et al. (1988), using FCC catalyst, showed that at a solids mass flux of 147 kg/(m^2•s) lowering the superficial gas from 9.1 to 4.7 m/s resulted in a significant densification of solids at the bottom of the riser. Figures 5.1 and 5.2 show the experimental and simulated apparent voidage at approximately the same mass flux but at different superficial gas velocities. At a superficial gas velocity of 8 m/s (Figure 5.1), the length of the acceleration zone is approximately 1.35 m while the simulated acceleration zone is roughly 1.5 m. Lowering the superficial gas velocity to 5 m/sec (Figure 5.2) the experimental acceleration increases to approximately 1.5 m while the simulated length increases to roughly 2.2 m. The large difference between the predicted and experimental acceleration length at the lower gas velocity was due to the slugging condition that existed in the riser. The slugging conditions in the riser was attributed to the almost periodic constricted flow in the line connecting the riser to the cyclone. Whenever there was some sort of clog in the line, the flow of solids was significantly reduced. After enough pressure built up from the fluidizing gas, the solids forming the choke were removed and a sudden increase in solid flow was initiated. The response of the CFB unit appeared to be analogous to the situation where a pulse input of tracer is applied to a

reactor system to determine the residence time distribution. After an initial delay which allowed the slug of solids to travel through the recirculation leg and into the riser, large fluctuations were noticed in the manometers used to measure the axial pressure drop along the riser. After the slug passed through the riser the fluctuations appeared to dissipate. However, because of the periodic constricted flow at the top of the CFB unit, it was very difficult to record the manometer readings and subsequently, the acceleration zone length with any reasonable degree of certainty. Even with the experimental difficulties encountered in performing Trial 1C (Figure 5.2), the results have been presented to illustrate how the performance of one part of a CFB unit affects all the other components that make up the rest of the system. Although the operating conditions of Trial 1C (superficial gas velocity, solids mass flux) are typical of those encountered in fast fluidization, the plugging of solids in the line connecting the riser and the cyclone resulted in gas and solid flow patterns vastly different from that of circulating fluidized beds. Figures 5.3 and 5.4 better illustrate the effect of superficial gas velocity in the acceleration region. In this instance the simulated and experimental acceleration lengths are almost exactly the same and it is evident that the higher the superficial gas velocity the shorter the acceleration zone. Furthermore, the greater solids concentration associated with the lower gas velocities is also evident at the bottom of the riser. In fact, in Figure 5.3 the low superficial gas velocity combined with the high solids mass flux creates a situation where the entire riser acts like an acceleration zone.

In the developed flow zone, increasing the superficial gas velocity at a constant solids mass flux leads to higher apparent voidages. The effect can again be attributed to

the fact that the higher the gas velocity the easier it is for the solids to be pushed out of the riser. As a result, at any point in the developed flow zone, the leaner the gas-solid suspension and hence the higher the apparent voidage. Examination of Figures 5.1 and 5.2 indicates the effect of superficial gas velocity on the apparent voidage in the developed flow zone for sand A. As the figures indicate the higher the gas velocity the higher the voidage. It should be noted that in Figure 5.2 the extent of densification of solids in the riser due to the plugging in the line connecting the riser to the cyclone is not known. If the densification effect is large enough, it may also increase the voidage in the developed flow zone. As previously mentioned, in Figure 5.3 the acceleration zone almost occupies the entire riser column and hence there is no developed flow zone. As a result, a comparison of apparent voidages as a function of superficial gas velocity could not be made for sand B.

Unlike the acceleration zone or the developed flow zone, it is not clear how various CFB operating conditions affect the segment of riser affected by an abrupt exit. The uncertainty is magnified by the lack of experimental studies involving CFB units equipped with abrupt exits. Figures 5.1 and 5.2 show the effect of superficial gas velocity on the apparent voidage at the upper part of the riser for sand A while Figures 5.3 and 5.4 show the corresponding effect for sand B. The experimental and simulated results suggest that the lower the superficial gas velocity the greater the abrupt exit effect. As shown in the acceleration and developed flow zones of the riser, increasing the superficial gas velocities at a constant solids flux leads to leaner gas-solid suspensions. The leaner the gas-solid suspensions, the smaller the amount of interaction between the solids

reflected off the top of the abrupt exit and the solids flowing up with the gas.

Generally, at a given superficial gas velocity, the higher the solids mass flux the greater the length of the acceleration zone. High solids fluxes result in a greater solids concentration in the riser. Consequently, at a given superficial gas velocity the higher the solids concentration the longer the time required for the solids to reach their steady state velocity. Consequently, there is a larger region at the bottom of the riser where there is a relatively high solids holdup. Figures 5.1 and 5.5 represent the axial apparent voidage profiles at constant superficial gas velocity but different solids fluxes. It is evident in both the simulated and experimental results that the higher the solids mass flux the greater the portion of riser making up the acceleration zone. At a solids flux of 106 kg/(m^2•s) the simulated acceleration zone length is approximately 1.5 m and the experimental length is 1.25 m while at a solids flux of 67 kg/(m^2•s) the predicted and experimental acceleration zones are around 1.0 m. Figures 5.4 and 5.6 show similar results but in this case the solids is sand type B. Similar results have been observed by Jotaki and Tomita (1976) and Yang and Keairns (1976) in experimental studies involving the acceleration region of vertical pneumatic transport lines.

Increasing solids mass flux at a constant superficial gas velocity results in lower apparent voidages in the developed flow zone. The effect of solids mass flux on the apparent voidage profile in the developed flow can be seen by examining Figures 5.4 and 5.6. The figures illustrate that the higher the solids mass flux, the greater the concentration of solids in the developed flow zone. Examination of Figures 5.1 and 5.5 illustrates a similar effect for sand A although the effect is not as evident as with sand

B. Both the simulated and experimental results suggest that for sand A the apparent voidage in the developed flow zone is relatively insensitive to the range of solids mass flux used. The different degree to which the solids mass flux affects the apparent voidage profile can be interpreted in terms of the degree of solid-solid interaction in the riser. Since sand A and sand B have the same solids density, solid-solid collisions will be more significant with sand B because of the larger diameter and hence, greater mass. The greater momentum exchange can lead to an increase in the lateral movement of solids within the core or between the core and annular regions which lengthens the amount of time solids stay in the riser. The net result is an increase in solids loading at any axial location. The effect is magnified by increasing the solids flux and solids mass. The same reasoning can be applied to the results shown in Figures 5.1 and 5.5. In this instance, the degree of solid-solid interaction is still expected to increase with increases in solids mass flux. However, because of the small solids diameter and the solids flux employed, the number and extent of solid collision is not large enough to have any appreciable effect on the axial apparent voidage.

Comparison of the experimental results in Figures 5.1 and 5.5 suggest that the lower the solids mass flux at a constant gas velocity the greater the degree of densification of solids at the top of the riser. However, experimental studies by Brereton (1987) and by Patience (1990) indicate the opposite effect; at a constant superficial gas velocity the greater the solids mass flux the greater the buildup of solids at the top of the riser. The higher the solids flux the greater the deflection of solids off the top or the sides of the abrupt exit. As a result, there is a greater degree of interaction between the

upward flowing solids and those falling down from the exit. The observed contradiction in Figures 5.1 and 5.5 can again be attributed to the constricted flow of gas and solids from the riser to the cyclone. As discussed earlier, the constricted flow increases the solids holdup in the upper portion of the riser above the amount that would normally exist. Examination of Figures 5.4 and 5.6 shows the correct trend. In both the simulated and experimental results the greater the solids mass flux at a constant gas velocity the greater the effect of the abrupt exit. It is interesting to note that even though the restricted flow in the line connecting the riser to the cyclone creates an additional amount of solids in the upper region of the riser, the experimental results suggest that the portion of the riser affected by the abrupt exit is approximately the same for a given solids type. In the case of sand A, which is shown in Figures 5.1 and 5.5 the abrupt exit affects only the upper 0.5 m of the riser. The simulation results also predict a similar effect but unlike the experimental results, the simulation results estimate that only the upper 0.15 m of the riser is affected by the abrupt exit configuration. Similar results have been observed in the experimental results of Patience (1990). It is difficult to speculate on the reasoning behind the observed effect. Visual observations were not possible because the abrupt exit could not be made out of plexiglass due to the 'sandblasting' effects of the sand. In the plexiglass section of the riser, the high superficial gas velocity and solids mass flux observations created an immense amount of turbulence so that visual observations could not be made. A possible explanation could be that the solids can only be reflected back a certain distance from the abrupt exit. Once the solids reach this point, they have lost all the momentum gained by reflecting off the top and are re-entrained with

the upward flowing gas.

Figures 5.6 and 5.7 provide an illustration of how the particle diameter affects the axial apparent voidage profile. The only visible differences lie in the lower and upper portions of the riser. A denser region exist at the bottom of the riser when the smaller sand is used. According to the Geldart classification system, sand A is a group A powder. Such solids can be moved from one area to another more easily than solids such as sand B. Perhaps at the bottom of the riser at the high superficial gas velocities typically found in fast fluidization, the fluidizing gas has so much momentum that it preferentially moves the smaller solids out towards the sides of the riser to a greater extent than with the larger solids. Thus, instead of the gas entraining the solids, the gas actually channels right through them. At the top of the riser, the larger the solids the greater the abrupt exit effect. The response is expected since for a constant density solid, the greater the solid the greater the mass and hence the greater the gain in momentum from deflection off the top of the exit. Furthermore, the larger the solids, the greater the chance of collisions between the particles at the top of the riser.

Simulations were also performed with data reported in literature to further validate the applicability of the model in predicting the axial apparent voidage profile in CFB risers. Figures 5.8 to 5.10 show the comparisons between the results of the simulations and the experimental data. The simulation conditions in Figures 5.8 through 5.10 were chosen so that the range of applicability of the model could be illustrated.

Very few experimental studies have been conducted on CFB units equipped with abrupt exits. To determine whether the model could simulate other CFB units equipped

with a right-angled type abrupt exit, simulations were conducted to model the experimental voidage profiles obtained by Patience (1990). Figures 5.8A and 5.8B compare the simulated and experimental apparent voidage profiles. The simulated riser is 5 m long and has an inside diameter of 0.0828 m. The column was operated at room temperature and atmospheric pressure. The simulated and experimental results follow the trends reported earlier. At the bottom of the riser, the voidage profile gradually increases with height because of solids acceleration. The largest difference between the simulated and experimental results occurs in this region. For example, in Figure 5.8A the percent difference in experimental and simulated apparent voidage at the bottom of the riser is approximately 10% whereas for the rest of the column the percent difference is well within 5%. As the figures show the greater the solids flux the longer the length of the acceleration zone. For a solids flux of 198 kg/(m^2•s) the experimental acceleration zone is approximately 2 m while reducing the solids flux to 20 kg/(m^2•s) the acceleration length decreases to approximately 1.25. Once the solids have stopped accelerating, the voidage profile becomes constant with increases in riser height. It is clearly evident in Figures 5.8A and 5.8B the slip factor criterion (Patience et al., 1991) provides an extremely good representation of the flow of gas and solids in the developed flow zone. A comparison of the two figures shows that the higher the solids mass flux the lower the apparent voidage in the developed flow zone. Because of the abrupt exit, there is a densification of solids at the top of the riser. It is interesting to note that unlike the experimental apparent voidage profiles shown earlier, in both Figure 5.8A and 5.8B the experimental apparent voidage at the top of the riser is almost constant. The result

FIGURE 5.8A - COMPARSION OF APPARENT VOIDAGE - DATA FROM
PATIENCE (1990)
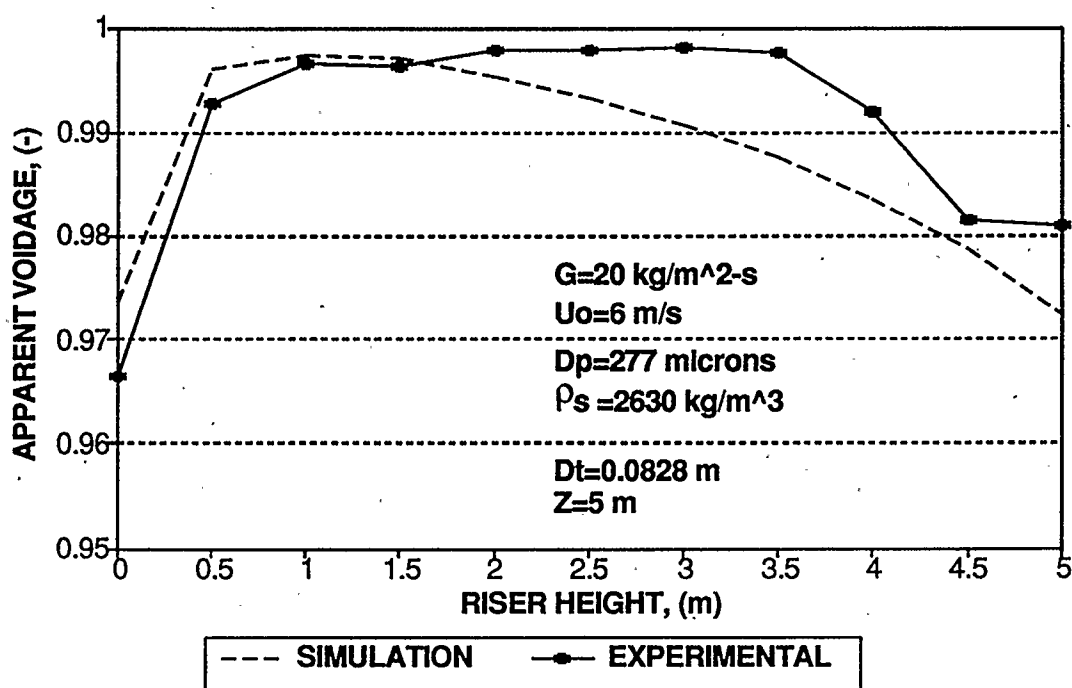
FIGURE 5.8B - COMPARISON OF APPARENT VOIDAGE - DATA FROM
PATIENCE (1990)

indicates that an abrupt exit can create many complex gas and solids flow patterns at the top of the riser. Clearly, further work is necessary to establish the role of an abrupt exit on gas and solid flow patterns in the riser.

According to Matsen (1976) in large industrial fluidized catalytic crackers, solid circulation rates typically range between 600 and 1500 kg/(m^2•s). Unfortunately, most experimental CFB units operate at moderate solids flux and furthermore, to the best of the author's knowledge, apparent voidage profiles and operating conditions of industrial CFB units have not been published in literature. Consequently, to determine whether the proposed hydrodynamic model can be used to predict the axial voidage profile at high circulation rates the experimental data of Arena et al. (1986) was simulated. Although the experimental CFB unit used by Arena et al. (1986) is only 6.4 m high and has a internal riser diameter of 0.04 m, the experimental study was performed at very high solid circulation rates. Figures 5.9A and 5.9B show the comparison between the simulation and experimental results for the column used by Arena et al. (1986). Unlike the results presented earlier, the experimental CFB unit used by Arena et al. (1986) is not equipped with an abrupt exit and consequently, as shown in the axial apparent voidage profiles there is no densification of solids in the upper region of the riser. The largest difference between the simulated and experimental results lies in the bottom portion of the riser. The main reason for the difference is due to inability of the bottom voidage correlation to predict the bottom voidage. Examination of Table 4.3 which shows the data used in the development of the bottom voidage correlation indicates that the operating conditions used by Arena et al. (1986) are outside the range of applicability of the correlation.
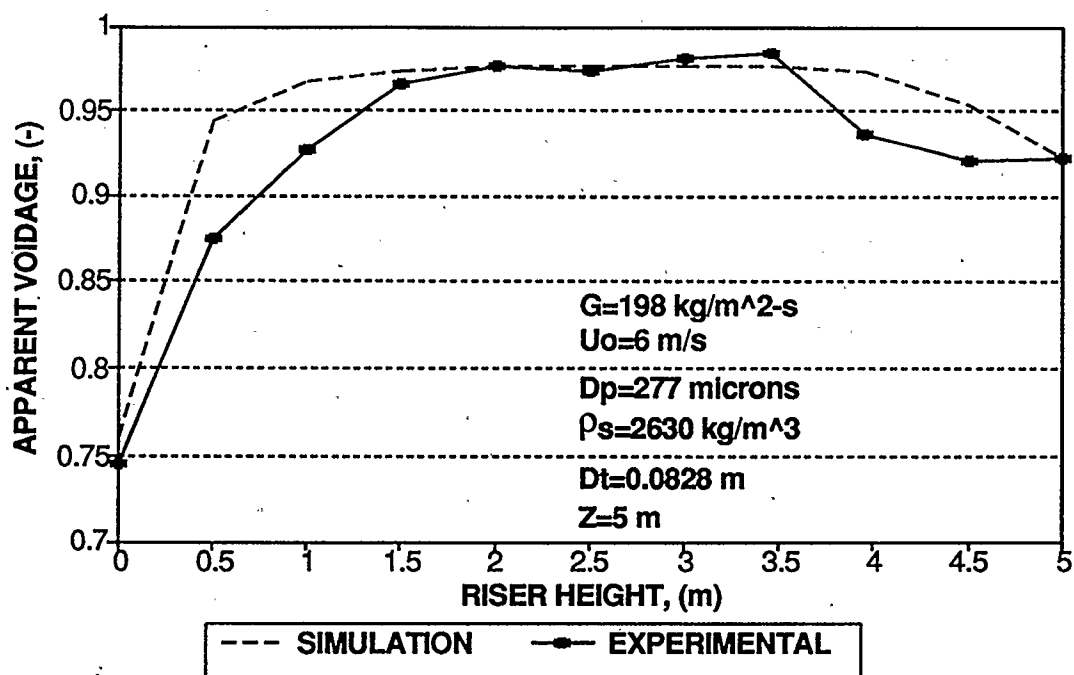
FIGURE 5.9A - COMPARISON OF APPARENT VOIDAGE - DATA FROM
ARENA ET AL. (1986)
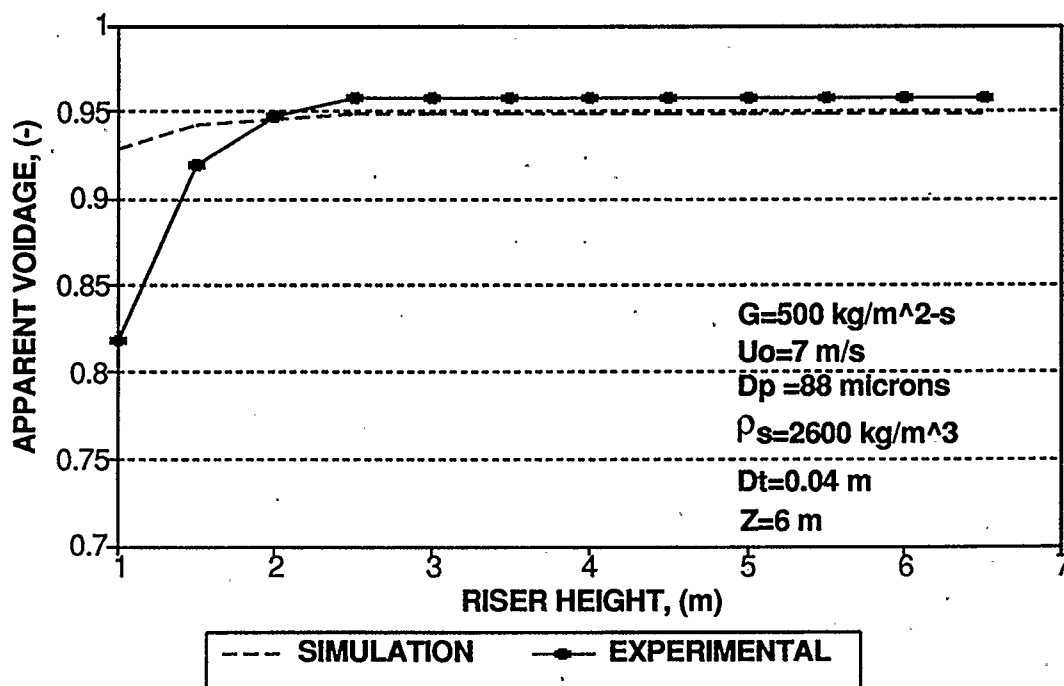
FIGURE 5.9B - COMPARSION OF APPARENT VOIDAGE - DATA FROM
ARENA ET AL. (1986)

Neglecting the differences that exist in the bottom portion of the riser, the agreement between the simulated and experimental results is very good. In the case of Figure 5.9A the percent difference is roughly 3% and in Figure 5.9B the error is only 0.25% in the developed flow zone.

So far all the experimental and simulated results presented have been for CFB risers with relatively small diameters. To determine whether the model could be applied to large diameter risers, the experimental risers used by Hartge et al. (1986) and by Bader et al. (1988) were simulated. Figure 5.10A shows the simulation results for the riser used by Hartge et al. (1986). The experimental unit has a internal riser diameter of 0.4 m and a riser height of 7.8 m. The figure shows the excellent agreement between the simulated and experimental voidage profiles. Figure 5.10B shows the simulated axial apparent voidage profile for the conditions used by Bader et al. (1988). The experimental unit is 12.5 m in height and has a diameter of 0.305 m. Again, the results show there is a very good match between the simulated results throughout the column.

The good fit between the simulated and experimental apparent voidage profiles suggests that the assumptions made in the formulation of the hydrodynamic model are reasonably correct. The assumption of predominant upflow of gas and solids in the acceleration region provides an extremely good first estimate of the apparent voidage. The true flow phenomena in the acceleration region is very complex. Besides solids acceleration there are also the effects of the mechanical device used to transfer solids from the recirculation leg to the riser and the movement of the fluidizing gas in the acceleration region which can impede the upward flow of gas and solids. Studies by
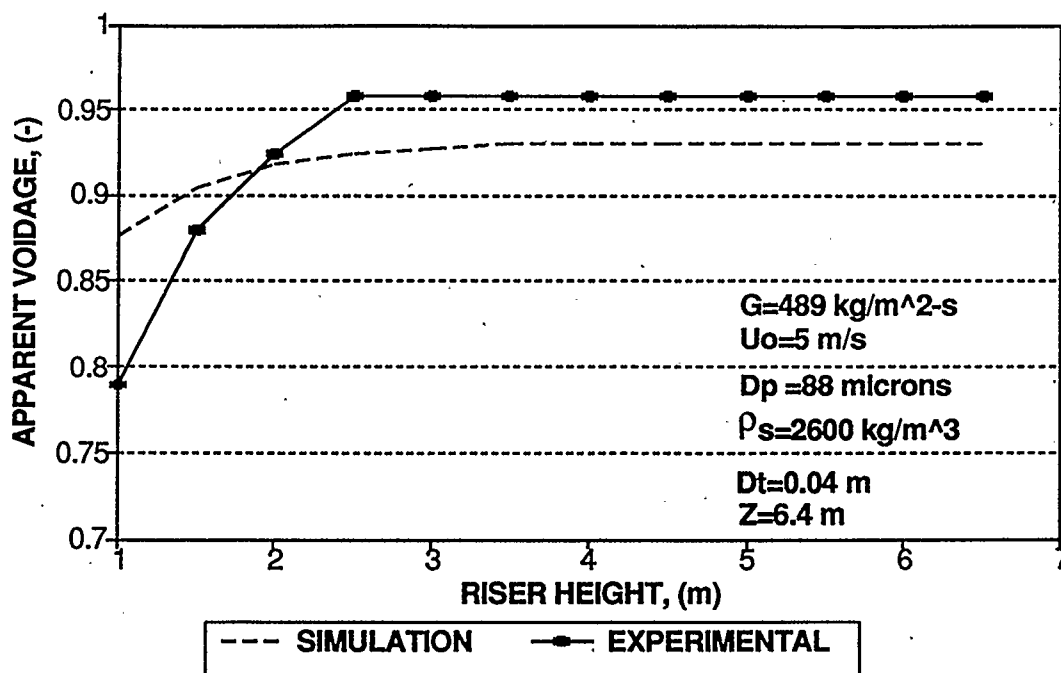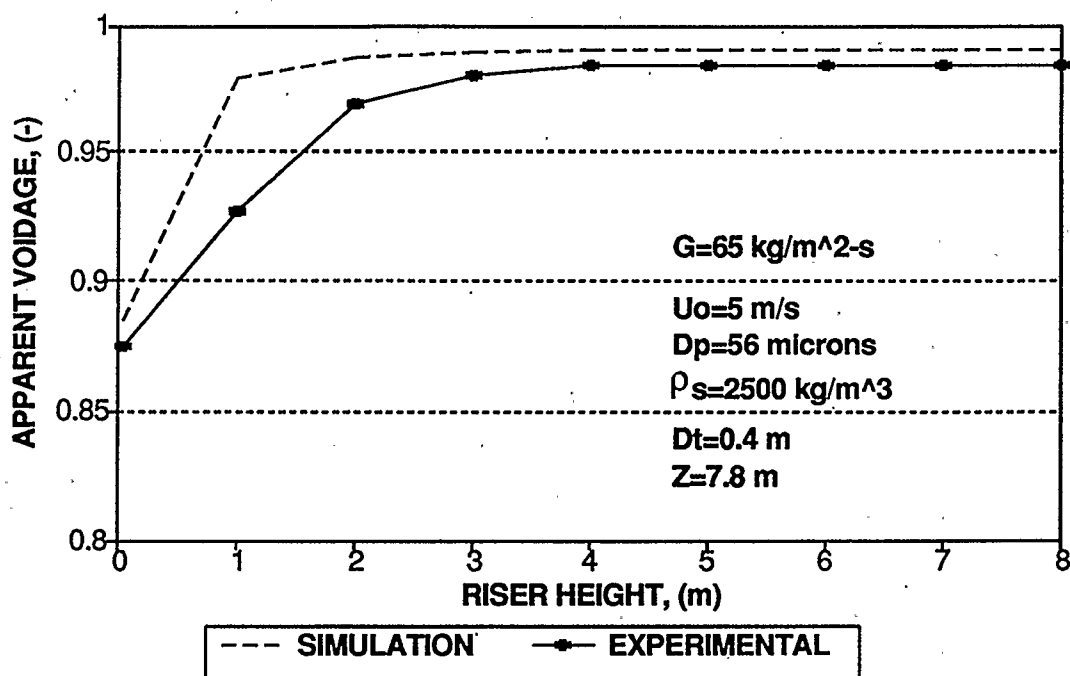
FIGURE 5.10A - COMPARSION OF APPARENT VOIDAGE - DATA FROM
HARTGE ET AL. (1986)
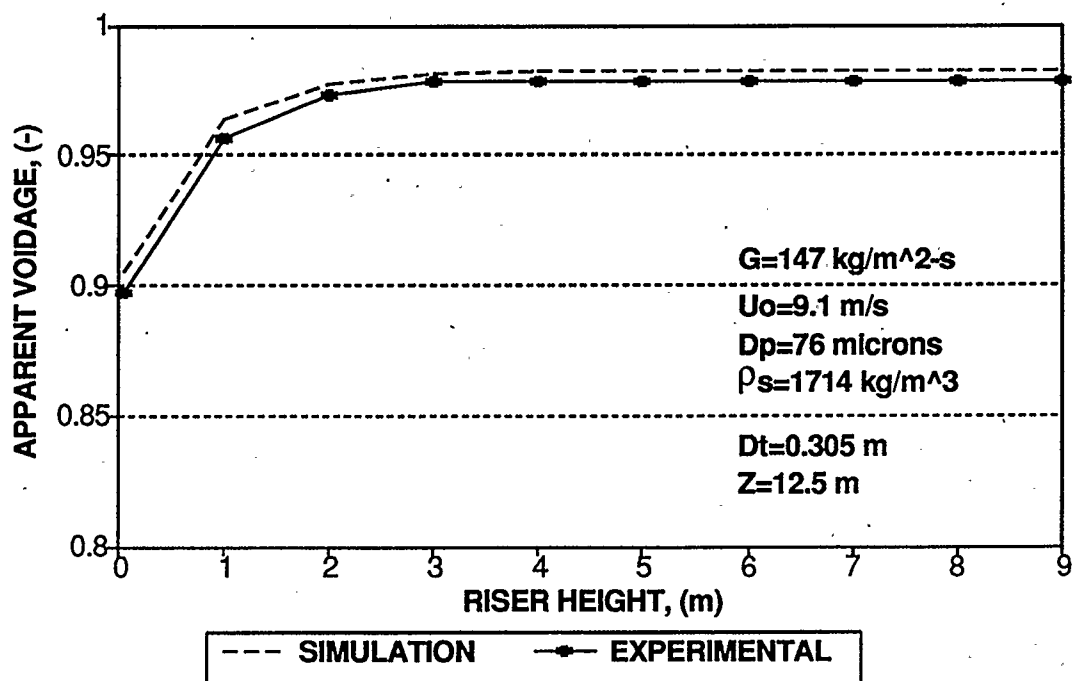
FIGURE 5.10B - COMPARSION OF APPARENT VOIDAGE - DATA FROM
BADER ET AL. (1988)

Rhodes et al. (1989) and Yang (1976,1988) in experimental CFB units and observations noted by Couturier et al. (1991) in an industrial unit have indicated that the design of the return transfer line, which controls the flow of solids into the riser can have a very important effect on gas-solid flow patterns at the bottom of the riser. For a inclined solids return line, Yang (1976, 1988) has indicated the angled downflow of solids can combine with the upward flowing gas to create a recirculation pattern in the lower regions of the riser. The internal recirculation (caused by the solids entering the riser) in the bottom region leads to an increased solids holdup due to the longer time the solids stay in the region. Studies by Rhodes et al. (1989) and Couturier et al. (1991) have illustrated that solids entering from one side of the riser can cause a radial maldistribution of solids across the riser cross-sectional area. Such "pockets" may lead to stagnant solids which increases the solids holdup in the lower regions of the riser. Because of the difficulty in determining the response of the apparent voidage to these effects, the proposed model neglects the internal recirculation due to solids entering the riser from the recirculation leg and the possibility of stagnant regions of solids due to the maldistribution of solids.

The inability of the model to predict exactly the apparent voidage at the top and bottom of the riser is due to the limitations of the proposed empirical correlations. Although a wide range of experimental data was used to develop the correlation for predicting the voidage at the bottom of the riser, differences such as the design of the solids return line connecting the riser and the recirculation leg could have superimposed an additional amount of solids holdup in the experimental results and hence, resulted in a false estimate of the bottom apparent voidage. Further work is necessary to determine

the extent to which the design of the solids transfer line affects the voidage at the bottom of the riser. Furthermore, most experimental CFB units, including the one at the University of Calgary, do not have a pressure tap situated at the very bottom of the riser. The first pressure tap is usually some distance away from the bottom. Consequently, one must extrapolate the experimental data to determine the voidage at the very bottom of the riser.

Similar arguments can be presented for the correlation used to predict the apparent voidage at the top of the riser. The experimental axial suspension profiles or equivalently, the axial apparent voidage profiles recorded by Patience (1990) demonstrated that the apparent voidage at the upper portion of the riser does not always decrease with increases in height. In some of his experiments the voidage actually increased at the top. Consequently, it is very difficult to extrapolate the data to any significant degree of accuracy since it is not clear how the abrupt exit affects solids behaviour. Furthermore, there have only been a few experimental studies reported on CFB units with abrupt exits. The work by Brereton (1987), Patience (1990) and the experimental work performed in this study involved small diameter columns (0.05-0.152 m) and a relatively narrow range of superficial gas velocities (5-8 m/s). As for the bottom voidage correlation, more extensive experimental studies involving various reactor geometries and gas and solids physical properties are required to increase the range over which the top voidage correlation applies. Nevertheless it should be emphasized that the correlations proposed to predict the apparent voidage at the top and bottom of the riser successfully predicted the experimental voidages to within 15% error.

The slip factor criterion (Patience et al., 1991) provides an extremely good way of calculating the apparent voidage in the developed flow zone. As Figures 5.1 through 5.8 indicate, the experimental and simulated results in the developed flow zone almost coincide. The results indicate that the ratio of interstitial gas to average solids velocity or the slip factor is indeed approximately two in CFB risers.

Based on the simulation of data from the experimental CFB unit at the University of Calgary and from the simulation of data reported in literature the proposed model has been shown to simulate well experimental CFB risers with diameter ranging from a 0.05 m up to 0.40 m, superficial gas velocities varying from 4 to 8 m/s and solids fluxes from 20 up to 200 kg/(m^2•s). The applicability of the model is mainly limited by the range of operating conditions and gas and solid physical properties used to develop the riser bottom and top voidage correlations. Because of the limited experimental data involving high solids mass fluxes, it cannot be surmised that the model can be used with high circulation rates, although simulation of the work by Arena et al. (1986) suggested that the model is indeed applicable.

5.3 INTERNAL FLOW STRUCTURE

An accurate evaluation of the model's ability to the internal flow characteristics is difficult because of the many uncertainties associated with experimental internal flow structure data. To simplify the modelling of the CFB riser, it is assumed that the core radius has a distinctly defined constant value at any axial location and that the internal flow structure parameters are averaged values over the core and annular regions. In

reality, because of solids interchange between the core and the annulus and because of interactions between the fluidizing gas and solids, it is expected that the core radius can be considered to be any number or radial locations. Furthermore, as shown by Rhodes et al. (1989) at a given axial location, the radial structure within the riser varies depending upon the angle the device used to measure the radial structure makes with the solids inlet position. For example, if some probe is used to measure the radial structure and if it is situated 180 degrees away from the solids inlet position, the radial profile is different than if the probe was situated at an angle of 90 degrees to the solids inlet position. Complicating matters even more is the fact that wall effects can be very important. The high circulation rates can cause significant erosion leading to indentations in the riser wall. The indentations act like obstacles in the path of the falling solids. As a result, instead of having a downward flow of solids along the riser wall, there can be lateral flow from the deflection of the solids off the indentations. The model does not take into account the change in flow patterns caused by erosion problems or maldistribution of solid flow. Finally, another problem obscuring the evaluation of the internal flow structure around the wall region is the type of equipment used to determine the radial structure. Herb et al. (1989) and Reh and Li (1990) indicate that the solid concentration determined from fibre-optic probes may be in error because a fibre-optic probe is dependent on the intensity of reflected light. Often, instead of just receiving light from solids in the riser, light reflected from the wall is also collected by the probe. Consequently, the measured solids concentration may be higher than it actually is. Irregardless of what type of probe is used, it is obvious that a probe will cause some sort

of disruption in the flow patterns of the gas and solids within the riser. Because of the lower concentration of solids in the middle of the riser, the disturbance is not as great as near the wall region. At or near the wall, solids may deflect off the probe and into the dilute core region or into other parts of the annular region. Consequently, the probe may actually dilute the amount of solids actually present in the annular region.

A set of the internal flow structure parameters as predicted by the model is shown in Figures 5.11 through 5.13. A typical core voidage profile is shown in Figure 5.11A while the corresponding core radius profile is shown in Figure 5.11B. Both profiles have similar shapes. The smallest core radius and voidage occurs at the bottom of the riser. As the solids accelerate from their initial value the core radius and voidage gradually increase to a constant value at which point the solids have reached their developed flow velocity. Like the apparent voidage, at the top of the riser, both the core voidage and radius decrease because of the abrupt exit effect. The figures indicate that the core radius is affected more than the core voidage at the top of the riser. For the same operating conditions Figure 5.12A and Figure 5.12B show the core gas and core solids velocity, respectively. Since the gas is assumed to travel only up the dilute core, the maximum core gas velocity occurs at the bottom of the riser where the core radius is the smallest. As the core radius increases and hence, the core cross-sectional area, the gas velocity decreases. At the top of the riser, the densification of solids leads to a reduced core cross-sectional area which increases the core gas velocity. Initially, the solids velocity at the bottom of the riser is approximately zero. The solids velocity rises until the solids stop accelerating. At the top of the riser, because of the way the solids core velocity is
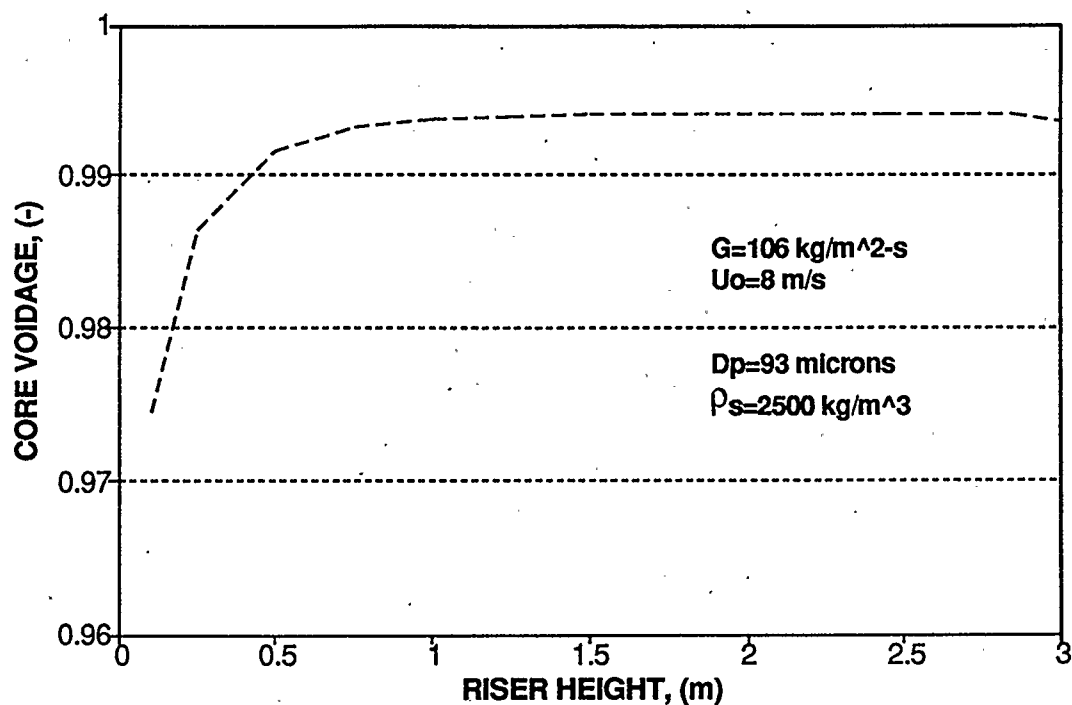
FIGURE 5.11A - SIMULATED CORE VOIDAGE PROFILE - TRIAL 2A
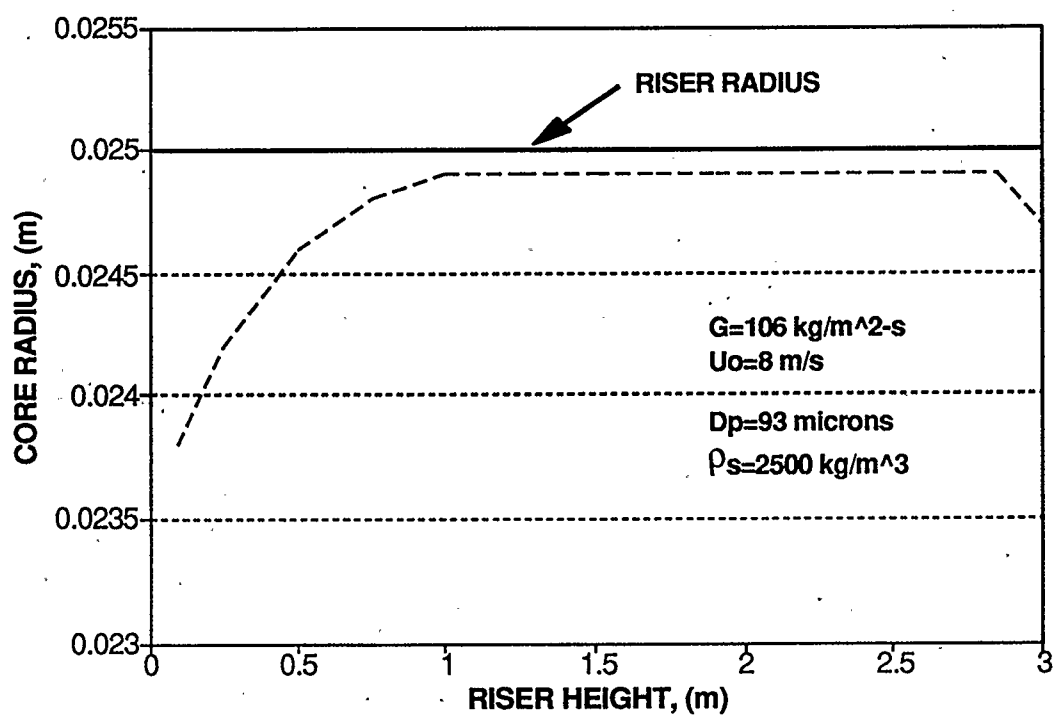
FIGURE 5.11B - SIMULATED CORE RADIUS PROFILE - TRIAL 2A
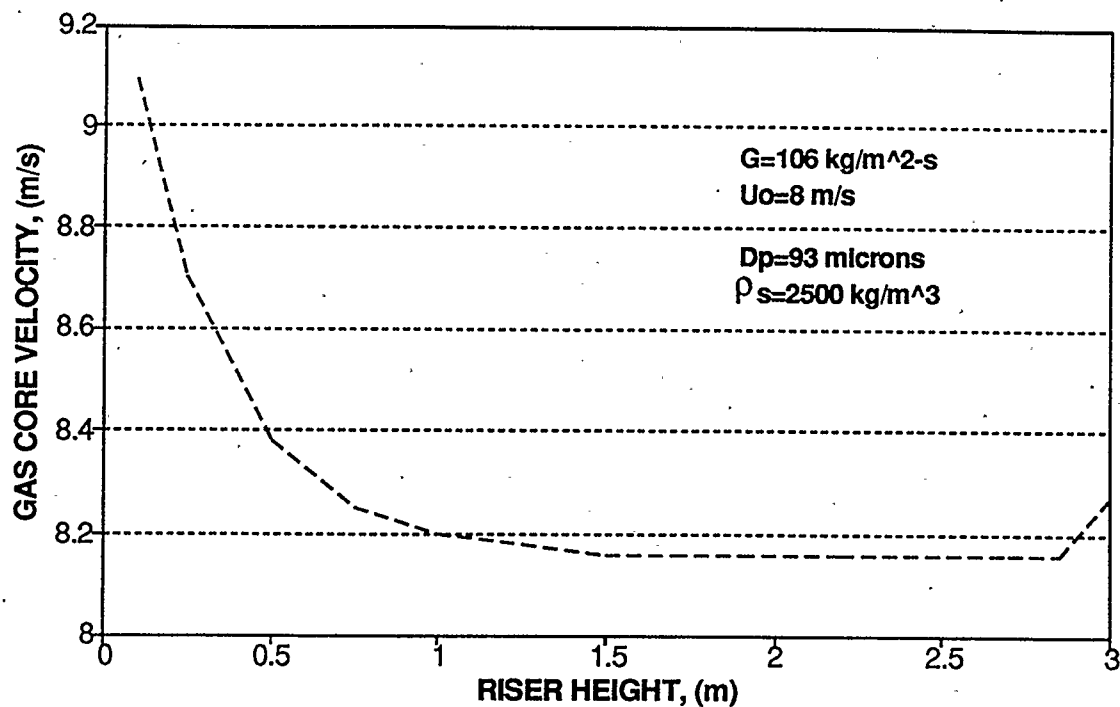
FIGURE 5.12A - SIMULATED GAS CORE VELOCITY PROFILE - TRIAL 2A

Chart labels: GAS CORE VELOCITY, (m/s) vs RISER HEIGHT, (m)

G=106 kg/m^2-s
Uo=8 m/s

Dp=93 microns
ρs=2500 kg/m^3
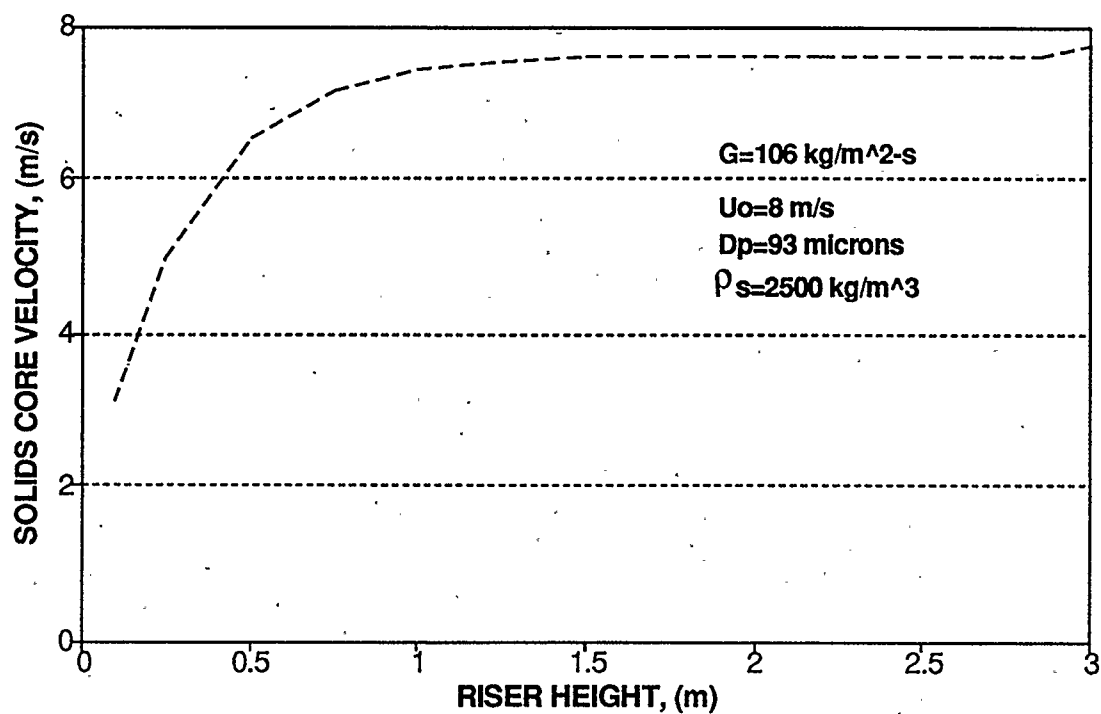
FIGURE 5.12B - SIMULATED SOLIDS CORE VELOCITY PROFILE - TRIAL 2A

Chart labels: SOLIDS CORE VELOCITY, (m/s) vs RISER HEIGHT, (m)

G=106 kg/m^2-s

Uo=8 m/s
Dp=93 microns
ρs=2500 kg/m^3

defined in the model formulation, the solids velocity increases because of the increase in core gas velocity. The corresponding solids interchange coefficients are shown in Figures 5.13A and 5.13B. The interchange coefficients follow the same shape although the core-to-annulus coefficient is approximately an order of magnitude larger than the annulus-to-core coefficient. At the bottom of the riser, there is a large transfer of solids from the core to the annulus as the core/annular structure is formed. With increases in riser height, K_{ca} decreases to a constant value in the developed flow zone. Besides the difference in magnitude the only other difference in the K_{ac} profile is the increase in value at the top of the riser. The value increases because of the abrupt exit which serves to transfer solids from the annulus to the core. Although a direct comparison cannot be made, the magnitude of K_{ca} is similar to the range determined by Senior and Brereton (1990). A comparison of the K_{ac} values cannot be made because of the lack of data in literature.

5.4 PARAMETER ANALYSIS

A parameter analysis was performed to determine the sensitivity of operating parameters such as superficial gas velocity, solids diameter, riser diameter and solids mass flux on the axial apparent voidage profiles. The simulation results are shown in Figures 5.14 to 5.16.

The effect of superficial gas velocity on the apparent voidage profile is shown in Figure 5.14A. The figure shows that increasing the superficial gas velocity results in a higher apparent voidage at any axial location. This is agreeable with the results presented earlier and consistent with results reported in literature. There does not seem to be one
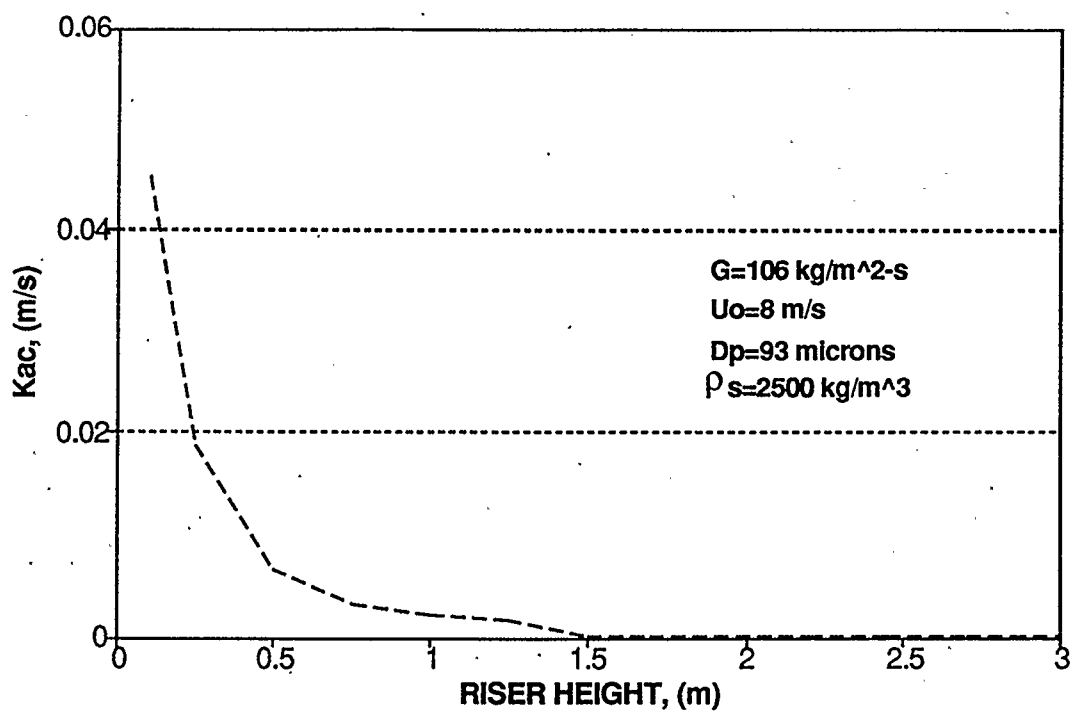
FIGURE 5.13A - SIMULATED ANNULUS-TO-CORE SOLIDS INTERCHANGE
COEFFICIENT - TRIAL 2A
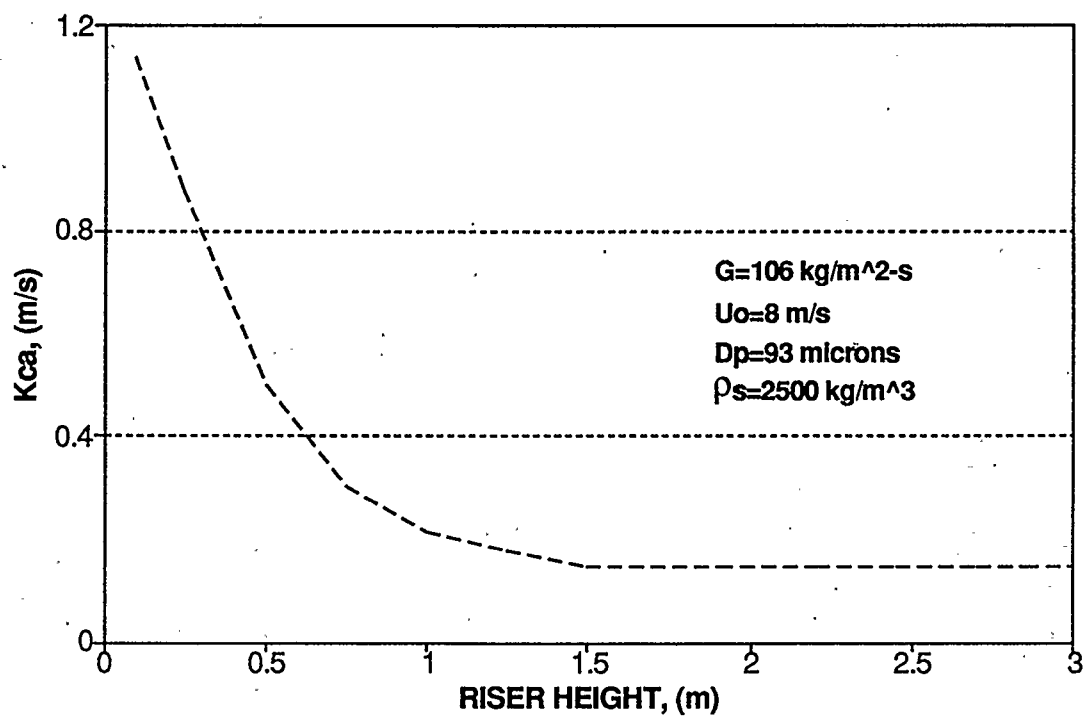
FIGURE 5.13B - SIMULATED CORE-TO-ANNULUS SOLIDS INTERCHANGE
COEFFICIENT - TRIAL 2A

FIGURE 14A - PARAMETER ANALYSIS - SIMULATED EFFECT OF SUPERFICIAL
GAS VELOCITY ON APPARENT VOIDAGE
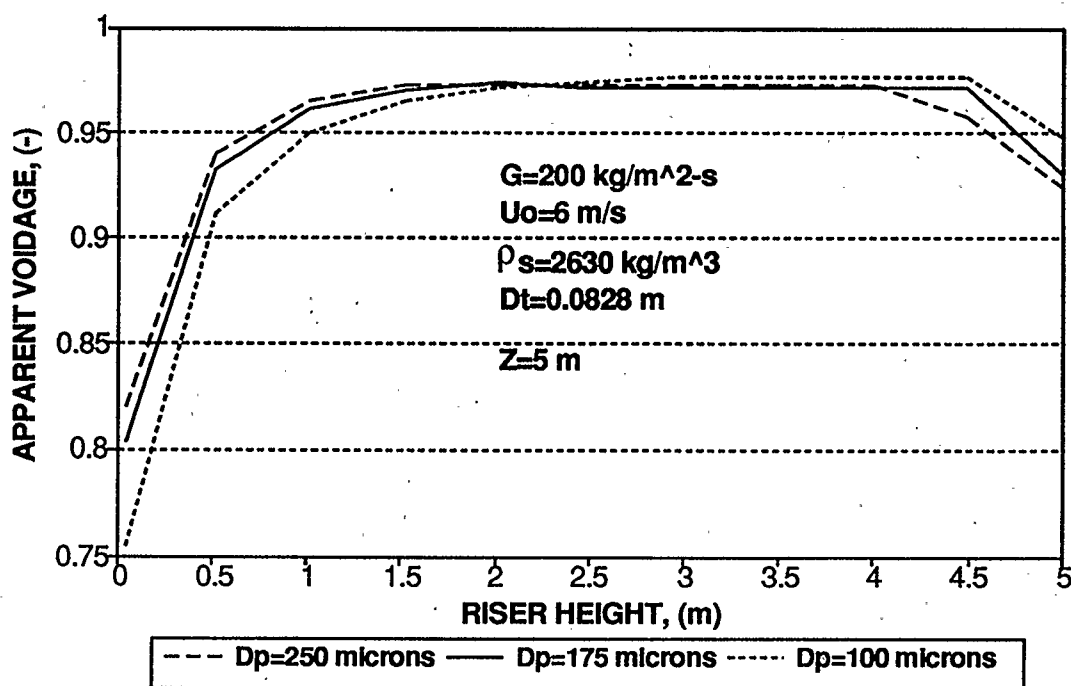
FIGURE 5.14B - PARAMETER ANALYSIS - SIMULATED EFFECT OF PARTICLE
DIAMETER ON APPARENT VOIDAGE

region that is affected more by the superficial gas velocity than any other region. For example, changing the gas velocity from 6 m/s to 8 m/s causes the voidage to increase by roughly 1% at every axial location.

Figure 5.14B shows how the solids diameter affects the axial apparent voidage profile. The figure shows that the solids diameter has the largest impact on the voidage at the bottom and top of the riser. At the bottom of the riser, the smaller the diameter the lower the apparent voidage. As noted earlier, the effect is attributed to the channelling of gas through the solids. At the top of the riser, the larger diameter solids have a more pronounced effect on the voidage profile. Because of their greater mass, the larger diameter solids create a greater amount of agitation in the region. The particle diameter does not really affect the apparent voidage in the developed flow zone, where, except for slight variations, the apparent voidage can be assumed to be a constant.

The effect of riser diameter on the apparent voidage profile is shown in Figure 5.15A. The figure indicates that variations in diameter can have a significant impact on the axial voidage profile at the top of the riser. At riser diameters of 0.0828 and 0.15 m, the apparent voidage at the top of the riser is similar in magnitude to the ones observed in experimental studies by Patience (1990) and Brereton (1987). However, increasing the riser diameter to 0.25 m results in a unreasonable top voidage. The reason for the unrealistic result is due to the limited data used to develop the top voidage correlation. As mentioned earlier, the diameter of the largest experimental riser equipped with an abrupt exit is 0.152 m. Consequently, using the top voidage correlation for diameter larger than 0.15 m results in erroneous results.

The variation in apparent voidage with changes in solids mass flux is shown in Figure 5.15B. As reported earlier, the higher the solids mass flux the greater the solids holdup at any axial location along the riser. It should be noted that the apparent voidage is most sensitive to the solids mass flux at the lower regions of the riser. The figure shows that increasing the solids flux from 100 to 200 kg/(m^2•s) results in a 10% change in the voidage at the very bottom of the riser. In both the developed flow zone and the abrupt exit zone the change is approximately 1%. The large change in the bottom region of the riser is due to the region required to accelerate the solids. At a solids flux of 100 kg/(m^2•s), the acceleration zone is approximately 1 m, while at a solids flux of 150 kg/(m^2•s) the length of the acceleration region increases to 1.5 m. Finally, increasing the solids flux to a value of 200 kg/(m^2•s) leads to an acceleration zone of 2 m.
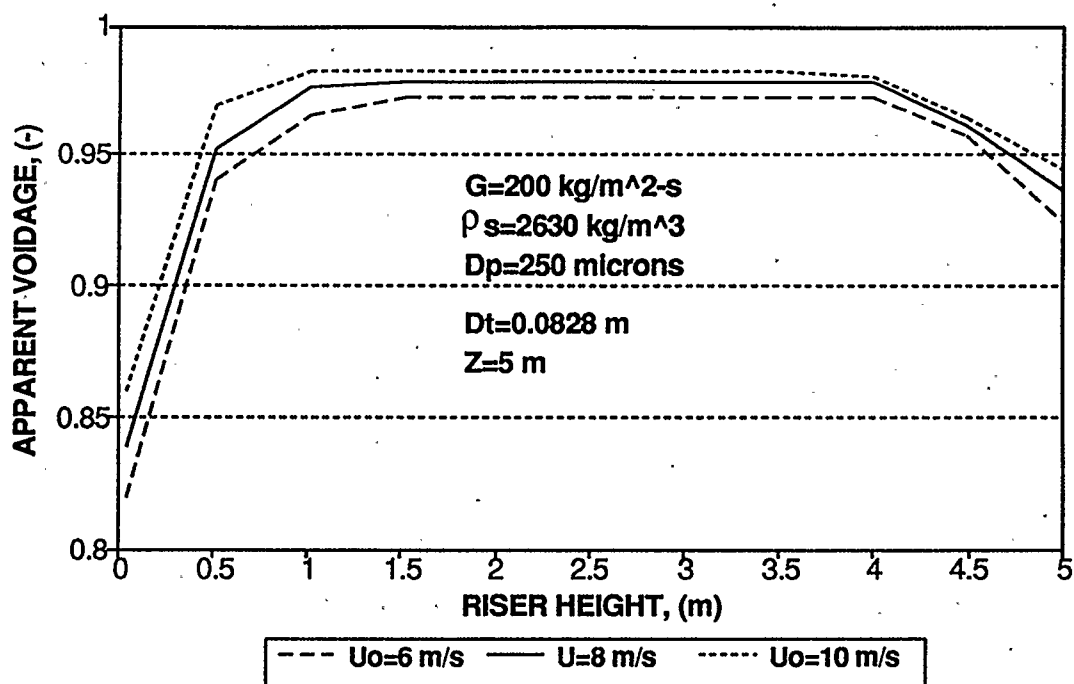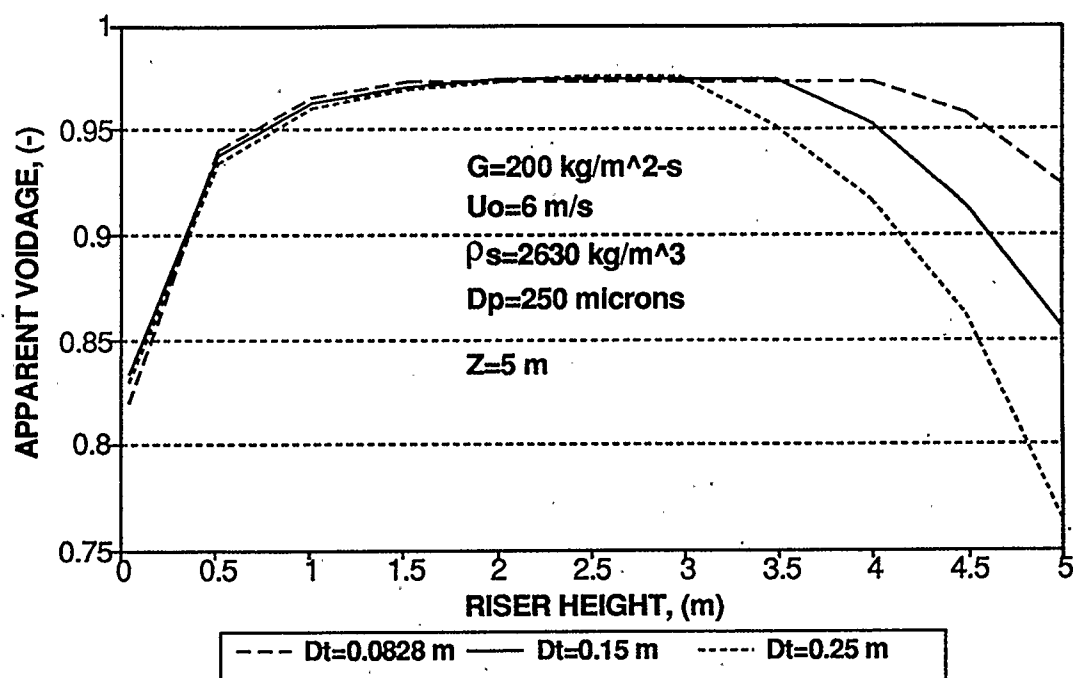
FIGURE 5.15A - PARAMETER ANALYSIS - SIMULATED EFFECT OF RISER
DIAMETER ON APPARENT VOIDAGE
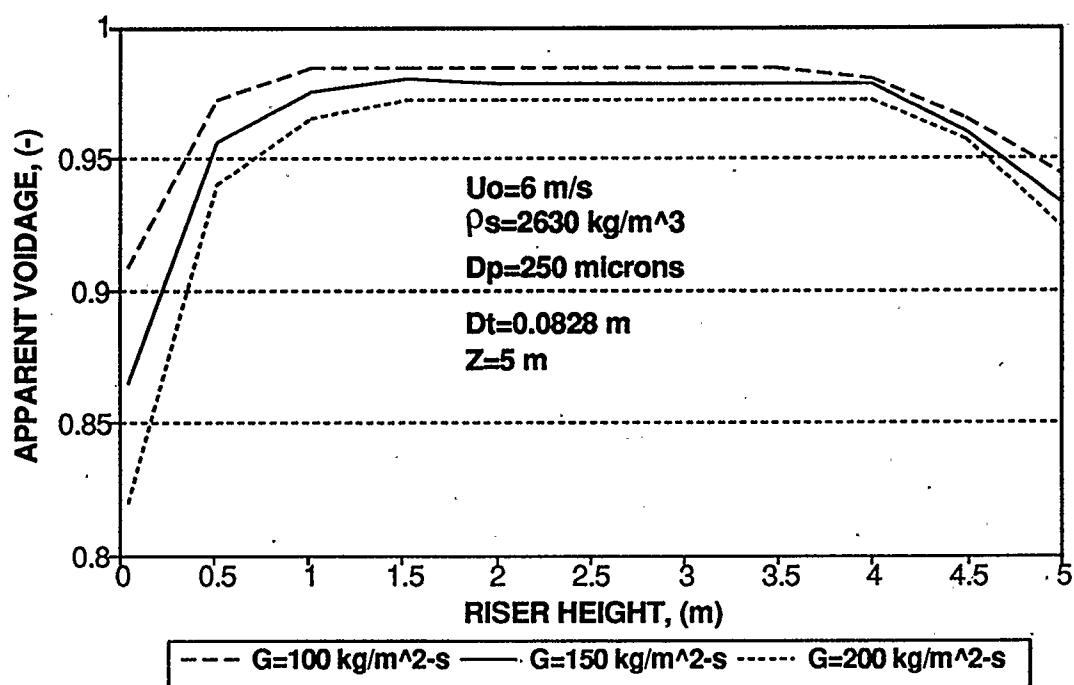
FIGURE 5.15B - PARAMETER ANALYSIS - SIMULATED EFFECT OF SOLIDS
MASS FLUX ON APPARENT VOIDAGE

CHAPTER 6
MODELLING OF SO_2 AND NO_x EMISSIONS FROM CFB COAL COMBUSTORS

6.1 INTRODUCTION

To illustrate an application of the proposed hydrodynamic model to reactor design, the model was used to simulate SO_2 and NO_x emissions from a CFB coal combustor. The burning of coal has widespread implications on society. As of 1989, 2777 billion kilowatt-hours of electrical power was generated in the United States, of which 56% was produced by burning coal, 19% from nuclear plants, 9.5% from hydroelectric sources, 9.5% from burning natural gas and the remaining 6% from petroleum, geothermal and other sources (Berruti and Wong, 1991). Unless there is a new economical way for producing energy, the usage of coal is expected to increase even more in the near future. As society increases its demand for technologically sophisticated products, which involve a lot more production steps, the amount of energy required to produce the products will undoubtedly increase. Moreover, coal accounts for approximately 85% of the potential U.S. fossil-fuel reserves and, as such, an increased exploitation would reduce the risk of a possible dependence on foreign fuel supplies. However, there are many environmental concerns associated with coal burning. Coal burning plants emit large quantities of sulfur dioxide, oxides of nitrogen and carbon dioxide that may fall back to the earth as acid rain and/or contribute to global warming. Of the various sources of air pollution in the U.S., coal-fired power plants contribute about 70% of the sulfur dioxide, 30% of the nitrogen oxides and approximately 35% of the carbon dioxide (Berruti and Wong, 1991). As environmental regulations become progressively stricter and coal consumption increases,

the popularity of CFB coal combustion technology has increased significantly over the last decade. According to Makansi and Schwieger (1987), out of 83 projects involving the combustion of coal, circulating fluidized bed are employed in 46 of the ventures. Furthermore, they say that many fluidized bed boilers suppliers have either eliminated the bubbling bed product line or have modified the boiler to approximate a CFB unit. Some of the attractive qualities of CFB coal combustors include a higher combustion efficiency which leads to more efficient coal usage and more environmentally friendly operation due to lower sulfur dioxide and nitrogen oxide emissions than conventional coal-fired furnaces or bubbling bed technologies.

6.2 CFB COAL COMBUSTOR

Figure 6.1 shows a schematic of a generic circulating fluidized bed combustor (CFBC) unit. The figure shows all of the parts that are typically employed in the design of a CFBC. The units include the fuel and sorbent preparation and feed systems, the fluidizing/combustion air supply, the combustion cell, the gas-solid separation devices and the convective pass system. The fuel and sorbent system consists of bins that store the fuel supply (in this case coal) and sorbents such as lime, limestone or dolomite which are used to control SO_2 emissions. Sometimes, the fuel and sorbents are larger than the design size and therefore, have to be "prepared" before they can be utilized in the CFBC. To help prepare the coal and sorbents, mechanical devices such as screw feeders are used to grind up the particles to the desired size. According to Stringer and Stallings (1991) of the Electric Power Research Institute, the coal feed size is typically less than 6 mm and
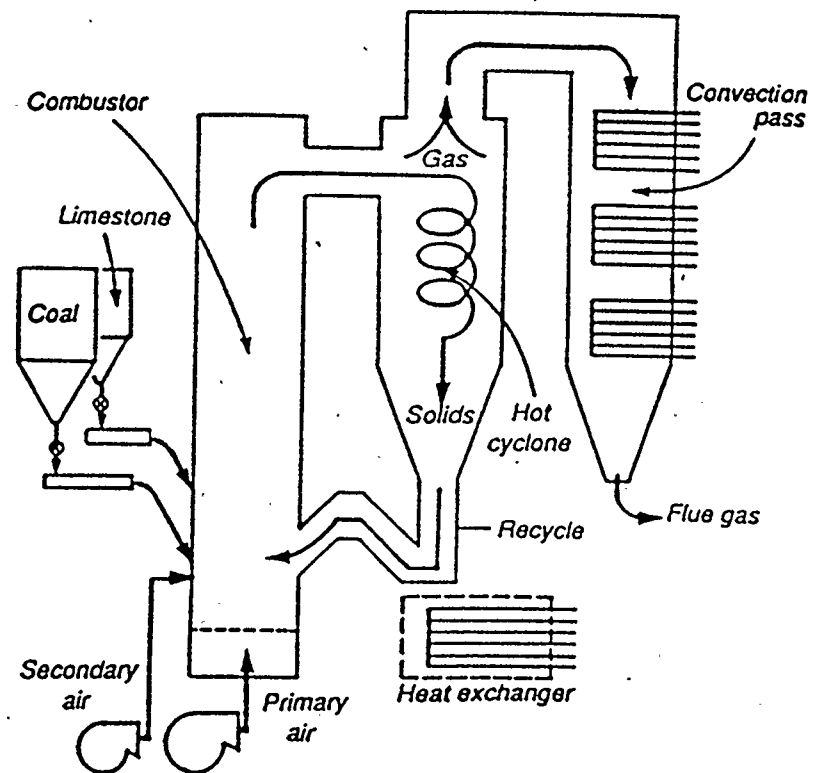
FIGURE 6.1 - SCHEMATIC OF GENERIC CIRCULATING FLUIDIZED BED COMBUSTOR (STRINGER AND STALLINGS, 1991)

sorbents such as limestone particles are usually less than 0.5 mm. However, it should be pointed out that the choice of solids size is dependent on the operating conditions of the CFBC and as mentioned by Makansi and Schwieger (1991) can vary widely from one CFBC supplier to another. The fuel and sorbents are usually fed separately into the combustor immediately above the distributor although, in some cases, to promote better mixing of the fuel and sorbent particles they are sometimes mixed before being sent into the combustor.

The fluidizing air system not only consists of the air required to maintain fast fluidization conditions in the combustor but also the air stoichiometrically required to carry out combustion. The fluidizing air system is set up so that staged combustion is possible. That is, the fluidizing/combustion air is usually split into two streams: a primary air stream containing between 50-70% of the stoichiometric requirements which is fed through the bottom of the riser and a secondary air stream added some distance up the riser. As will be explained later, staged combustion is primarily designed to minimize the formation of NO_x, although reducing the amount of combustion in the lower regions of the combustor provides a way to control heat release distribution. Air is also introduced into the recirculation leg to control solids flow and into the fuel and sorbent feed ports to prevent bridging in the feed lines. According to Grace (1990), superficial gas velocities in CFBCs typically range from 5-9 m/s.

The combustion cell or the riser is the part of a CFBC unit where the reactions associated with combustion occurs. The fluidized fuel and sorbent particles mix with an inert medium such as river sand and react with the oxygen in air to initiate coal

combustion and the reactions that result in the formation of NO_x and SO_2 emissions. According to Basu and Fraser (1991), the majority of solids within the riser is the inert medium. The fuel and sorbent particles make up only 1-3% of the total solids inventory within the combustion cell. According to Grace (1990) and Dry and La Nauze (1990), the net solids circulation rate within a CFBC unit is usually between 10 and 100 $kg/(m^2 \cdot s)$. The solids circulation rate is mainly determined by costs (Dry and La Nauze, 1990). Although higher solids circulation rates would lead to better gas-solid mixing and generally, a better combustion environment, the blowers required to provide the large volume of combustion air would become too costly. The purpose of the inert medium is to promote better mixing between the solids and to act like a thermal ballast which helps to help maintain both the axial and radial temperature approximately constant (Senior and Brereton, 1990; Zhao et al., 1989). The usual operating temperature of a CFB combustor is between 800-900°C. The operating temperature is a compromise between efforts to ensure high combustion efficiency which is a measure of carbon burnout and efforts to minimize air pollutants. Generally, the higher the operating temperature, the greater the combustion efficiency. However, high combustion temperature lead to high levels of NO_x and SO_2 emissions. The combustion cell is one of three areas within a CFBC system where heat removal occurs. Because of the high gas velocities found in CFBCs and the resulting erosion problems, it is not recommended that in-bed heat recovery tubes similar to those employed in bubbling bed combustors be used for heat exchange. Instead, heat exchange is accomplished by the use of water-cooled membrane walls surrounding the riser walls. To increase the available surface area

for heat exchange, the combustion cell is usually square in cross sectional area. According to Stringer and Stallings (1991), wing walls, which are vertical panels perpendicular to the wall and extending into the combustion cell have also been used for heat exchange purposes.

The gas-solids separation system consists of the cyclone(s) and the standpipe arrangement used to separate the solids and recycle them back to the base of the combustion cell. The cyclone(s) if integrated with the combustion cell and the water walls is known as a hot cyclone since it operates at approximately the same temperature as the combustion cell, thus enhancing the combustion efficiency of the process. The return of the solids from the bottom of the cyclone to the combustion cell is achieved through a vertical pipe with a turn at the bottom. The turn acts like a valve and is referred as a J-valve, L-valve or loop seal. Heat removal can also occur in the solids recirculation leg. The heat exchanger surrounded by the dashed box in Figure 6.1 can be placed in the recycle leg and used to cool the solid material coming from the gas-solid separation device. The heat exchanger in the recirculation leg is known as an external heat exchanger and is essentially a bubbling fluidized bed containing immersed tube bundles. According to Makansi and Schwieger (1987), one advantage of an external heat exchanger is its ability to help regulate the heat absorption rate in a CFBC. Sometimes, when the fuel type is changed or when the combustor is operated at part-load conditions, the absorption rate will change in the combustion cell. The overall absorption rate can be maintained constant by changing the operating conditions within the external heat exchanger.

The flue gas leaving the cyclone is cooled as it is directed through a convective heat transfer boiler known as the convective pass system. It is then sent through a baghouse or electrostatic precipitator to further remove any particulates before being released into the atmosphere.

6.2.1 COAL COMBUSTION

The combustion of coal is a very complicated process. Figure 6.2 shows the basic phenomena involved in coal combustion and the relative time to complete each step (Keairns et al., 1984). As the figure shows, coal combustion involves three steps: 1) heating of the coal particle to ignition temperature and vaporization of any trapped moisture, 2) pyrolysis or devolatilization of volatile matter and subsequent combustion of the volatiles outside the particle surface and 3) combustion of the remaining char particle.

Devolatilization involves breaking the weak carbon-carbon bonds found in coal. At temperatures around 350°C, the bonds break releasing aromatic hydrocarbons and gases. Many of the heavier hydrocarbons react with the coal and crack to yield lighter compounds and carbon. The devolatilization products subsequently diffuse through the internal pores of the coal particle and to the particle surface where the volatiles undergo combustion (Ehrlich, 1987).

Despite extensive research on coal devolatilization, reliable rate expressions for coal devolatilization in CFB coal combustors are not available (Rajan and Wen, 1980; Borghi et al., 1985; Stubington and Chan, 1988). In the present study, it is assumed that
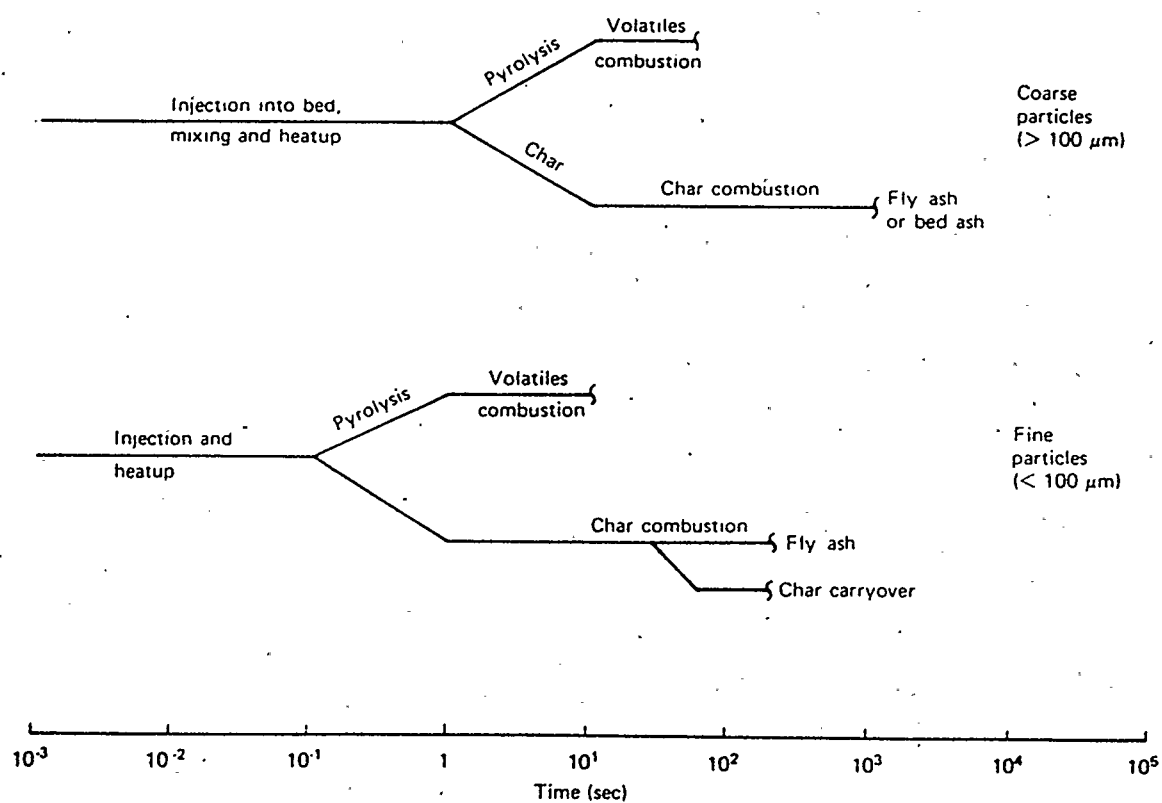
FIGURE 6.2 - STEPS IN COAL COMBUSTION (KEAIRNS ET AL., 1984)

the only devolatilization products are sulfur which is emitted as SO_2 and nitrogen which is emitted as NH_3. The weight fraction of sulfur released during the devolatilization process is estimated from (Fine et al., 1974)

$$X_s = 0.001\,T - 0.6 \qquad\qquad 6.1$$

where T is the temperature of the bed in Kelvin.

Similarly, the weight fraction of volatile nitrogen emitted during devolatilization (Fine et al., 1974) is

$$X_n = 0.001\,T - 0.06 \qquad\qquad 6.2$$

Although species such as methane, hydrogen, carbon dioxide, water and tar are also products of the devolatilization process, the lack of kinetic data makes an estimation of their composition extremely difficult. Any nitrogen or sulfur that is not released through the devolatilization process is assumed to be released during the char combustion process, at a rate proportional to the rate of char combustion.

Once devolatilization has occurred, a relatively porous and pure carbon particle called char remains. The type of coal, particle size, temperature, oxygen concentration and fluidizing characteristics are factors that influence the rate of combustion of char. According to Rajan and Wen (1980), the reaction describing the burning of residual char is given by

$$C + \frac{1}{\delta}O_2 \Rightarrow (2 - \frac{2}{\delta})CO + (\frac{2}{\delta} - 1)CO_2 \qquad 6.3$$
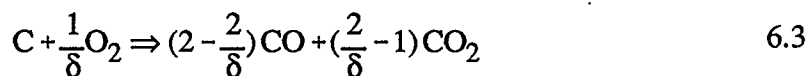
where δ is a mechanism factor which is a function of particle diameter and bed temperature and takes the value 1 when CO_2 is transported away from the char particle and 2 when carbon monoxide is transported away during char combustion (Field et al., 1967). According to Rajan and Wen (1980), with small particles, carbon monoxide formed during char combustion diffuses out fast because of rapid mass transfer whereas with large particles, because of the slow rate of mass transfer, carbon monoxide burns within the boundary layer of the particle. The parameter δ is expressed by

$$\delta = \frac{2p+2}{p+2}, \quad d_c < 0.005 \text{ cm} \qquad 6.4$$

$$\delta = \frac{(2p+2) - p(d_c - 0.005)/0.095}{p+2}, \quad 0.005 < d_c < 0.1 \text{ cm} \qquad 6.5$$

where d_c is the diameter of the char particle.

The parameter p in Equations 6.4 and 6.5 is defined as the ratio of carbon monoxide to carbon dioxide formed during char combustion and is expressed by Arthur (1951) as

$$p = 2500 \exp(-\frac{5.19 \times 10^7}{R'T}) \qquad 6.6$$

where R' is the universal gas constant and is equal to 8314 J/(kmol•K).

Reviews on char combustion have been presented by Mulcahy (1978), Essenhigh (1981) and Smith (1982). Because each coal type has a different composition and structure, the best way to model char combustion is to experimentally determine the

chemical reaction rate expression. Because experiments were not possible, the char combustion rate expression developed by Field et al. (1967) is used in the present reactor model simulation. The rate expression is given by

$$r_{char} = \pi d_c^2 k_c C_{O_2}$$

6.7

where k_c is defined as the overall rate constant and can be expressed as

$$k_c = \frac{R_g T}{\frac{1}{k_{cr}} + \frac{1}{k_{cd}}}$$

6.8

R_g is also the universal gas constant and is equal to 82.06 atm cm^3/(mol·K) and k_{cr} and k_{cd} are the chemical reaction rate and diffusion rate constants, respectively. The chemical reaction rate constant can be expressed as

$$k_{cr} = 8710 \exp\left(-\frac{1.497 \times 10^8}{R' T_c}\right)$$

6.9

while the diffusion rate constant can be expressed as

$$k_{cd} = \frac{24 \delta D}{d_c R_g T}$$

6.10

where D is the molecular diffusivity for oxygen-nitrogen and T_c is the char particle temperature which can be determined through a thermal balance over a char particle or from an experimentally determined expression. Very few studies under fast fluidization have been conducted to determine parameters such as the convective heat transfer coefficient or emissivity which are required to solve the particle thermal balance.

Furthermore, because the hydrodynamic conditions are vastly different, there is much conjecture as to whether correlations developed from bubbling bed studies can be used in situations involving fast fluidization conditions. In the present study, in order to get an estimate of the char particle temperature, the empirical correlation of Ross and Davidson (1981) is used:

$$T_c = T + 66000 C_{O_2} \qquad 6.11$$

where T_c is the char particle temperature in Kelvin and C_{O_2} is the molar concentration of oxygen in the combustion cell. The validity of the equation in CFBs was illustrated by Basu et al. (1981) who, using the Ross and Davidson (1981) correlation, was able to predict the burning rate of carbon particles in a circulating fluidized bed.

The carbon monoxide formed during char combustion can react with oxygen to produce carbon dioxide. That is,

$$CO + \frac{1}{2}O_2 \Rightarrow CO_2 \qquad 6.12$$

According to Hottel et al. (1965), the rate expression for the above reaction is

$$r_{CO} = 3 \times 10^{10} \left(\frac{P}{R_g T} \right)^{1.8} \exp\left(-\frac{6.699 \times 10^7}{R'T} \right) y_{H_2O}^{0.5} \, y_{CO} \frac{17.5 y_{O_2}}{1 + 24.7 y_{O_2}} \qquad 6.13$$

In the present reactor model simulation, it is assumed that char combustion can be represented by using a coal particle with a diameter equivalent to the Sauter mean diameter. It is postulated that the greater rate of combustion associated with smaller particles will be compensated by the slower combustion rate of larger particles. Through

contact with other particles and/or the walls of the combustion cell and possibly during devolatilizaton, attrition or breakup of the coal particles will occur. Because it is difficult to estimate the degree of attrition that occurs within the combustion cell, the effects of attrition is neglected in the reactor model.

6.2.2 SULFUR CAPTURE AND SO$_2$ EMISSIONS

The sulfur dioxide emitted during coal combustion comes from either the combustion of sulfur in pyrite (FeS$_2$) or from the sulfur contained in the organic molecules of the coal. Typically, coal may contain between 1 and 5% sulfur content. The release of SO$_2$ into the atmosphere is a major environmental and health concern. The SO$_2$ emissions can combine with water vapour to form solutions of sulfuric acid which are then washed out of the air during a rain or snowfall. Acid rain has been attributed to the destruction of numerous biological ecosystems and damage to the surface of buildings, cars and monuments.

Of all the schemes proposed for controlling the SO$_2$ emissions, addition of sorbents such as limestone (CaCO$_3$) or dolomite (CaCO$_3$·MgCO$_3$) into the combustion chamber to react chemically with SO$_2$ is the simplest and most direct. Sulfur capture with limestone or dolomite is a high temperature process. Calcination, which is the process by which limestone is converted to calcium oxide requires a temperature over 750°C. The resulting calcium oxide then reacts with SO$_2$ to form solid calcium sulfate which can be removed by electrostatic collectors, bag filters or simply drained from the bed. Depending upon its purity, the CaSO$_4$, better known as gypsum, can be used as a

soil stabilizer, a filler in concrete or a filler in drywall. The reaction of interest, between calcium oxide and SO_2 is as follows:

$$CaO(s) + SO_2(g) + \frac{1}{2}O_2(g) \Rightarrow CaSO_4(s) \qquad 6.14$$
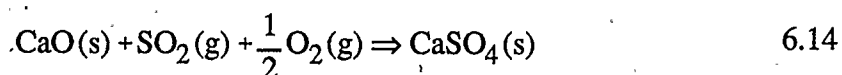
The reaction is an example of a non-catalytic gas-solid reaction. That is, a solid reactant (CaO) reacts with gases to produce another solid product. Since calcium sulfate ($CaSO_4$) has a larger molar volume than the original limestone, a product layer forms around the grains and pores of the sorbent and reaction eventually stops before all the limestone has reacted. Typically, only 50% of the limestone reacts and it must, therefore, be fed at a rate greater than the stoichiometric amount (Dry and La Nauze, 1990). The amount of limestone required is usually expressed in terms of the ratio of the amount of calcium in the limestone sorbent to the amount of sulfur in the coal. According to Dry and La Nauze (1990), typical Ca/S requirements in CFB combustors range from 2 to 4. Equipment needed is limited to conveyors for handling the sorbent, pulverizers for reducing the size of the sorbent, a system for injecting the sorbent into the reactor and means of removing the solid product.

Over thirty models have been proposed in the literature to describe the SO_2 - CaO reaction. An excellent review of the models has been given by Dogu and Dogu (1991). The particle-pellet or the grain model as applied by Hartman and Coughlin (1976) to sulfur capture is used in the proposed CFB coal combustor model. According to the grain model, a porous particle is comprised of spherical grains of uniform size separated by pores through which the reacting gases diffuse. A shell of the reaction product is formed

on the surface of the grains as the reaction proceeds. The product layer increases to a point where the pores between the grains become plugged and the reaction stops.

According to Wen (1968), the rate at which the reaction layer moves is small with respect to the rate of transport of SO_2. Consequently, the transport of sulfur dioxide within a spherical pellet of lime can be described utilizing the pseudo steady state approximation. Assuming a spherical limestone pellet, the transport of SO_2 within the pellet can be described by

$$\frac{1}{R_p^2}\frac{\partial}{\partial R_p}\left(D_{eff}R_p^2\frac{\partial C}{\partial R_p}\right) - r_{SO_2} = 0 \qquad 6.15$$

where R_p is the pellet radius, r_{SO_2} is the rate at which sulfur dioxide reacts within the pellet and D_{eff} is the effective diffusivity in the pores of the limestone pellet. The boundary conditions for Equation 6.15 are

$$C = C_o \text{ at } R_p = R_{po} \qquad 6.16$$

and

$$\frac{\partial C}{\partial R_p} = 0 \text{ at } R_p = 0 \qquad 6.17$$

In Equation 6.16, it is assumed that, because of the high slip velocity between solid and gas, a film does not develop around the particle and consequently, there is no external film resistance. The boundary condition of Equation 6.17 is simply the condition of symmetry for a spherical particle.

The effective diffusivity can be calculated from

$$D_{eff} = D\varepsilon_x \qquad 6.18$$

where D is the molecular diffusivity of SO_2 in the limestone particle and ε_x relates the porosity of the reacting particle and the progress of the sulfation reaction.

From the experiments of Hartman and Coughlin (1974), ε_x is given by

$$\varepsilon_x = 1 - (1-\varepsilon_{ls})\left(\frac{\rho_{ls}y}{mw_{CC}}[V_{CO} + (1 - \frac{r_g^3}{r_{go}^3})(V_{CS} - V_{CO})] - (1-y)\frac{\rho_{ls}}{\rho_{CC}} \right) \qquad 6.19$$

where ε_{ls} is the porosity of natural limestone, y is the content of calcium carbonate in limestone, ρ_{ls} and ρ_{CC} are the density of limestone and calcium carbonate, respectively, and V_{CO} and V_{CS} are the molar volumes of calcium oxide and calcium sulfate. The densities and molar volumes, as well as the magnitude of y, can be obtained through experiments.

If it is assumed that the reaction between the gas and grains is first order with respect to sulfur dioxide, the rate at which sulfur dioxide reacts within the pellet can be expressed as (Hartman and Coughlin, 1976)

$$r_{SO_2} = 3(1-\varepsilon_{lsc})\frac{r_g^2}{r_{go}^3}k_{SO_2}C_c \qquad 6.20$$

where ε_{lsc} is the porosity of calcined limestone, r_g is the radius of the reaction interface within a spherical grain, r_{go} is the initial grain radius, k_{SO_2} is the chemical reaction rate constant per unit area of reaction interface and C_c is the concentration of SO_2 at the reaction interface within a grain. The term $3(1-\varepsilon_{lsc})r_g^2/r_{go}^3$ converts the reaction rate constant from a per unit surface area basis to a per unit volume pellet basis.

The chemical reaction rate constant is specific to each type of sorbent. As shown by Borgwardt and Harvey (1972), physical properties such as grain size-distribution or crystal structure and chemical composition of the original rock can greatly affect the reaction rate constant. The grain size distribution affects the ease with which SO_2 can diffuse within a pellet, while certain chemicals such as sodium or potassium may retard absorption because they occlude or obstruct reactive surfaces (Makansi and Schwieger, 1987). Thus, to rigorously and properly model sulfur capture with limestone particles, experiments must be conducted to determine the chemical reaction rate. In the proposed simulation, the kinetic data obtained by Hartman and Coughlin (1976) is used.

Assuming that the unreacted shrinking core model can be applied to a spherical grain, C_c, the SO_2 concentration at the reaction interface within a grain can be determined. The concentration of SO_2, C_{pl}, at any radial location r_{pl} in the product layer can be determined from

$$\frac{\partial^2 C_{pl}}{\partial r_{pl}^2} + \frac{2}{r_{pl}} \frac{\partial C_{pl}}{\partial r_{pl}} = 0 \qquad\qquad 6.21$$

with the following boundary conditions:

$$C_{pl} = C(R_p) \text{ at } r_{pl} = r_{go} \qquad\qquad 6.22$$

$$D_s \left(\frac{\partial C_{pl}}{\partial r_{pl}} \right)_{r_{pl} = r_g} = k_{SO_2} C_c \qquad\qquad 6.23$$

where D_s is the solid product layer diffusivity.

Integration of Equation 6.21 with the boundary conditions shown in Equations 6.22 and

6.23 yields

$$C_c = \frac{D_s C}{D_s + k_{SO_2} r_g (1 - \dfrac{r_g}{r_{go}})}$$

6.24

The rate at which the reaction interface moves inward may be expressed by

$$\frac{\partial r_g}{\partial t} = -\frac{k_{SO_2}}{\rho} C_c \quad \text{for } r_g > 0$$

6.25

where ρ is the molar density of calcium oxide.

The boundary and initial conditions for Equation 6.25 are

$$r_g = r_{go} \quad \text{at } t = 0$$

6.26

and

$$\frac{\partial r_g}{\partial t} = 0 \quad \text{at } r_g = 0$$

6.27

The grain (local) and pellet (overall) calcium oxide conversion per pellet can be expressed in terms of the position of the reaction interface. The local conversion is given by

$$X_L = 1 - \frac{r_g^3}{r_{go}^3}$$

6.28

while the overall conversion is calculated by

$$X_O = \frac{3}{R_p^3} \int_0^{R_{po}} R_p^2 (1 - \frac{r_g^3}{r_{go}^3}) dR_p \qquad \text{6.29}$$

Equations 6.15 to 6.29 describes the concentration profile within a spherical limestone pellet, position of the reaction interface within the individual grains of the limestone pellet and the local and overall calcium oxide conversion per pellet during the reaction. The solution to the sulfur capture problem involves the solution of Equations 6.15 and 6.25. The equations can be discretized and solved in an semi-implicit manner. At t=0, the grain reaction interface is equal to the grain radius and the concentration of SO_2 at each grid point in the limestone pellet is known. Thus, Equation 6.25 can be solved to yield the reaction front position at time step t+1. Knowing the reaction front position at each grid point, the method of lines can be used to solve Equation 6.15 implicitly to determine the SO_2 concentration profile within the pellet at time step t+1. The SO_2 concentration profile is updated and the entire procedure is repeated again.

6.2.3 NO$_x$ EMISSIONS

Nitrogen oxides (NO_x) emitted from the burning of coal include nitrous oxide (N_2O), nitrogen dioxide (NO_2) and nitric oxide (NO). Furthermore, when air is heated to elevated temperatures, oxygen and nitrogen can dissociate to their atomic forms and recombine to form thermal NO_x. There is a considerable amount of evidence indicating that nitrogen oxides are deleterious components of air pollution (Sticksel and Engdahl, 1984). The presence of smog creates significant respiratory problems for people suffering

from bronchitis, emphysema or asthma. Nitrogen oxides can cause fading of textiles and weaken metals by the formation of acids. Combination of water with nitrogen oxides can lead to the formation of nitrous and nitric acid which contribute to acid rain. Furthermore, nitric oxides such as nitrous dioxide can react with ozone in the upper atmosphere (stratosphere) to cause a reduction in ozone concentration (Moritomi et al., 1991; Wojtowicz et al., 1991). Changes in the ozone concentration in the upper atmosphere would alter the quantity of ultraviolet radiation reaching the earth's surface and can subsequently lead to global warming. Recently, reductions in stratospheric ozone, which acts to protect the earth from harmful solar radiation have been linked to increased cases of skin cancer.

Many methods have been devised for controlling the formation of NO_x emissions during coal combustion. Examples include ammonia and/or urea injection and thermal deNO$_x$ procedures. A review of the various emission control strategies is given by Berruti and Wong (1991). Staged combustion is one of the most popular methods. Air staging aims at reducing NO_x emissions by capitalizing on the enhanced NO_x destruction that occurs under sub-stoichiometric conditions. All the coal is injected into the primary stage so that the bed is maintained at or near sub-stoichiometric conditions creating NO_x reduction. Partial combustion of coal in the reducing environment produces carbon monoxide and char, which tends to reduce NO_x by the following reactions:

$$NO + CO \Rightarrow \frac{1}{2}N_2 + CO_2 \qquad\qquad 6.30$$

and

$$NO + C \Rightarrow \frac{1}{2}N_2 + CO \qquad\qquad 6.31$$

According to Ehrlich (1987), in a fluidized bed coal combustion system there are five mechanisms responsible for NO_x formation and four mechanisms for NO_x reduction. The NO_x formation mechanisms are 1) reactions of atmospheric nitrogen and oxygen to form thermal NO_x, 2) reaction of atmospheric nitrogen and oxygen via a solids intermediate such as calcium cyanimide (CaNCN), 3) reaction of organic nitrogen with air via a solid intermediate, 4) reaction of organic nitrogen directly with air and 5) reaction of volatiles with air via a gaseous intermediate such as hydrogen cyanide (HCN). The mechanisms responsible for the destruction of NO_x include 1) reaction with char to form carbon monoxide, carbon dioxide or nitrogen, 2) reaction with gaseous intermediates such as NH_2, 3) reaction with hydrocarbon volatiles and 4) reaction via a heterogeneous catalyst. Direct reaction of organic nitrogen with air is the most likely NO_x formation mechanism whereas reaction with char to form carbon dioxide appears to be the most favourable destruction route. Other NO_x formation and reduction pathways have been proposed by Gibbs and Hampartsoumian (1984), Furusawa et al. (1985), Johnsson (1989), Wojtowicz et al. (1991) and Moritomi et al. (1991).

Unlike the many mechanisms that have been proposed for the formation and destruction of NO_x, the number of studies that have been conducted to determine NO_x kinetic information has been very limited. Johnsson (1989) developed a kinetic model to describe NO_x formation in a bubbling bed combustor. Using kinetic data reported in literature, Johnsson (1989) concluded that the majority of the kinetic data could not be

used with respect to modelling NO_x formation in a bubbling bed combustor. Most of the kinetic rate expressions were developed outside the operating conditions (temperature and concentration) typically encountered in fluidized bed combustion, and many of the reaction rate expressions were derived from different types of coal. In order to properly model NO_x formation, the kinetic data should be derived from the same coal type under the proper operating conditions. As indicated by Ishizuka et al. (1988), Mulcahy and Smith (1969) and Tsuoboi and Iwasaki (1988), coal composition and type has a large impact on NO_x formation. For example, bituminous coal particles combust three to six times faster than an anthracite coal particle of equivalent size (Mulcahy and Smith, 1969) and hence can result in a greater degree of NO_x emissions in a given time interval. Although Kramlich et al. (1989) and Kilpinen and Hupa (1990) have proposed kinetic models for the homogeneous formation of N_2O and kinetic studies have been done by Miller and Bowman (1988), there is still no conclusive picture on N_2O formation and destruction mechanisms.

The intrinsic kinetic data obtained by Johnsson and Dam-Johansen (1991) is used in the present work to model the formation and reduction of NO_x in a CFB combustor. Their experimental study focused only on the heterogeneous reduction of NO and oxidation of NH_3 to NO. As a result, the proposed simulation only looks at the NO form of NO_x emissions and involve only coal types similar to the ones used by Johnsson and Dam-Johansen (1991). It is assumed that thermal NO formed from the oxidation of molecular nitrogen has only minor significance in a CFB coal combustor. Studies by Furusawa et al. (1978), Pereira et al., (1974) and Bonn and Richter (1990) have validated

this assumption. Table 6.1A, 6.1B and 6.1C show the NO forming and reducing reactions considered in the present simulation along with their corresponding rate expressions. It should be pointed out that intrinsic kinetic rate data do not take into account intraparticle or interparticle effects. The overall kinetic rate expression can be severely affected by the degree of interparticle or intraparticle resistance. As with bubbling beds, because of the high degree of gas-solid mixing, it is assumed that interparticle resistance is negligible. To determine the degree of intraparticle resistance, the effectiveness factor is calculated. Assuming a spherical pellet and a first order irreversible reaction, the effectiveness factor is given by

$$\eta = \frac{1}{\psi}\left(\frac{1}{\tanh(3\psi)} - \frac{1}{3\psi}\right) \qquad 6.32$$

where ψ is the Thiele modulus.

The Thiele modulus is given by

$$\psi = \frac{R_{sol}}{3}\sqrt{\frac{k_v}{D_{eff}}} \qquad 6.33$$

where R_{sol} is the radius of the solid particles, k_v is the volumetric reaction rate constant for a first order irreversible reaction and D_{eff} is the effective solid diffusivity.

D_{eff} can be determined experimentally or from one of the many models available in literature. The evaluation of k_v is more difficult since most reaction rate expressions are not first order. In order to estimate k_v, the half life was calculated for each of the reactions that were not first order. Then, assuming a pseudo first order reaction, the half life is evaluated and used to back calculate the pseudo first order reaction rate constant.

TABLE 6.1A - SUMMARY OF REACTIONS USED IN REACTOR MODEL

REACTION 1:

$$C + \frac{1}{\delta}O_2 \Rightarrow (2 - \frac{2}{\delta})CO + (\frac{2}{\delta} - 1)CO_2$$
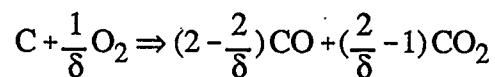
$$-r_1 = -r_{char} = \pi d_c^2 k_c C_{O_2}$$

where $-r_1$ is in gmol/(s•particle) and k_c is from Field et al. (1967)

REACTION 2:

$$CO + \frac{1}{2}O_2 \Rightarrow CO_2$$
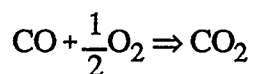
$$-r_2 = -r_{CO} = k_{12}y_{H_2O}^{0.5} y_{CO} \frac{k_{22}y_{O_2}}{1 + k_{32}y_{O_2}}$$

where $-r_2$ is in gmol/(cm^3•s) and k_{12}, k_{22} and k_{32} are from Hottel et al. (1965)

REACTION 3:

$$NO + C \Rightarrow \frac{1}{2}N_2 + CO$$
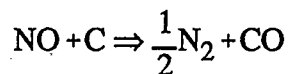
$$-r_3 = -r_{NO} = \frac{k_{13}k_{33}C_{NO}}{k_{13}C_{NO} + k_{33}}$$

where $-r_3$ is in kmol/(kg•s) and k_{13} and k_{33} are from Johnsson and Dam-Johansen (1991)

TABLE 6.1B – SUMMARY OF REACTIONS USED IN REACTOR MODEL

REACTION 4:

$$NO + CO \Rightarrow \frac{1}{2}N_2 + CO_2$$
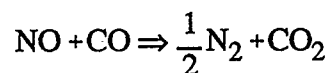
with char and bed material as catalyst

$$-r_4 = -r_{NO} = \frac{k_{14}C_{NO}[k_{24}C_{CO} + k_{34}]}{k_{14}C_{NO} + k_{24}C_{CO} + k_{34}}$$

where $-r_4$ is in kmol/(kg•s) and k_{14}, k_{24} and k_{34} are from Johnsson and Dam-Johansen (1991)

REACTION 5:

$$NO + \frac{2}{3}NH_3 \Rightarrow \frac{5}{6}N_2 + H_2O$$
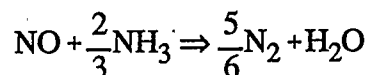
with char and bed material as catalyst

$$-r_5 = -r_{NO} = k_5 C_{NO}^{a5} C_{NH_3}^{b5}$$

where $-r_5$ is in kmol/(kg•s) and k_5, a5 and b5 are from Johnsson and Dam-Johansen (1991)

REACTION 6:

$$NH_3 + \frac{5}{4}O_2 \Rightarrow NO + \frac{3}{2}H_2O$$
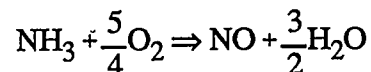
with CaO as catalyst

$$-r_6 = -r_{NH_3} = k_6 C_{NH_3}^{a6} C_{O_2}^{b6}$$

where $-r_6$ is in kmol/(kg•s) and k_6, a6 and b6 are from Johnsson and Dam-Johansen (1991)

TABLE 6.1C - SUMMARY OF REACTIONS USED IN REACTOR MODEL

<u>REACTION 7:</u>

$$2NH_3 + \frac{3}{2}O_2 \Rightarrow N_2 + 3H_2O$$
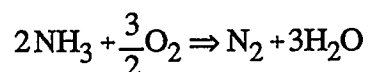
with char catalyst

$$-r_7 = -r_{NH_3} = k_7 C_{NH_3}^{a7} C_{O_2}^{b7}$$

where $-r_7$ is in kmol/(kg•s) and k_7, a7 and b7 are from Johnsson and Dam-Johansen (1991)

<u>REACTION 8:</u>

$$CaO(s) + SO_2(g) + \frac{1}{2}O_2(g) \Rightarrow CaSO_4(s)$$
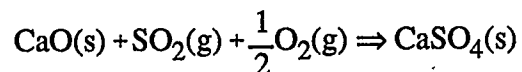
$$-r_8 = -r_{SO_2} = 3(1 - \varepsilon_{lsc}) \frac{r_g^2}{r_{go}^3} k_{SO_2} C_{SO_2}$$

where $-r_8$ is in gmol/(cm^3•s) and k_{SO_2} is from Hartman and Coughlin (1976)

For a first order irreversible reaction, the half life is related to the rate constant by

$$t_{0.5} = \frac{\ln(2)}{k_v}$$
6.34

If the effectiveness factor is close to one, then there is no intraparticle resistance whereas if the effectiveness factor is close to zero, then there is a significant amount of intraparticle resistance.

6.3 REACTOR MODEL

The solids holdup along the CFB combustor is obtained from the proposed hydrodynamic model described earlier in this work. Although the hydrodynamic model was developed with data from experimental CFB units at room temperature, it is assumed that the axial voidage profile can be applied to units that operate typically between 800-900°C. Increasing the operating temperature as shown by Senior and Brereton (1990) causes a reduction in gas viscosity and would lower the axial solids holdup. The lower gas viscosity makes it easier for the solids to move through the riser. The proposed reactor model described in the following paragraphs only qualitatively describes the SO_2 and NO emissions from a CFB coal combustor. There is not enough information available in literature to quantitatively model the emissions from an actual industrial or experimental CFB unit. The kinetic information pertaining to the coal and sorbent type used in CFB units are usually not given and, at this point in time, only some of the reactions responsible for NO_x formation and reduction are known. For example, although HCN is known to play an important role in NO_x formation, there is no kinetic

information available (Johnsson, 1989).

It is assumed that all chemical reactions considered in Tables 6.1A, 6.1B and 6.1C occur only in the core region of the riser. The assumption follows from the development of the hydrodynamic model; the majority of gas is assumed to go only through the centre region of the riser. In addition, the flow and quantity of gas and solids in the recirculation leg and in downstream equipment is not known and as a result, it is hard to estimate what reactions are possible and to what extent the reactions can occur.

As shown by Rhodes (1989) and Bader et al. (1988), the flow of gas in the core region can be approximated as plug flow. Furthermore, studies by Senior and Brereton (1990) and Zhao et al. (1989) have shown that there is very little radial or axial variation of temperature in the riser of a CFB combustor. Assuming the gases to be flowing in plug flow and assuming isothermal conditions, material balances can be written for each component in the system. The plug flow reactor design equation, for homogeneous reactions, can be expressed as

$$\frac{dF_i}{dV} = \sum r_i \varepsilon \qquad 6.35$$

where V is the volume of the reactor, F_i is the molar flowrate of species i, ε is the voidage, r_i is the reaction rate based on unit volume of reactor and referenced with respect to species i. The summation in Equation 6.35 is carried out over all reactions involving species i in the system.

Because chemical reactions are assumed to occur only in the core region of the riser, the volume of the reactor is determined from the core radius obtained from the

hydrodynamic model and, by similar reasoning, the voidage term refers to the core voidage.

For heterogeneous reactions, the corresponding plug flow reactor design equation is given by

$$\frac{dF_i}{dV} = \sum r_i^* (1-\varepsilon) \rho_{bulk} \eta \qquad 6.36$$

where r_i^* is the reaction rate based on a unit mass of catalyst and ρ_{bulk} is the bulk density of the catalyst, which is used to convert the reaction rate to a reactor volume basis. As an illustration of the plug flow design equation, the following is a material balance for NO:

$$\frac{dF_{NO}}{dV} = -r_3 - r_4 - r_5 + r_6 + (1-X_n)\frac{wf_n mw_c}{wf_c mw_n} r_1 \qquad 6.37$$

where the r_i's are the reaction rates based on NO as illustrated in Tables 6.1A, 6.1B and 6.1C and have been converted to a reactor volume basis. The last term in Equation 6.37 represents the amount of nitrogen that is converted to NO through char combustion. The quantities wf_n, wf_c are the weight fractions of nitrogen and coal, determined from the ultimate coal analysis, while mw_n and mw_c are the molecular weights of nitrogen and coal. X_n is the fraction of coal released through the devolatilization process. The last term of Equation 6.37 indicates the rate of release of nitrogen into NO from char combustion is such that the ratio of nitrogen to carbon always remain the same. Similar balances can be written for oxygen, nitrogen, carbon monoxide, carbon dioxide, water, sulfur dioxide and ammonia. Knowing the initial concentration of each species, the

material balances can be solved to yield the concentration profiles of each species along the riser.

Table 6.2 shows the typical physical parameters and operating conditions arbitrarily chosen for the proposed reactor model. It should be pointed out that quantities such as riser diameter, solids circulation rate and superficial gas velocities are limited by the range of operating conditions over which the hydrodynamic model can be applied.

6.4 REACTOR MODEL SOLUTION METHOD

In order to solve the reactor model, the proposed hydrodynamic model must be solved simultaneously with the reactions associated with coal combustion, sulfur capture and NO formation and reduction. First, knowing the operating temperature, the reaction rates and the density and concentration of each species in the system can be calculated. Then, the inlet molar calcium-to-sulfur ratio and primary air ratio are chosen so that the limestone, coal feedrate and superficial gas velocity can be determined. As mentioned earlier, the amount of coal and limestone is much smaller than the amount of sand in the system. Consequently, the properties of the sand are used to determine the initial hydrodynamic structure. The main iteration loop is then started. The solids core velocity is known from the hydrodynamic model and can be combined with the solids flowrate to determine the solids residence time between two consecutive grid points. The sulfur capture subroutine is then called to determine the calcium oxide conversion per pellet. The conversion can be converted to a mass basis knowing the density of calcium oxide and the dimensions of the limestone particle. Using the initial species concentration at

TABLE 6.2 - SUMMARY OF PARAMETERS USED IN REACTOR MODEL

Coal Composition		Sulfur Capture Model Constants	
Component	**wt%**	$CaCO_3$ density, ρ_{CC}, kg/m^3	2710
carbon	71.80	$CaCO_3$ content, y, (-)	0.982
sulfur	0.39	molar volume-CaO, V_{CO}, m^3/mol	16.9×10^{-6}
nitrogen	1.00	molar volume-$CaCO_3$, V_{CC}, m^3/mol	52.2×10^{-6}
hydrogen	3.70	weight fraction-CaO wf_{CaO}, (-)	0.55
oxygen	12.51	product layer diffusivity, D_s, m^2/s	6×10^{-13}
ash	9.90	limestone diffusivity, D, m^2/s	7.5×10^{-6}
		limestone porosity, ε_{ls}, (-)	0.
Coal Physical Properties		calcined limestone porosity, ε_{lsc}, (-)	0.52
diameter, dp_c, mm	1.5-3.5	initial grain size, r_{go}, m	1×10^{-7}
density, ρ_c, kg/m^3	1500		
effective diffusivity, De_{char}, m^2/s	1×10^{-5}	**Reactor Operating Conditions**	
		solids circulation rate, G, $kg/(m^2 \cdot s)$	50-100
Limestone Physical Properties		superficial gas velocity, U_o, m/s	6-12
diameter, dp_{ls}, mm	1.2-5	riser diameter, D_t, m	0.1-0.6
density, ρ_{ls}, kg/m^3	2710	riser height, Z, m	5-8

grid point i, the reaction rate expressions can be solved to yield the reaction rate. The effectiveness factor is also calculated to determine the effect of intraparticle resistance on the reaction rates. The mass balances obtained from the plug flow reactor design equation (in either the homogeneous or heterogeneous form) are then solved to yield the flowrates and subsequently concentration, mole or mass fractions at the next grid point i+1. The flowrate of the individual species are added together to determine the new superficial gas velocity which if different, is used to update the hydrodynamic flow structure. If the grid point corresponds to the location where secondary air is added, then the additional amount of oxygen and nitrogen are added to the material balances before the hydrodynamic flow structure is updated. The procedure is repeated until the end of the riser is reached.

6.5 REACTOR MODEL RESULTS

The simulation results from the proposed reactor model are shown in Figures 6.3 through 6.9. As mentioned earlier, the simulation results from the proposed reactor model are only qualitative results. The omission of reactions pertaining to the formation and reduction of NO_2, N_2O and hydrocarbons means that the model cannot be used to fully simulate an actual CFB combustor. Furthermore, reactions in the cyclone, standpipe and in the downstream separation devices (baghouse) were assumed to be negligible. Depending upon the extent to which reactions occur in these units, the emission out of the CFB combustor can be significantly different from those out of the top of the riser. Figure 6.3 shows the effect of excess air on NO and SO_2 emissions for two molar Ca/S ratios while Figure 6.4 shows the effect of staged combustion on the same emissions.

The excess air refers to the amount of air required not only to fluidized the bed of solids but also the reactions associated with coal combustion, sulfur capture and NO forming and reducing reactions. Figure 6.3 shows that in the case of NO emissions, the greater the quantity of excess air, the greater the NO emissions. The effect is partly due to the fact that the large concentration of oxygen associated with the higher excess air values increases the extent to which NO forming reactions occur. Studies by Hiltunen and Tang (1988), Tsuboi and Iwasaki (1988) and Brown and Muzio (1991) have shown that oxidizing conditions drastically increase the amount of NO_x emissions in both experimental and industrial sized CFB combustors. The effect is also due to the larger degree of combustion that occurs at higher excess air levels. Experimental studies by Salim et al. (1989) and Lee et al. (1984) have shown that combustion efficiency, which is a measure of carbon burnout, increases with increasing excess air ratios. The higher combustion efficiencies indicate that the coal burns to a greater degree and hence the NO contribution from char combustion also increases. It is interesting to note that at excess air levels greater than 1.4, NO is formed to a greater extent than at lower excess air values (change in slope). A possible explanation for the increased NO formation could be that for the given simulation conditions, the amount of oxygen available is such that there is an enhanced degree of coal combustion. It should also be pointed out that the higher the excess air level the greater the gas velocity and the shorter the gas residence time within the riser. Theoretically, the decrease in gas residence time combined with the lower solids concentration due to the higher gas velocity should decrease the rate of any chemical reaction. However, based on the NO emission results shown in Figure 6.3, it
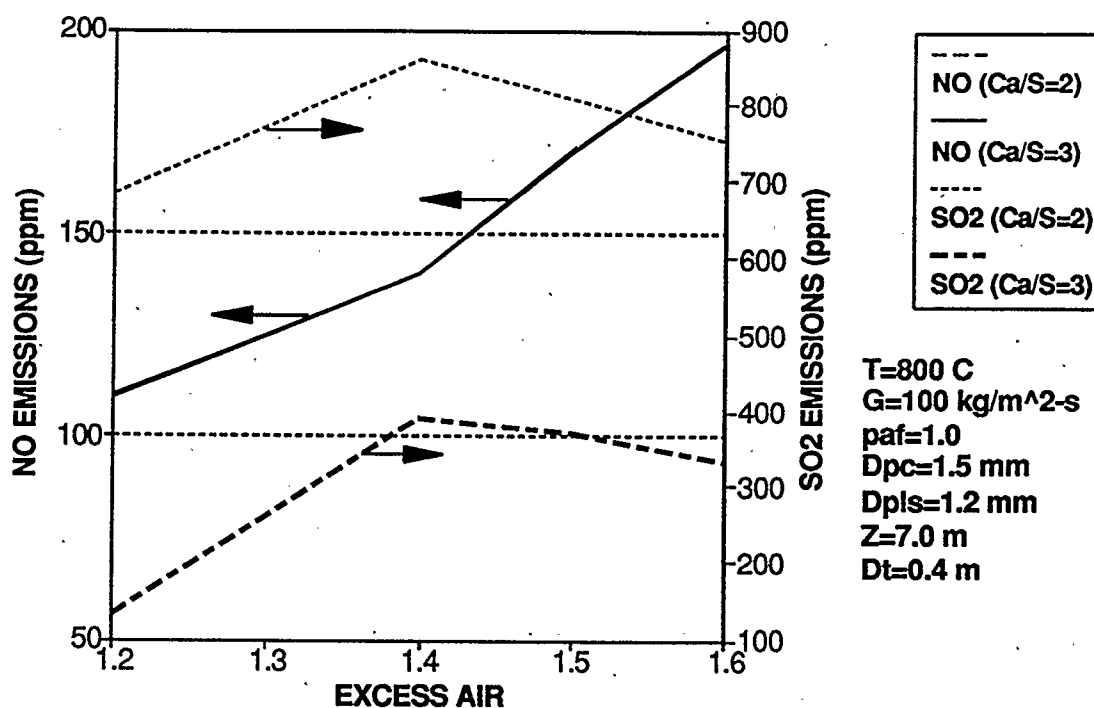
FIGURE 6.3 - EFFECT OF EXCESS AIR ON NO AND SO2 EMISSIONS
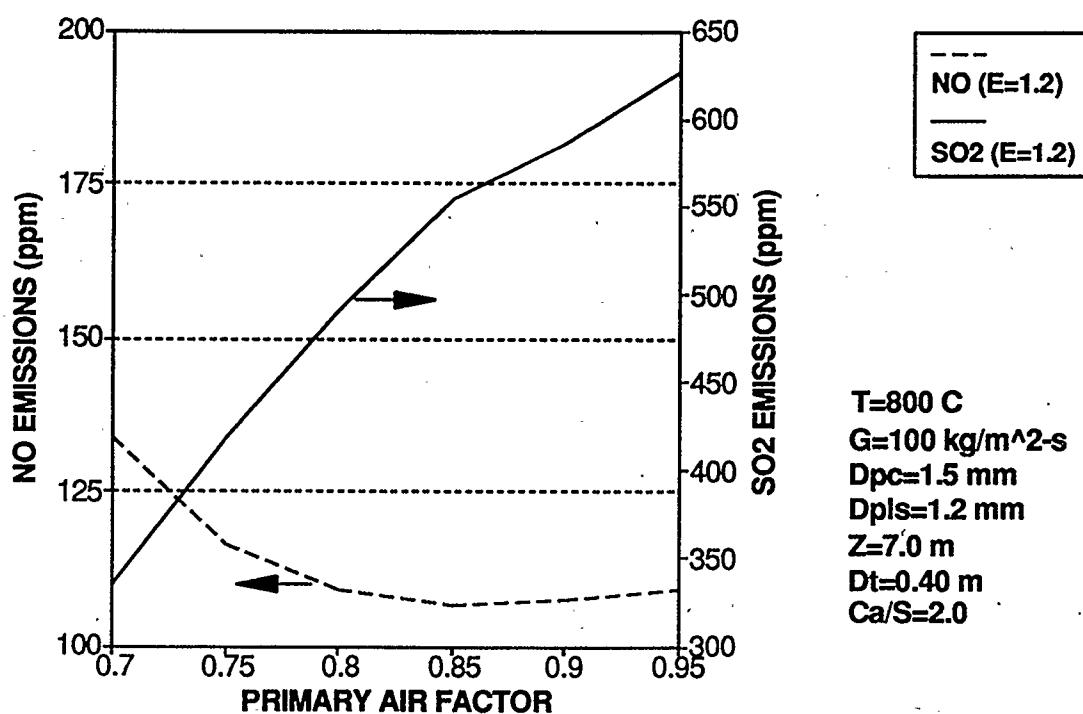
FIGURE 6.4 - EFFECT OF PRIMARY AIR FACTOR ON NO AND SO2 EMISSIONS

appears that increasing the amount of oxygen has a more dominant effect on NO emission than a reduction in gas residence time. The figure further shows that for the simulated operating conditions, the molar Ca/S ratio does not seem to affect the NO emissions. Examination of the data used to develop Figure 6.3 indicates that NO emissions actually increase with molar Ca/S ratio although the difference is small. For example, at an excess air level of 1.2 and a Ca/S ratio of 2, the simulated NO emission at the top of the riser is 109.78 ppm while at the same excess air level and at a Ca/S ratio of 3, the NO emission is 109.88 ppm. Reports by Dry and La Nauze (1991), Schaub et al. (1989) and Lin and van den Bleek (1990) have indicated strong interactions between sulfur capture and NO_x emissions in CFB combustors. The difference between the simulated and experimental results could be attributed to the omission of key reactions responsible for NO_x and SO_2 interaction in the reactor model. A more detailed discussion on the effect of limestone on NO emissions will be provided later. The SO_2 profile shown in Figure 6.3 increases with excess air level up to a value of approximately 1.4 and then subsequently decreases with further increases in excess air level. The increase in SO_2 emissions with excess air levels can be explained in terms of the impact of solids concentration and gas residence time on the SO_2 emissions. Low excess air levels result in lower superficial gas velocities which according to the proposed hydrodynamic model results in a higher solids concentration along the riser. Higher solid concentrations not only increases the amount of limestone particles but also coal particles at any axial location. Any available oxygen must be shared between the char combustion reaction, NO forming and reducing reactions and sulfur capture reaction and hence, lowers the

chance of sulfur capture by the limestone particles. Since the SO_2 profile increases with increasing excess air levels, the results show that the char combustion and NO formation and reduction reactions occur to a greater extent than the sulfur capture or sulfation reaction. As with the NO emissions, at an excess air level greater than 1.4, there is a change in the SO_2 emissions. Unlike the NO emissions, the SO_2 emissions actually decrease with further increases in excess air. Even though the superficial gas velocity increases and hence, solids concentration decreases, the amount of oxygen may be high enough to cause a marked increase in sulfur capture.

The simulated effect of staged combustion on the NO and SO_2 emissions being emitted out of the top of the riser is shown in Figure 6.4. The degree of staged combustion is expressed in terms of the primary air factor (paf), defined as the fraction of fluidizing gas that is sent into the combustor as primary air. The NO emission profile shows an optimum paf value of approximately 0.85. The NO profile can be partially explained in terms of the hydrodynamic conditions that exist within the riser. Low paf values lead to low inlet superficial gas velocities which according to the axial solids holdup model results in an increased solids concentration. Although reducing conditions exist in the lower portion of the riser, the rate of char combustion is still significant enough to cause a large amount of NO to be released. If the NO formed is not reduced enough in the bottom zone, it may not have enough opportunity to be reduced in the rest of the riser. There is a significant increase in superficial gas velocity at and above the secondary air location because of the introduction of secondary air. As the primary air factor is increased, the amount of solids in the lower region is not as high and the amount

of NO formed through char combustion is not as significant as with a lower paf value. When the primary air factor is increased, the amount of secondary air added becomes smaller and smaller. Consequently, the effect of secondary air on the axial solids holdup and on the gas residence time is not as significant. The effect is reflected in a lower amount of NO emissions with an increase in primary air factor values. The SO_2 profile in Figure 6.4 indicate that the lower the primary air factor, the greater the degree of sulfur capture. Experimental studies by Beacon and Lundqvist (1991) and Khan and Gibbs (1991) have shown that reducing conditions in a CFB riser can lead to decreased sulfur retention efficiency. The effect is attributed to a combination of lower oxygen concentration in the bed available for the sulfation reaction and increased sulfur regeneration from $CaSO_4$ in the reducing region of the bed. The main reason why the experimental observations were not achieved in the simulated results was due to the difficulties in determining the extent to which sulfur capture is hampered by reducing conditions in the reactor. Studies by Hansen et al. (1990) have shown that reducing conditions in the riser can reduce the effectiveness of sulfur capture using limestone particles.

The effect of molar Ca/S ratio and the effect of limestone particle diameter on NO and SO_2 emissions is shown in Figures 6.5 and 6.6, respectively. Figure 6.5 shows that in the case of NO emissions, at a constant excess air level, there is no significant effect caused by changes in the Ca/S ratio. In the case of SO_2 emissions, the simulated results show that the greater the molar Ca/S ratio the greater the degree of sulfur capture. As expected, increasing the amount of limestone in the reactor encourages greater sulfur
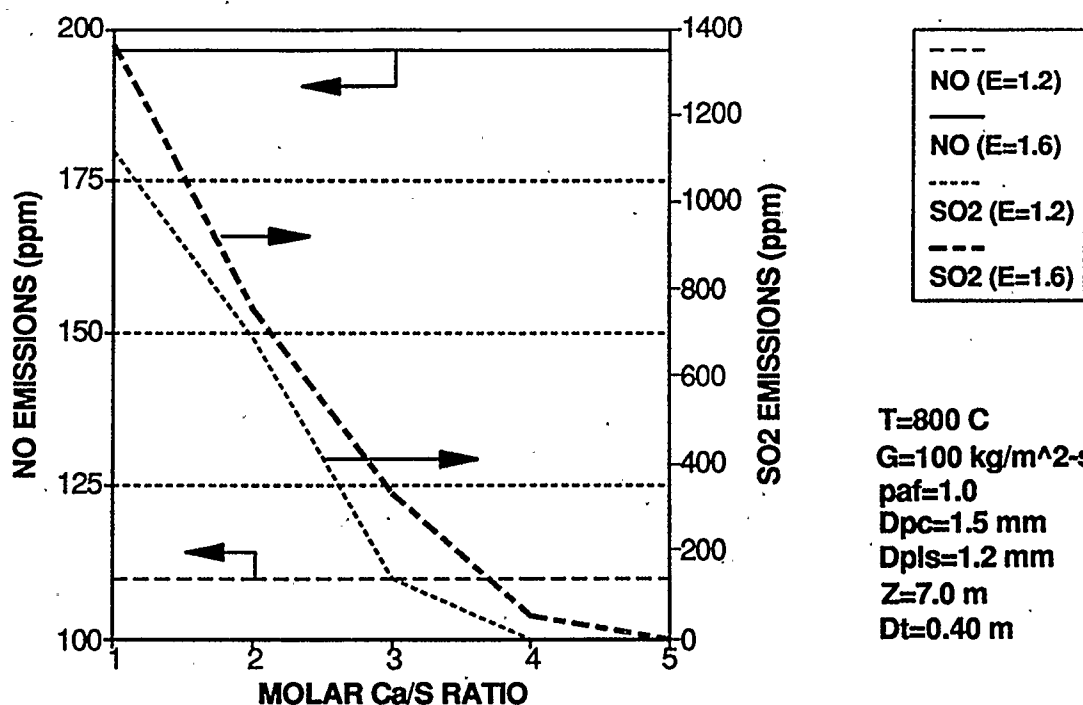
FIGURE 6.5 - EFFECT OF MOLAR Ca/S RATIO ON NO AND SO2 EMISSIONS
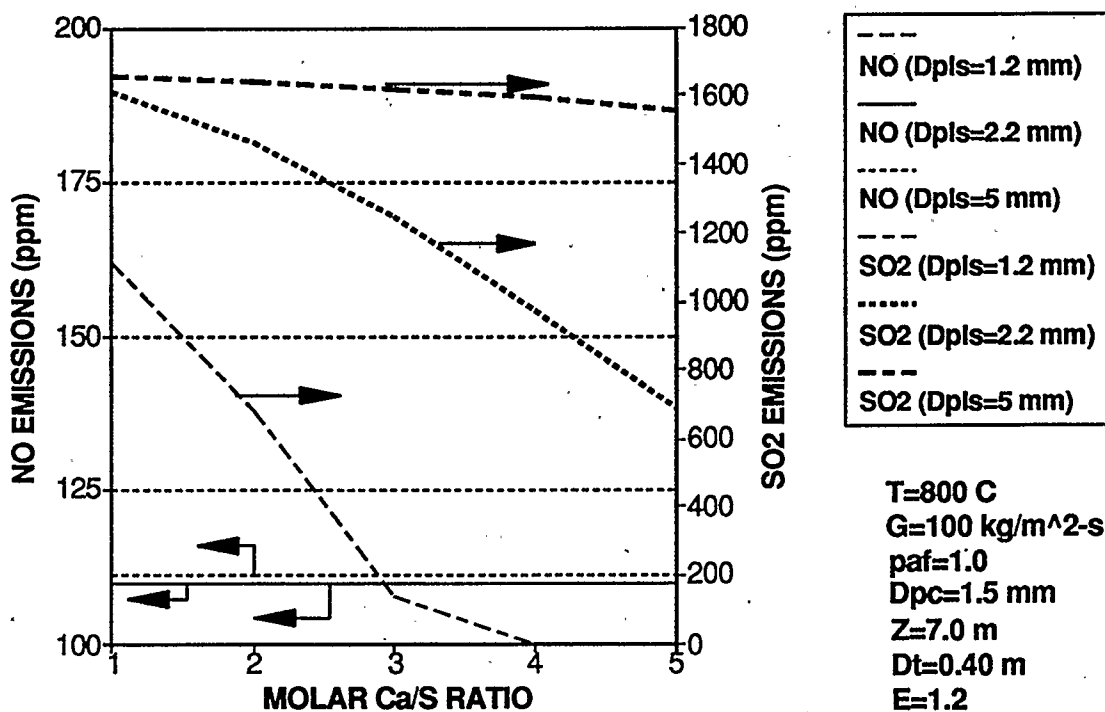
FIGURE 6.6 - EFFECT OF LIMESTONE PARTICLE DIAMETER
NO AND SO2 EMISSIONS

capture. As shown earlier the greater the excess air level the increased quantity of NO and SO_2 emissions.

As shown in Figure 6.5 and confirmed again in Figure 6.6, the reactor model predicts that NO emissions are not affected by increases in Ca/S ratio. The greatest impact of limestone particle diameter is on the SO_2 emissions. As the figure shows, the larger the particle size the higher the SO_2 emissions. The effect is due to the increased difficulty in capturing the SO_2 with larger particles (Hartman and Coughlin, 1976). For the simulation conditions shown in Figure 6.6, using a limestone particle diameter of 1.2 mm and a Ca/S ratio of approximately 4 would result in 100% sulfur retention. Increasing the limestone particle diameter to 2.2 mm would require a Ca/S ratio of around 7 to achieve 100% sulfur retention. The difference in Ca/S ratio becomes even more significant if one thinks in terms of the amount of limestone required. The simulated results suggest that for limestone particles with diameters around 5 mm, 100% sulfur retention is possible without using an excessive amount of limestone. It is important to point out that with the high degree of mixing in a CFB riser, attrition of limestone particle through contact with sand or char particles or with the walls can play an important role in the amount of sulfur retention that occurs. Attrition can prolong the usefulness of the calcined limestone particle by exposing fresh calcium oxide for reaction with SO_2. Although limestone attrition was not considered in the model, the SO_2 emission results shown in Figure 6.6 indicate the worst case scenarios for the simulation conditions chosen. For example, with attrition effects, 100% sulfur retention might be achievable at a Ca/S ratio well below 4.

Figures 6.7 and 6.8 show the effect of coal particle diameter and riser diameter on NO and SO_2 emissions, respectively. The effect of coal particle diameter is to influence the amount of NO emitted from the top of a CFB riser. Figure 6.7 shows that at any excess air level, the larger the coal particle, the lower the NO emission. The effect is due to the lower rate of char combustion associated with larger char particles. According to the Fine et al. (1974) correlation, the amount of NH_3 (which is subsequently converted to NO) released through the devolatilization process is only a function of temperature. Therefore, for a given operating temperature, the NH_3 released is a constant. Consequently, the change in NO emissions is due entirely to the reduction in NO formed from char combustion. The higher the excess air level the greater the difference between the NO emitted at different particle diameters. This is directly related to the increased combustion that occurs at higher oxygen levels. The SO_2 profile is essentially independent of coal particle diameter. The effect is again due to the Fine et al. (1974) correlation used to estimate the amount of sulfur released through the devolatilization process. According to the conditions shown in Figure 6.7, all of the sulfur contained in the coal is released in the devolatilization process. If it is assumed that only a fraction of the sulfur contained in the coal is released through the devolatilization process then results similar to those of the NO emission are expected. The larger the coal particle, the lower the rate of char combustion and hence the lower the SO_2 emitted.

The effect of riser diameter is shown in Figure 6.8 at two different excess air levels. The effect of riser diameter on SO_2 emissions is different from that of NO emissions. Increasing the riser diameter and keeping all other operating conditions
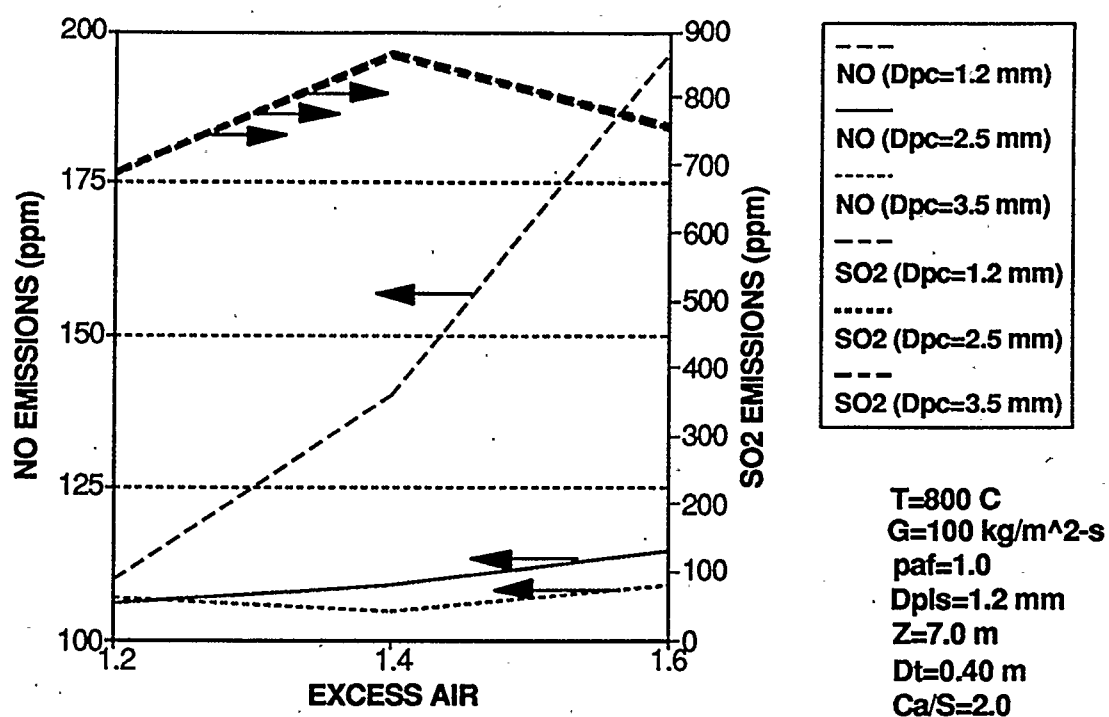
FIGURE 6.7 - EFFECT OF COAL PARTICLE DIAMETER ON
NO AND SO2 EMISSIONS

Legend:
- NO (Dpc=1.2 mm)
- NO (Dpc=2.5 mm)
- NO (Dpc=3.5 mm)
- SO2 (Dpc=1.2 mm)
- SO2 (Dpc=2.5 mm)
- SO2 (Dpc=3.5 mm)

T=800 C
G=100 kg/m^2-s
paf=1.0
Dpls=1.2 mm
Z=7.0 m
Dt=0.40 m
Ca/S=2.0
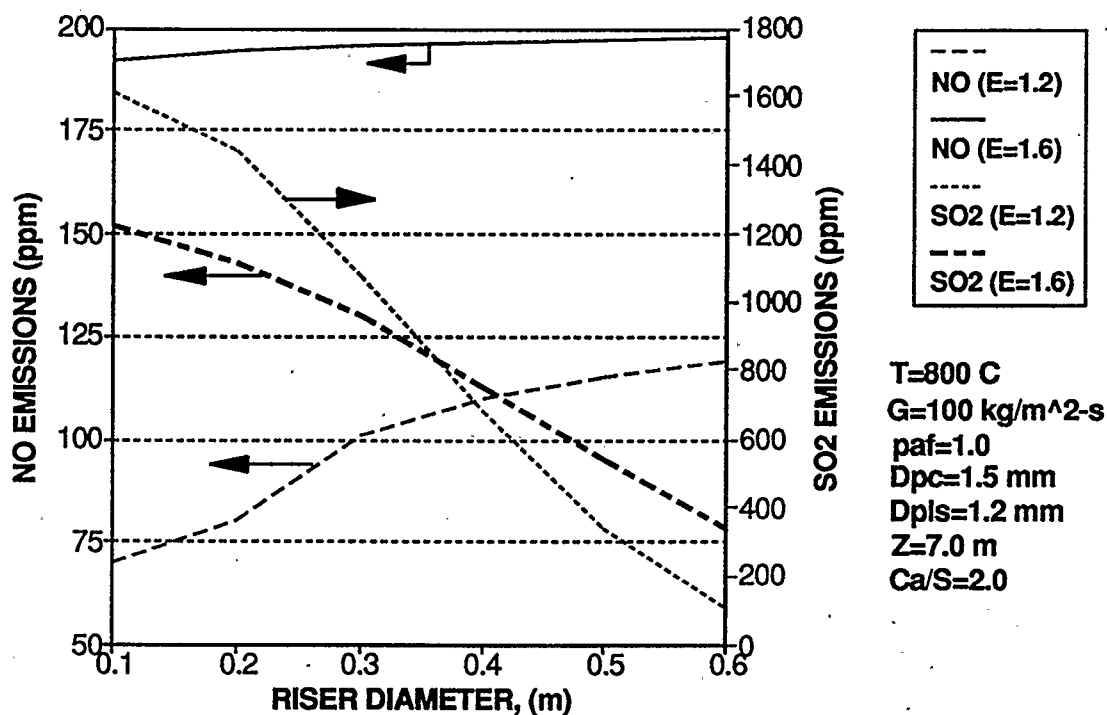
FIGURE 6.8 - EFFECT OF RISER DIAMETER ON NO AND SO2 EMISSIONS

Legend:
- NO (E=1.2)
- NO (E=1.6)
- SO2 (E=1.2)
- SO2 (E=1.6)

T=800 C
G=100 kg/m^2-s
paf=1.0
Dpc=1.5 mm
Dpls=1.2 mm
Z=7.0 m
Ca/S=2.0

constant lead to an increase in gas and solids residence times. In the case of NO, the effect is to increase the emissions at the top of the riser. At smaller diameters, for the same volumetric flow, the superficial gas velocity is increased so much that there is very little chance for any type of reaction to occur. Again, the higher the excess air level, the greater the NO emission. In the case of SO_2, the larger the diameter the longer the solids residence time and hence, the greater the degree of sulfur retention. As Figure 6.8 shows the SO_2 emission profiles crossover at a riser diameter around 0.38 m. At smaller diameters, the SO_2 emissions at an excess air level of 1.2 is greater than the SO_2 emissions at an excess air level of 1.6. The results seem to indicate that the reduction in gas residence time is not as important as the oxygen concentration in affecting the sulfur capture reaction for riser diameters less than 0.38 m. This is mainly due to the fact that with the small diameter and consequently, high superficial gas velocity, the solids concentration does not vary enough to affect sulfur capture to any significant degree. At riser diameters greater than 0.38 m the SO_2 emissions are higher for the higher excess air level. At these riser diameters the effect of solids concentration is more important.

Figure 6.9 shows the effect of riser height on NO and SO_2 emissions at the outlet of a CFB riser and at two different riser diameters. As expected, the greater the riser height, the longer the limestone residence time and hence, the lower the SO_2 emissions. The NO emissions are not affected to the same extent as the SO_2 emissions. As Figure 6.9 shows, the NO emissions remain reasonably constant with changes in riser height. At a riser diameter of 0.20 m, the NO emissions initially decreases slightly and then gradually increases as the riser height is raised. The changes to the NO emission profile
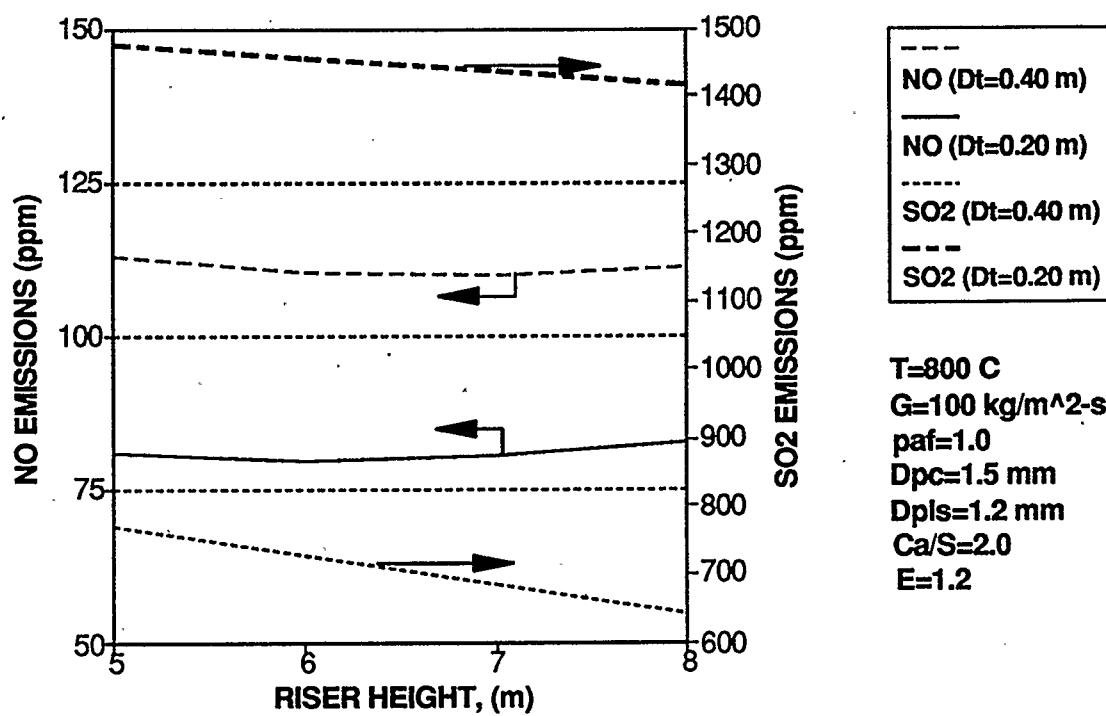
FIGURE 6.9 - EFFECT OF RISER HEIGHT ON NO AND SO2 EMISSIONS

can be explained by considering the fact that increasing the riser length, increases the amount of char combustion that can occur to form NO. However, as indicated in Figure 6.9, the amount of char combustion due to the increased riser length is very small. In all likelihood, the oxygen concentration is so small that the rate of char combustion is very small. Although it should be emphasized that there are many assumptions used in generating Figure 6.9, the figure suggests that increasing the riser height only benefits the control of SO_2 emissions.

CHAPTER 7
CONCLUSIONS AND RECOMMENDATIONS

7.1 CONCLUSIONS

A predictive model based on core/annular flow has been developed to estimate the axial voidage profile and internal flow structure of risers under fast fluidization conditions. The model assumes the riser to consist of three sections: 1) an acceleration zone where the solids accelerate upon entry into the riser, 2) a developed flow zone where the flow of gas and solids is assumed to be hydrodynamically developed and 3) an abrupt exit zone for CFB units equipped with an abrupt exit at the top of the riser. Using empirically developed equations for predicting the apparent voidage at the bottom of the riser, the length of the acceleration zone and the apparent voidage at the top of the riser (for CFBs with abrupt riser exits), the three sections of the riser are solved to yield the average voidage, core voidage, core radius, gas core velocity, solids core velocity, core-to-annulus solids interchange coefficient and annulus-to-core solids interchange coefficient as a function of axial location.

The validity of the proposed model was demonstrated by performing computer simulations to compare the apparent axial voidage profile and/or internal flow structure characteristics predicted using the model with data obtained in experimental CFB units. Generally, the simulated results compared favourably with the experimental results. The model was able to qualitatively and quantitatively predict the effect of operating variables such as superficial gas velocity, solids mass flux, solids diameter and density and riser geometry on the apparent voidage profile. Because of the uncertainties associated with

experimental internal flow structure measurements, a meaningful comparison between the simulated and experimental internal flow structure results could not be made.

The applicability of the model is mainly limited by the range of operating conditions and gas and solid physical properties used to develop the riser bottom and top voidage correlations. Using the model outside the range of applicability of the empirical equations would undoubtedly lead to erroneous results.

To illustrate an application of the hydrodynamic model to reactor design, the model was used to study the formation and evolution of environmentally damaging air pollutants such as SO_2 and NO_x emissions generated during circulating fluidized bed coal combustion. However, due to a combination of unreliable kinetic data and uncertainty in the mechanisms responsible for the formation and reduction of NO_x emissions like NO_2 and N_2O, the hydrodynamic model was only used to study the SO_2 and NO emissions from a CFB coal combustor. This study represents a first attempt to model emissions from CFB combustors and may serve as a basis for more comprehensive simulations.

The results of the reactor model agreed reasonably well with the trends reported in literature. The reactor model showed that the greater the reducing conditions in the combustion cell the lower the NO emissions. Increasing the overall excess air resulted in an increase in NO emission out of the riser. The Ca/S ratio and limestone particle diameter were shown to be important parameters affecting limestone utilization. Increasing the Ca/S ratio results in better sulfur retention but also increases the amount of limestone required, while increasing limestone particle diameter decreases the

effectiveness of sorbent. Simulations involving riser diameter and riser height as independent variables illustrated that both gas and solids residence times have an important effect of the amount of SO_2 and NO emitted from a CFB riser.

7.2 RECOMMENDATIONS

Presently, mainly because of the limited data reported in literature, the model is restricted to experimental CFB units with small diameters and short riser lengths operating over a narrow range of solids circulation rates. Further experimental studies should be performed in order to gather more data so that the range of conditions over which the axial solids holdup model is applicable can be increased. Specifically, studies should be conducted on industrial sized units operating at high circulation rates and at various operating temperatures and pressures.

Although many mechanisms for NO_x formation and reduction have been proposed, the kinetic studies that have been conducted to validate the mechanisms has been limited. More studies should be conducted to determine kinetic data for NO_x formation and reduction. Once the information is available, it can be incorporated into the proposed reactor model to make it more comprehensive.

CHAPTER 8
REFERENCES

8.1 REFERENCES

Ambler, P.A., "Residence Time Distribution of Binary Solids Mixtures in a Circulating Fluidized Bed", M.A.Sc Thesis, University of Waterloo, Canada (1988)

Ambler, P.A, B.J. Milne, F. Berruti and D.S. Scott, "Residence Time Distribution of Solids in a Circulating Fluidized Bed: Experimental and Modelling Studies", Chem. Eng. Sci., 45, 8, 2179-2186 (1990)

Arastoopour, H. and D. Gidapow, "Vertical Pneumatic Conveying Using Four Hydrodynamic Models", Ind. Eng. Chem. Fundam., 18, 123 (1979)

Arena, U., A. Cammarota and L. Pistane, "High Velocity Fluidization Behaviour of Solids in A Laboratory Scale Circulating Fluidized Bed", in Circulating Fluidized Bed Technology, P. Basu, Ed., Pergamon Press, Toronto, 119-125 (1986)

Arena, U., A. Malandrino, A. Marzocchella and L. Massimilla, "Flow Structures in the Risers of Laboratory and Pilot CFB Units", in Proc. of 3rd Int. Conf. on Circulating Fluidized Beds, Oct. 15-18, Nagoya, Japan, 4-10-1 to 4-10-12 (1990)

Arthur, J.R., "Reactions Between Carbon and Oxygen", Trans. Faraday Soc, 47, 164 (1951)

Bader, R., J. Findlay and T.M. Knowlton, "Gas/Solids Flow Patterns in a 30.5 cm Diameter Circulating Fluidized Bed", in Circulating Fluidized Bed Technology, P. Basu and J.F. Large, Eds., Pergamon Press, Toronto, 123-137 (1988)

Basu, P., C. Ritchie and P.K. Halder, "Burning Rates of Carbon Particles in a Circulating Fluidized Bed", in Circulating Fluidized Bed Technology, P. Basu, Ed., Pergamon Press, Toronto, 229-237 (1986)

Basu, P. and S.A. Fraser, "Circulating Fluidized Bed Boilers-Design and Operations", Butterworth-Heinemann, Toronto (1991)

Beacon, D. and R. Lundqvist, "Advanced Emission Controls at Mt. Poso Pyroflow Circulating Fluidized Bed Boiler", in Proc. of 11th Int. Conf. on Fluidized Bed Combustion, 233-239 (1991)

Berruti, F. and N. Kalogerakis, "Modelling the Internal Flow Structure of Circulating Fluidized Beds", Can. J. Chem. Eng., 67, 1010-1014 (1989)

Berruti, F. and R. Wong, "Strategies For Low Emissions From Circulating Fluidized Bed Boilers", paper presented at the NATO-Advanced Study Institute Chemical Reactor Technology for Environmentally Safe Reactors and Products Conference, Aug. 25-Sept. 4, London, Canada (1991)

Bolton, L.W. and J.F. Davidson, "Recirculation of Particles in Fast Fluidized Risers", in Circulating Fluidized Bed Technology II, P. Basu and J.F. Large, Eds., Pergamon Press, Toronto, 139-146 (1988)

Bonn, B. and E. Richter, "Aspects of Coal Combustion in Atmospheric and Pressurized Fluidized Beds", Fuel Processing Tech., 24, 319-353 (1990)

Borghi, G., A.F. Sarofim and J.M. Beer, Comb. Flame, 61,1 (1985)

Borgwardt, R.H. and R.D. Harvey, "Properties of Carbonate Rocks Related to SO_2 Reactivity", Environ. Sci. Technol., 4, 350-360 (1972)

Breault, R.W. and V.K. Mathur, "High Velocity Fluidized Bed Hydrodynamic Modelling. 1. Fundamental Studies of Pressure Drop", Ind. Eng. Chem. Res., 28, 684-688 (1989)

Brereton, C.M.H., "Fluid Mechanics of High Velocity Fluidized Beds", Ph.D. Dissertation, U.B.C., Vancouver, B.C., Canada (1987)

Brown, R.A. and L. Muzio, "N_2O Emissions from Fluidized Bed Combustion", in Proc. of 11th Int. Conf. on Fluidized Bed Combustion, 719-724 (1991)

Burkell, J.J., J.R. Grace, J. Zhao and C.J. Lim, "Measurement of Solids Circulation Rates in Circulating Fluidized Beds", in Circulating Fluidized Bed Technology II, P. Basu and J. F. Large, Eds., Pergamon Press, Toronto, 501-509 (1988)

Chandok, S.S. and D.C.T. Pei, "Particle Dynamics in Solids-Gas Flow in a Vertical Pipe", Progress in Heat and Mass Transfer, 6, 465-474 (1972)

Choi, J.H., C.K. Yi and J.E. Son, "Axial Voidage Profile in a Cold Mode Circulating Fluidized Bed", in Proc. of 3rd Int. Conf. on Circulating Fluidized Beds, Oct. 15-18, Nagoya, Japan, 4-9-1 to 4-9-6 (1990)

Contractor, R.M., "Butane Oxidation to Maleic Anhydride in a Recirculating Solids Riser Reactor", in Circulating Fluidized Bed Technology II, P. Basu and J.F. Large, Eds., Pergamon Press, Toronto, 467-474 (1988)

Couturier, M., B. Doucette, D. Stevens, S. Pooplol and V. Razbin, "Temperature, Gas Concentration and Solid Mass Flux Profiles Within a Large Circulating Fluidized Bed Combustor", in Proc. of 11th Int. Conf. of Fluidized Bed Combustion, 107-114 (1991)

Dinrong, B., J. Yong and Y. Zhiqing, "The Two-Channel Model for Fast Fluidization", in Fluidization'88, M. Kwauk and D. Kunii, Eds., Science Press, Beijing, China, 155-164 (1988)

Dogu, G. and T. Dogu, "Kinetics of Capture of Sulfur Dioxide and Applications to Flue Gas Desulfurization", paper presented at the NATO-Advanced Study Institute Chemical Reactor Technology for Environmentally Safe Reactors and Products, Aug. 25-Sept. 4, London, Canada (1991)

Dry, R.J. and R.D. La Nauze, "Combustion in Fluidized Beds", Chem. Eng. Prog., 86(7), 31-47 (1990)

Dukler, A.E., "Characterization, Effects and Modelling of The Wavy Gas-Liquid Interface", in Progress in Heat and Mass Transfer, Volume 6, G. Hetsroni, S. Sideman and J.P. Hartnett, Eds., Pergamon Press, Toronto, 207-235 (1970)

Ehrlich, S., "Fluidized Bed Combustion", in Encyclopedia of Physical Science and Technology, R.A. Meyers, Ed., Academic Press (1987)

Enick, R., K.L. Falkenberg and G.E. Klinzing, "Acceleration Length Model for Pneumatic Transport", in Particulate and Multiphase Processes, T. Ariman and T.N. Vezirglu, Eds., Hemisphere Publishing Corporation, New York, 307-317 (1987)

Essenhigh, R.H., in "Chemistry of Coal Utilization", M.A. Elliot, Ed., 2nd Suppl. Vol, John Wiley, New York, 1153-1312 (1981)

Field, M.A., D.W. Gill, B.B. Morgan and P.G.W. Hawksley, "Combustion of Pulverized Coal", BCURA (1967)

Fine, D.H., S.M. Slater, A.F. Sarofim and G.C. Williams, "Nitrogen in Coal as a Source of Nitrogen Oxide Emissions from Furnaces, Fuel, 53, 120 (1974)

Furusawa, T., T. Honda, J. Takano and D. Kunii, "Nitric Oxide Reduction in an Experimental Fluidized Bed Coal Combustor, in Fluidization, Cambridge University Press, 314-319 (1978)

Furusawa, T., M. Tsujimura, M. K. Yasunaga and T. Kojima, "Fate of Fuel Bound Nitrogen within Fluidized-Bed Combustor under Staged Air Firing", in Proc. of 8th Int. Conf. on Fluidized Bed Combustion, 1095-1104 (1985)

Geldart, D., "Gas Fluidization Technology", John Wiley & Sons, Toronto (1986)

Geldart, D; and M.J. Rhodes, "From Minimum Fluidization to Pneumatic Transport- A Critical Review of the Hydrodynamics", in Circulating Fluidized Bed Technology, P.Basu Ed., Pergamon Press, Toronto, 21-31 (1986)

Gibbs, B.M. and E. Hampartsoumian, in "Fluidized Bed Boilers: Design and Application", P. Basu, Ed.. Pergamon Press, Toronto (1984)

Grace, J.R., "High-Velocity Fluidized Bed Reactors", Chem. Eng. Sci. 45, 1953-1966 (1990)

Grewal, N.S., R.D. Maurer, W. Fox and M.D. Mann, "Axial Particle Loading in a Circulating Fluidized Bed", in Proc. of 11th Int. Conf. on Fluidized Bed Combustion, Montreal, 317-323 (1991)

Hansen, P.F.B., K. Dam-Johansen, L.H. Bank and K. Ostergaard, "Sulfur Capture on Limestone under Periodically Changing Oxidizing and Reducing Conditions", in Proc. of 3rd Int. Conf. on Circulating Fluidized Beds, Oct. 15-18, Nagoya, Japan, 1-22-1 to 1-22-6 (1990)

Hartge, E.U., Y. Li. and J. Werther, "Analysis of the Local Structure of Two Phase Flow in a Fast Fluidized Bed", in Circulating Fluidized Bed Technology, P. Basu, Ed., Pergamon Press, Toronto, 153-160 (1986)

Hartman, M. and R.W. Coughlin, "Reaction of Sulfur Dioxide with Limestone and the Influence of Pore Structure", Ind. Eng. Chem. Process Des. Dev., 13, 3, 248-253 (1974)

Hartman, M. and R.W. Coughlin, "Reaction of Sulfur Dioxide with Limestone and the Grain Model", AIChE J., 22, 490-498 (1976)

Herb, B., K. Tuzla and J.C. Chen, "Distribution of Solids Concentrations in Circulating Fluidized Bed", in Fluidization VI, J.R. Grace, L.W. Shemilt and M.A. Bergougnou, Eds., Engineering Foundation, New York, 65-72 (1989)

Hiltunen, M. and J.T. Tang, "NO_x Abatement in Ahlstrom Pyroflow Circulating Fluidized Bed Boilers", in Circulating Fluidized Bed Technology II, P. Basu and J.F. Large, Eds., Pergamon Press, Toronto, 429-436 (1988)

Horio, M., K. Morishita, O. Tachibana and N. Murata, "Solid Distribution and Movement in Circulating Fluidized Beds", in Circulating Fluidized Bed Technology II, P. Basu and J.F. Large, Eds., Pergamon Press, Toronto, 147-154 (1988)

Horio, M. and Y. Takei, "Macroscopic Structure of Recirculating Flow of Gas and Solid in Circulating Fluidized Beds", in Proc. of 3rd Int. Conf. on Circulating Fluidized Beds, Oct. 15-18, Nagoya, Japan, 4-15-1 to 4-15-6 (1990)

Hottel, H.C., G.C. Williams, N.M. Nerheim and G.R. Schneider, "Burining Rate of Carbon Monoxide", 10th International Symposium on Combustion, 111 (1965)

Ishii, H., T. Nakajima and M. Horio, "The Clustering Annular Model of Circulating Fluidized Beds", Jap. J. Chem. Eng., 22, 5, 484-490 (1989)

Ishizuka, H., K. Hyvarinen, A. Morita, T. Suzuki, K. Yano and R. Hirose, "Experimental Study on NO_x Reduction in CFB Coal Combustion", in Circulating Fluidized Bed Technology II, P. Basu and J.F. Large, Eds., Pergamon Press, Toronto, 437-444 (1988)

Johnsson, J.E., "A Kinetic Model for NO_x Formation in Fluidized Bed Combustion", in Proc. of 10th Int. Conf. on Fluidized Bed Combustion, 1111-1118 (1989)

Johnsson, J.E. and K. Dam-Johansen, "Formation and Reduction of NO_x in a Fluidized Bed Combustor", in Proc. of 11th Int. Conf. on Fluidized Bed Combustion, 1389-1396, Montreal (1991)

Jotaki, T. and Y. Tomita, "Flow in the Acceleration Region of Pneumatic Transport of Granular Solids in Vertical Pipes", in Proc. of Pneumotransport 3, Apr. 7-9, Bath, England, D8-99 to D8-108 (1976)

Kalpakov, V.M. and E.V. Donat, "An Investigation of the Pressure Drop in the Acceleration Zone of a Vertical Pipeline for Conveying Solid Particles", Int. Chem. Eng. 10, 3, 394-397 (1970)

Kato, K., Y. Ozawa, H. Endo, M. Hiroyasu and T. Hanzawa, "Particles Hold-up and Axial Pressure Drop in Vertical Pneumatic Transport Reactor (Riser)", in Fluidization V, K. Ostergaard and A. Sorensen, Eds., Engineering Foundation, New York, 265-272 (1986)

Kato, K., H. Shibasaki, K. Tamura, S. Arita, C. Wang, and T. Takarada, "Particle Holdup in a Fast Fluidized Bed", Jap. J. Chem. Eng., 22, 130-136 (1989)

Kato, K., T. Takarada, T. Tamura and K. Nishino, "Particle Hold-up Distribution in a Circulating Fluidized Bed", in Proc. of 3rd Int. Conf. on Circulating Fluidized Beds, Oct. 15-18, Nagoya, Japan, 4-11-1 to 4-11-6 (1990)

Keairns, D.L., R.A. Newby and N.H. Ulerich, in Fluidized Bed Boilers: Design and Application, Pergamon Press, P. Basu, Ed., Pergamon Press, Toronto (1984)

Kehoe, P.W.K. and J.F. Davidson, Inst. Chem. Eng. (London) Symp. Ser., Vol. 33, 97 (1971)

Khan, W.U.Z. and B.M. Gibbs, "The Effects of Bed Temperature and Oxygen Stoichiometry on Sulfur Capture by Limestone in a Fluidized Bed Combustor", in Proc. of 11th Int. Conf. on Fluidized Bed Combustion, 1503-1510 (1991)

Kilpinen, P. and M. Hupa, "Homogeneous N_2O Chemistry at Fluidized Bed Conditions: a Kinetic Modelling Study", Combustion and Flame (in press) (1991)

Kmiec, A. and K. Leschonski, "Acceleration of the Solid Phase During Pneumatic Conveying in Vertical Pipes", Chem. Eng. J., 36, 59-70 (1987)

Kojima, T., K. Ishihara, I. Guilin and T. Furusawa, "Measurement of Solids Behaviour in a Fast Fluidized Bed", Jap. J. Chem. Eng., 22, 4, 341-346 (1989)

Kramlich, J.C., J.A. Cole, J.M. McCarthy and W.S. Lanier, "Mechanisms of Nitrous Oxide Formation in Coal Flames", Combustion and Flame, Vol 77, 375 (1989)

Kunii, D. and O. Levenspiel, "Flow Modelling of Fast Fluidized Beds" in Proc. of 3rd Int. Conf. on Circulating Fluidized Beds, Oct. 15-18, Nagoya, Japan, 4-7-1 to 4-7-8 (1990)

Kwauk, M., W. Ningde, L. Youchu, C. Bingyn and S. Zhiyuan, "Fast Fluidization at ICM", in Circulating Fluidized Bed Technology, P. Basu, Ed., Pergamon Press, Toronto, 33-62 (1986)

Lanneau, K.P, "Gas-solid Contacting in Fluidized Beds", Trans. Instn. Chem. Engrs., Vol. 38, 125-143 (1960)

Lee, G.S., G. Young Han and S.D. Kim, "Coal Combustion Characteristics in a Circulating Fast Fluidized Bed", Kor. J. Chem. Eng.,1, 71-76 (1984)

Li, Y. and M. Kwauk, "The Dynamics of Fast Fluidization" in Fluidization, J.R. Grace and J.M. Matsen Eds., Plenum Press, New York, 537-544 (1980)

Lin, W. and C.M. van den Bleek, "The SOx/NO_x Emissions in the Circulating Fluidized Bed Combustion of Coal", in Proc. of 3rd. Int. Conf. on Circulating Fluidized Beds, Oct. 15-18, Nagoya, Japan, 6-2-1 to 6-2-6 (1990)

Makansi, J. and R. Schwieger, "Fluidized-Bed Boilers", Power, May, S1-S16 (1987)

Matsen, J.M., "Some Characteristics of Large Solids Circulation Systems", in "Fluidization", D.L. Keairns, Ed., Hemisphere, New York, 135-149 (1976)

McCabe, W.L., J.C. Smith and P. Harriot, "Unit Operations of Chemical Engineering", 4th Edition, McGraw Hill, Montreal (1985)

Miller, J.A. and C.T. Bowman, "Mechanism and Modelling of Nitrogen Chemistry in Combustion", paper presented at the 1988 Fall Meeting of the Western State Section/ The Combustion Institute, Dana Point, California, October 17-18 (1988)

Milne, B.J. and F. Berruti, "Modelling the Mixing of Solids in Circulating Fluidized Beds", in Proc. of 3rd Int. Conf. on Circulating Fluidized Beds, Oct. 15-18, Nagoya, Japan, 6-4-1 to 6-4-6 (1990)

Min, K., "Intensity of Particle Motion in Solid-Gas Suspension Flow", J. Appl. Physics, 38, 564-567 (1967)

Minchener, A.J. and G.J. Kelsall, "The Control of NO_x Emissions from PFBC Systems", J. Inst. Energy, 85-91, June (1990)

Mori, S., Y. Yan, K. Kato, K. Matsubara and D. Liu, "Hydrodynamics of a Circulating Fluidized Bed", in Proc. of 3rd Int. Conf. on Circulating Fluidized Beds, Oct. 15-18, Nagoya, Japan, 4-5-1 to 4-5-6 (1990)

Moritomi, H., Y. Suzuki, N. Kido and Y. Ogius, "NO_x Formation Mechanism of Circulating Fluidized Bed Combustion", in Proc. of 11th Int. Conf. on Fluidized Bed Combustion, 1005-1011 (1991)

Morooka, S., K. Kawazuishi and Y. Yato, Powder Tech., 26, 75 (1980)

Morooka, S., H. Kawamura, S. Yan, T. Okubo and K. Kusakabe, "Surface Modification of Milled Carbon Fiber by Low-Temperature Oxygen Plasma in a Fast Fluidized Bed", in Proc. of 3rd Int. Conference on Circulating Fluidized Beds, Oct. 15-18, Nagoya, Japan, 2-4-1 to 2-4-6 (1990)

Mulcahy, M.F.R., in "Oxygen in the Metal and Gaseous Fuel Industries", 175-208, The Chemical Society, London (1978)

Mulcahy, M.F.R. and J.W. Smith, "Kinetics of Combustion of Pulverized Fuel: A Review of Theory and Experiment", Rev. Pure and Appl. Chem., Vol 81, 107-114 (1969)

Nakamura, K. and C.E. Capes, "Vertical Pneumatic Conveying: A Theoretical Study of Uniform and Annular Particle Flow Models", Can. J. Chem. Eng., 51, 39-46 (1973)

Nakamura, S., Y. Ito, M. Shirakashi, and M. Kanno, "Development of CFB Adsorber for Recovery of Uranium From Seawater", in Proc. of 3rd Int. Conf. on Circulating Fluidized Beds, Oct. 15-18, Nagoya, Japan, 2-2-1 to 2-2-6 (1990)

Patience, G.S., "Circulating Fluidized Beds: Hydrodynamics and Reactor Modelling", Ph.D. Dissertation, Ecole Polytechnique, Montreal, Quebec, Canada (1990)

Patience, G.S., J. Chaouki, F. Berruti and R. Wong, "Scaling Considerations for Circulating Fluidized Bed Risers", submitted to Powder Tech. for publication

Pereira, F.J., J.M. Beer, B. Gibbs and A.B. Hedley, "NO_x Emissions from Fluidized Bed Coal Combustors", in Proc. of 15th Int. Symp. on Combustion, 1149-1156 (1974)

Rajan, R.R. and C.Y. Wen, "A Comprehensive Model for Fluidized Bed Coal Combustors", AIChE J., 24, 4, 642-655 (1980)

Reh, L., "The Circulating Fluid Bed Reactor - a Key to Efficient Gas/Solid Processing", in Circulating Fluidized Bed Technology, P. Basu, Ed., Pergamon Press, Toronto, 105-118 (1986)

Reh, L. and J. Li, "Measurement of Voidage in Fluidized Beds by Optical Probes", in Proc. of 3rd Int. Conf. on Circulating Fluidized Beds, Oct 15-18, Nagoya, Japan, 4-16-1 to 4-16-9 (1990)

Rhodes, M.J. and D. Geldart, "The Hydrodynamics of Recirculating Fluidized Beds", in Circulating Fluidized Bed Technology, P. Basu Ed., Pergamon Press, Toronto, 193-200 (1986)

Rhodes, M.J. and D. Geldart, "A Model for the Circulating Fluidized Bed", Powder Tech., 53, 155-162 (1987)

Rhodes, M.J., T. Hirama, G. Cerutti and D. Geldart, "Non-uniformities of Solids Flow in the Risers of Circulating Fluidized Beds", in Fluidization VI, J.R. Grace, L.W. Shemilt and M.A. Bergougnou, Eds., Engineering Foundation, New York, 73-80 (1989)

Rhodes, M.J., "Modelling the Flow Structure of Upward-Flowing Gas-Solids Suspensions", Power Tech., 60, 27-38 (1990)

Rose, H.E. and R.A. Duckworth, "Transport of Solid Particles in Liquids and Gases", The Engineer, 227,392-396 (1969)

Ross, I.B. and J.F. Davidson, "The Combustion of Carbon Particles in a Fluidized Bed", Trans. Instn. Chem. Engrs., Vol 59, 108-112 (1981)

Salam, T.F., F. Sibtain and B.M. Gibbs, "Reduction of NO_x by Staged Combustion Combined with Ammonia Injection in a Fluidized Bed Combustor: Influence of Fluidizing Velocity and Excess Air Levels", in Proc. of 10th Int. Conf. on Fluidized Bed Combustion, 69-76 (1989)

Schaub, R., R. Reimert and J. Albrecht, "Investigations of Emission Rates From Large Scale CFB-Combustion Plants", in Proc. of 10th Int. Conf. on Fluidized Bed Combustion, 685-691 (1989)

Senior, R.C. and C.M.H. Brereton, "Modelling of Circulating Fluidized Bed Flow Structure and Heat Transfer", Report from Department of Chemical Engineering, University of British Columbia, Sept. (1990)

Smith, I.W. "The Combustion Rates of Coal Chars: A Review", in Proc. of 19th Int. Symp. on Combustion, 1045-1065, Combustion Institute, Pittsburgh, Pennsylvania (1982)

Sticksel, P.R. and R.B. Engdahl, "Air Pollution", in Encyclopedia of Chemical Technology, Volume 1, 3rd Edition, John Wiley and Sons, Toronto, 624-649 (1984)

Stringer, J. and J. Stallings, "Materials Issues in Circulating Fluidized Bed Combustors", in 11th Int. Conf. on Fluidized Bed Combustion, 589-608 (1991)

Stubington, J.F. and S.W. Chan, Austr. Coal Sci. Conf., Adelaide, Paper B3:4 (1988)

Takeuchi, H. and T. Hirama, "Flow Visualization in the Riser of a Circulating Fluidized Bed", in Proc. of 3rd Int. Conf. on Circulating Fluidized Beds, Oct. 15-18, Nagoya, Japan 4-29-1 to 4-29-6 (1990)

Tsuo, Y.P. and D. Gidaspow, "Computation of Flow Patterns in Circulating Fluidized Beds", AIChE J., 36, 6, 885-896 (1990)

Tsuboi, H. and T. Iwasaki, "Coal Combustion in Circulating Fluidized Beds", in Circulating Fluidized Bed Technology II, P. Basu and J.F. Large, Eds., Pergamon Press, Toronto, 327-334 (1988)

Van Swaaij, W.P.M., C. Buurman and J.W. Van Breugel, "Shear Stresses on the Wall of a Dense Gas-solids Riser", Chem. Eng. Sci., 25, 1818-1820 (1970)

Wallis, G.B., "One-Dimensional Two-Phase Flow", McGraw-Hill Inc., Toronto (1969)

Weinstein, H., M. Meller, J. Shao and R.J. Parisi, "The Effect of Particle Density on Holdup in a Fast Fluidized Bed" in Fluidization and Fluid Particle Systems: Theories and Applications, T. M. Knowlton, Ed., AIChE Symp. Ser., NO. 234, Vol 80, 52-59 (1984)

Weinstein, H., M. Shao and M. Schnitzlein, "Radial Variation in Solid Density in High Velocity Fluidization", in Circulating Fluidized Bed Technology, P. Basu, Ed., Pergamon Press, Toronto, 201-206 (1986)

Weinstein, H. and J. Li, "An Evaluation of the Actual Density in the Acceleration Section of Vertical Risers" (Letter), Powder Tech., 57, 77-79 (1989)

Wen, C.Y., "Noncatalytic Heterogeneous Solid Fluid Reaction Models", Ind. Eng. Chem, 60, 9, 34 (1968)

Wen, C.Y. and L.H. Chen, "Fluidized Bed Freeboard Phenomena: Entrainment and Elutriation", AIChE J.,1 , 117-120 (1982)

Wojtowicz, M.A., J.A. Oude Lohuis, P.J.J. Tromp and J.A. Moulijn, "N_2O Formation in Fluidized Bed Combustion of Coal", in Proc. of 11th Int. Conf. on Fluidized Bed Combustion, 1013-1020 (1991)

Yang, W.C. and D.L. Keairns, "Estimating the Acceleration Pressure Drop and the Particle Acceleration Length in Vertical and Horizontal Pneumatic Transport Lines", in Proc. of Pneumotransport 3, Apr. 7-9, Bath, England, D7-89 to D7-98 (1976)

Yang, W.C., "A Unified Theory on Dilute Phase Pneumatic Transport", J. Powder and Bulk Solids Technology, 1, 89-95 (1977)

Yang, W.C., "A Model for the Dynamics of a Circulating Fluidized Bed Loop", in Circulating Fluidized Bed Technology II, P. Basu and J.F. Large, Eds., Pergamon Press, Toronto, 181-191 (1988)

Yerushalmi, J. "The Interaction of Gas and Solid in the Fast Fluidized Bed", in Proc. of Pneumotransport 3, April 7-9, Bath, England, E4-41 to E4-48 (1976)

Yerushalmi, J., N.T. Cankurt, D. Geldart and B. Liss, "Flow Regimes in Vertical Gas-Solid Contact Systems", AIChE Symp. Ser., No. 176, Vol. 74, 1-13, 1978

Yerushalmi, J. and N.T. Cankurt, "Further Studies of the Regimes of Fluidization", Powder Technology, 24, 187-205, (1979)

Yerushalmi, J. "High Velocity Fluidized Beds", in Gas Fluidization Technology, D. Geldart, Ed., John Wiley and Sons, Toronto (1986)

Yong, J., Y. Zhiqing, Q. Chunming and B. Dingrong, "The Influence of Exit Structures on The Axial Distribution of Voidage in Fast Fluidized Bed", in Fluidization'88, M. Kwauk and D. Kunii, Eds., Science Press, Beijing, China, 165-173 (1988)

Zhang, H., Y. Xie, Y. Chen and M. Hasatani, "Mathematical Modelling for Vertical Longitudinal Distribution of Fast Fluidized Beds" in Proc. of the 3rd. Conf. on Circulating Fluidized Beds, Oct. 15-18, Nagoya, Japan, 4-13-1 to 4-13-6 (1990)

Zhao, J., R.L. Wu, R.C. Senior, R. Legros, C.M.H. Brereton, J.R. Grace and C.J. Lim, "Spatial Variations Inside a Pilot Scale Circulating Fluidized Bed Combustion Unit", in Proc. of the EPRI Workshop on Material Properties in CFBC, Argonne (1989)

APPENDIX A

EXPERIMENTAL PRESSURE GRADIENTS

TRIAL #	1A	1B	1C	2A
Height, m	dP/dx, Pa/m	dP/dx, Pa/m	dP/dx, Pa/m	dP/dx, Pa/m
0.10	804	6000	3104	1387
0.25	603	3888	1940	817
0.50	333	2716	1096	666
0.74	235	2101	706	511
0.99	219	1347	706	187
1.24	185	590	706	187
1.49	185	312	706	187
1.68	185	261	706	187
1.93	185	261	746	187
2.18	197	261	1052	187
2.43	197	261	1563	187
2.68	416	261	1700	485
2.83	574	550	1800	490

TABLE A1 - EXPERIMENTAL PRESSURE GRADIENTS (TRIALS 1A TO 2A)

TRIAL #	2B	3A	3B	3C	3D
Height, m	dP/dx, Pa/m	dP/dx, Pa/m	dP/dx, Pa/m	dP/dx, Pa/m	dP/dx, Pa/m
0.10	1387	2400	3814	2155	810
0.25	1059	1600	3051	1272	571
0.50	883	1200	2746	909	376
0.74	519	960	1907	430	270
0.99	490	872	1430	214	162
1.24	379	436	1040	214	162
1.49	204	282	320	214	162
1.68	204	282	320	214	162
1.93	204	282	320	214	162
2.18	204	282	320	214	162
2.43	204	320	520	214	162
2.68	441	400	1443	1010	606
2.83	588	480	2286	1136	693

TABLE A2 - EXPERIMENTAL PRESSURE GRADIENTS (TRIALS 2B TO 3D)

TRIAL #	4A	4B	5A	5B	6A
Height, m	dP/dx, Pa/m	dP/dx, Pa/m	dP/dx, Pa/m	dP/dx, Pa/m	dP/dx, Pa/m
0.10	5775	5087	809	1416	392
0.25	3850	4545	539	927	294
0.50	1980	4040	320	726	196
0.74	990	2484	245	492	196
0.99	990	2480	245	492	140
1.24	990	1325	245	492	131
1.49	990	1325	245	492	131
1.68	990	1325	245	492	131
1.93	990	1325	245	492	146
2.18	990	1325	245	674	148
2.43	990	1325	245	1118	197
2.68	1732	1325	525	1150	336
2.83	2310	1325	715	1180	586

TABLE A3 - EXPERIMENTAL PRESSURE GRADIENTS (TRIALS 4A TO 6A)

TRIAL #	6B	7A	7B	8A	8B
Height, m	dP/dx, Pa/m	dP/dx, Pa/m	dP/dx, Pa/m	dP/dx, Pa/m	dP/dx, Pa/m
0.10	1796	2525	905	864	1716
0.25	1320	2424	746	495	1287
0.50	832	1683	566	448	1250
0.74	532	1154	364	226	1100
0.99	300	932	364	226	715
1.24	300	504	364	226	498
1.49	300	504	364	226	498
1.68	300	504	364	226	498
1.93	300	504	364	226	498
2.18	300	504	364	226	498
2.43	1122	505	364	394	667
2.68	1150	932	506	605	794
2.83	1220	1010	776	770	1110

TABLE A4 - EXPERIMENTAL PRESSURE GRADIENTS (TRIALS 6B TO 8B)